JOURNAL OF APPLIED PHYSICS

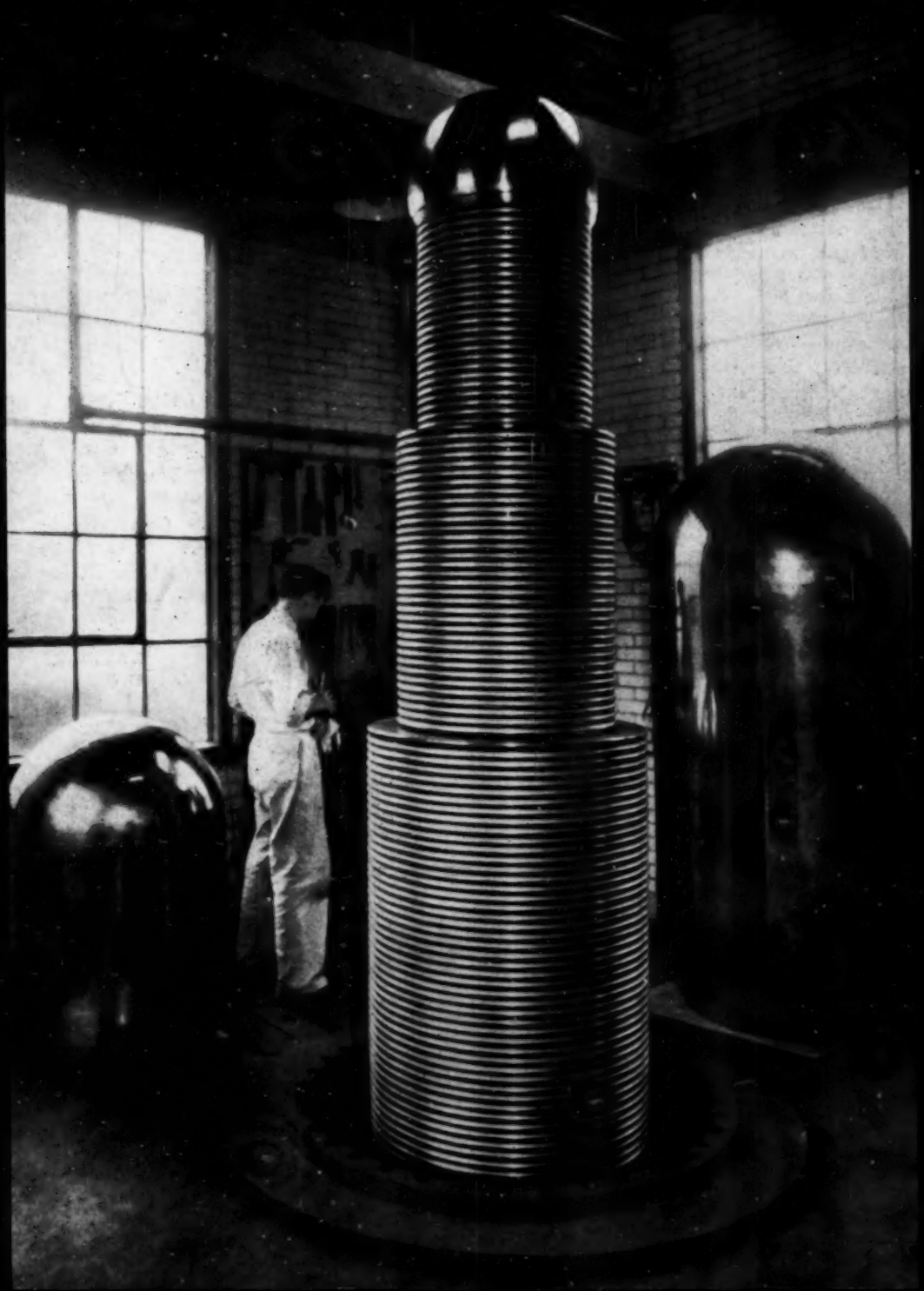

JOURNAL OF APPLIED PHYSICS

Vol. 19, No. 7 JULY, 1948

In This Issue

Page

Shipping of Radio-Isotopes KARL Z. MORGAN 593

Contributed Original Research

Irradiation of Biological Materials by High Energy Roentgen Rays and Cathode Rays J. G. TRUMP AND R. J. VAN DE GRAAFF 599

Biological and Photo-Chemical Effects of High Energy, Electrostatically Produced Roentgen Rays and Cathode Rays CECIL G. DUNN, WILLIAM L. CAMPBELL, HARVEY FRAM, AND ARDELIA HUTCHINS 605

Analysis of Retarded Control Systems LOUIS A. PIPES 617

Erratum: Response of Linear Resonant Systems to Excitation of Frequency Varying Linearly with Time GUNNAR HOK 623

Rising Sun Magnetrons with Large Numbers of Cavities A. V. HOLLENBERG, N. KROLL, AND S. MILLMAN 624

Transmission Losses in 2*n*-Terminal Networks VITOLD BELEVITCH 636

Transmission of Monoenergetic Slow Neutrons through Solid Solutions and Mechanical Mixtures of TiC and WC S. S. SIDHU 639

Experimental Results on Standing Wave Type Linear Accelerators for Electrons ELLIOTT J. LAWTON AND W. C. HAHN 642

Method for Measuring the Complex Dielectric Constant of Gases at Microwave Frequencies by Using a Resonant Cavity C. K. JEN 649

Carbon Film Formation and Commutator Brush-Wear As Revealed by the Electron Microscope ERNEST F. FULLAM AND ROBERT H. SAVAGE 654

Radiation Patterns of Dielectric Rods—Experiment and Theory R. B. WATSON AND C. W. HORTON 661

Attenuation of Spherical Shock Waves in Air RICHARD G. STONER AND WALKER BLEAKNEY 670

Chromatic Aberration and Resolving Power in Electron Microscopy E. G. RAMBERG AND J. HILLIER 678

Young's Modulus and Strain Coefficient of Resistivity of Some Bismuth Rich Alloys G. C. KUCZYNSKI AND J. T. NORTON 683

Letter to the Editor:

Electron Optical "Schlieren" Effect L. MARTON 687

In Every Issue

Calendar of Meetings 635

Here and There 688

New Booklets 688

Index to Advertisers xxxii

BOARD OF EDITORS

ELMER HUTCHISSON, *Editor*

Associate Editors

R. BOWLING BARNES
OTTO BEECK
W. F. BUSSE
W. JAMES LYONS
PHILIP MORRISON
PAUL E. SABINE
FREDERICK SEITZ
J. R. TOWNSEND
JOHN VON NEUMANN

Publication of the

American Institute of Physics

ADMINISTRATIVE STAFF

HENRY A. BARTON, *Director*

CLEVELAND NORCROSS, *Assistant Director*

RUTH F. BRYANS, *Publication Manager*

THEODORE VORBURGER, *Business Manager*

JOHN T. TATE, *Adviser on Publications*

GOVERNING BOARD

GEORGE R. HARRISON, *Chairman*

WALLACE WATERFALL, *Secretary*

GEORGE B. PEGRAM, *Treasurer*

LUIS W. ALVAREZ
ROBERT B. BRODE
E. U. CONDON
A. J. DEMPSTER
W. F. FAIR, JR.
HARVEY FLETCHER
R. C. GIBBS
W. V. HOUSTON
PAUL E. KLOPSTEG
F. W. LOOMIS
PHILIP M. MORSE
A. H. PFUND
JOHN T. TATE
M. W. WHITE
A. G. WORTHING

The JOURNAL OF APPLIED PHYSICS, published monthly at Prince and Lemon Sts., Lancaster, Pa., is devoted to physics in its role as the science basic to other natural sciences and to the arts and industries. Previous to 1937 this publication was known as PHYSICS. The JOURNAL OF APPLIED PHYSICS publishes editorials, news of physicists, and reviews, as well as technical papers of applied physics.

Manuscripts should be submitted to Elmer Hutchisson, Editor, Case Institute of Technology, Cleveland 6, Ohio.

Subscriptions and orders for back numbers should be addressed to Prince and Lemon Streets, Lancaster, Pa. or to the American Institute of Physics, 57 East 55 Street, New York 22, N. Y.

Subscription Price

	U.S. AND CANADA	ELSEWHERE
To members and associate members of the American Institute of Physics	$6.00	$7.00
To all others	8.00	9.00

Back Number Prices

Complete set: Vol. 1, July, 1931–Vol. 18, 1947—$132.00
Yearly back number rate: $10.00
Single copies: $1.00 each.

Changes of address should be sent to the Business Manager, American Institute of Physics; **corrected proofs** should be sent to the Publication Manager, American Institute of Physics.

Advertising rates supplied on request. Orders, advertising copy, and cuts should be sent to the American Institute of Physics.

Entered as second class matter January 22, 1937, at the Post Office at Lancaster, Pennsylvania, under the Act of March 3, 1879.
Accepted for mailing at the special rate of postage provided for in the Act of February 28, 1925, authorized May 2, 1932.

Copyright 1948, by the American Institute of Physics.

Journal
of
Applied Physics

Volume 19, Number 7 July, 1948

Shipping of Radio-Isotopes*

KARL Z. MORGAN
Oak Ridge National Laboratory, Oak Ridge, Tennessee

(Received December 19, 1947)

A. GENERAL DISCUSSION OF THE PROBLEM

THE need for suitably revised regulations governing the shipment of radioactive materials has been recognized for several years. Present regulations prohibit the shipment of radioactive materials by mail[1] and specify the conditions under which 100 mc or less of radium and radon can be shipped by railway express and by air.[2] A few years before the past war the shipment of radioactive materials from Van de Graff machines and cyclotrons began, and the magnitude and number of such shipments has increased rapidly since because of the development of other high voltage accelerators and the widespread expanding use of radio-isotopes in research, medicine, and industry. It was not until the large scale production of radio-isotopes by uranium piles began and until the relaxing of security regulations since the war that it became possible to furnish fission products and pile-induced radio-isotopes on a large scale so that serious efforts were made to formulate a completely new set of shipping regulations. It was recognized that suitable regulations should be developed for radioactive shipments by air as well as by rail because many of the radioactive materials are short-lived and often the most practical and economical method of shipment is the fastest method available. Also, regulations dealing specifically with radioactive materials other than radium, polonium, radon, and thorium were badly needed. All the prewar regulations were developed with particular emphasis on the protection of photographic and x-ray films from radiation exposure during shipment. Now the large increase in frequency of radio-isotope ship-

* Dr. K. Z. Morgan, Director of Health Physics at Oak Ridge National Laboratory, gave this paper before the Conference on Radiobiology and Medicine held at Brookhaven National Laboratory on October 18, 1947.

[1] One gram of luminous paint made from pure polonium, free of other radioactive members, may be shipped by mail if properly packaged. Dials painted with pure polonium are mailable. Otherwise, the following statement of the Postmaster General describes the case. "Any radioactive material, including radium, thorium, or other radioactive substances, or any materials containing radioactive substances, such as powders containing radium or thorium, liquids containing radium emanation, radium salts, or radioactive minerals, is prohibited transmission in the mails."

[2] The regulations at present (referring to the old regulations that were superseded January 26, 1948) prohibit the shipment of more than 100 mg of radium unless special arrangements are made with the local shipping agent. A table is available (L. F. Curtiss, J. App. Phys. **12**, 346 (1941)) which gives the lead shielding thickness required for up to 600 mg of radium and for different times of transit. The radioactive shipment must be placed 15 ft. or more from x-ray film and 10 ft. or more from ordinary film. The radioactive material must be securely packaged with labels indicating the radium or "equivalent radium" content. According to Mr. R. B. Wilsey these regulations were intended to limit on the average the exposure to 11 mr to x-ray film and 25 mr to other types of film. Supplement 5 to the Railway Express Agency, Air Express Division, Tariff No. 8 (May 31, 1946) lists regulations for shipment of radio-isotopes by air.

ments and the fact that (potentially, at least) single sources can be made up rather cheaply for shipment, which produce a gamma-radiation equivalent to thousands of curies of radium, make it urgent that regulations be provided which will protect man as well as films.

During this interim period the Health Physics Divisions of the Plutonium Projects (at the University of Chicago, Hanford, Washington, and Oak Ridge, Tennessee) have set up their own more rigid and complete protective measures for the shipment of radio-isotopes. They have maintained what is considered to be safe radiation protection standards for these shipments. For example, Oak Ridge National Laboratories solves this problem by specifying the type of shipping container, by limiting the radiation in the cab of a truck to a tolerance dose per day, by limiting the radiation level at the surface of a package to 50 mr/hr. for truck and rail shipment and 15 mr/hr. for plane shipment, by forbidding contamination on the surface of a package, etc.

Ideally, perhaps, one would like to require that radio-isotopes be so packaged that no radiation escapes from or through the surface, but this criteria must be ruled out as impractical because it would make the packages cumbersome and heavy and would lead to excessive shipping expense.

Recognizing the desirability of establishing shipping regulations that were safe and suitable to all interested parties, H. A. Campbell of the Bureau of Explosives called together, on May 22, 1946, representatives from the film industry, the radium industry, the shipping industry, the Bureau of Standards, the Atomic Energy Projects, the universities and hospitals, the Air Transport Association, the National Research Council, and the National Research Council of Canada. Many exchanges of letters between these representatives during the following months led to a further understanding of what the final shipping regulations should be like.

All during this period the Committee on Radioactivity of the National Research Council (now the Committee on Nuclear Science of the NRC) had indicated an interest in this problem and on February 1, 1947, the Subcommittee on Shipment of Radioactive Materials** was called together by the chairman, R. D. Evans of M.I.T. A number of other meetings of this committee have been held and the present form of the Regulations for the Shipment of Radio-Isotopes has been arrived at after many ramifications and a healthy exchange and development of ideas, and through the assistance of the Bureau of Explosives and with the valuable advice of such men as R. C. Gibbs, G. Failla, J. E. Rose, H. M. Parker, J. J. Quinn, T. C. George, and others.

An act of Congress authorizes the Interstate Commerce Commission to formulate regulations governing the transportation of dangerous articles, and the I.C.C. is authorized to call upon the Bureau of Explosives to maintain safe transportation of explosives and other dangerous articles. It is the responsibility of the Bureau of Explosives to assist in preparing and enforcing regulations governing the transportation of dangerous articles such as radioactive materials by rail freight, rail express, and by common contract and private carriers by motor vehicle. If penalization of a shipper is necessary, the Bureau of Explosives reports the case to the I.C.C. which directs it to the proper federal authorities for prosecution. The Post Office Department is responsible for setting up its own regulations governing (or prohibiting) radioactive shipments. It is not certain at present when the Civil Aeronautics Board will publish regulations for radioactive shipments by air. For the present some of the airlines have agreed to carry shipments of radio-isotopes packaged in such a manner that the gamma-radiation does not exceed 14 mr at 30 ft. Other airlines will not accept such shipments unless the surface radiation of the package does not exceed 15 mr/hr., and unless other presently proposed regulations for rail and motor vehicle shipments are adhered to. Mr. R. D. Speas of the American Airlines and John Lawrence and Harold Crouch of the Eastman Kodak Company have been working with R. D. Evans of M.I.T. since 1943, laying the ground work for

** Members consist of R. D. Evans of M.I.T., L. F. Curtiss of the National Bureau of Standards, H. S. Youngs of Air Transport Association, R. B. Wilsey of Eastman Kodak Company, A. Morrison of National Research Council of Canada, W. G. McKenna of the Bureau of Explosives, and K. Z. Morgan of Oak Ridge National Laboratories.

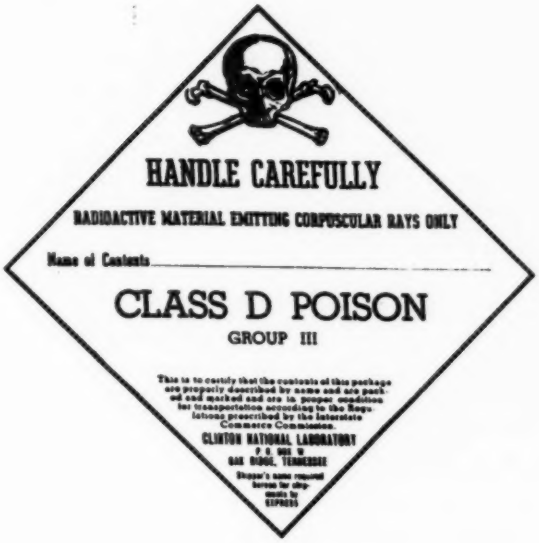

FIG. 1.

HANDLE CAREFULLY
RADIOACTIVE MATERIAL
CLASS D POISON
GROUP I or II
NO PERSON SHALL REMAIN WITHIN THREE FEET OF THIS CONTAINER UNNECESSARILY
Do Not Place Undeveloped Film Within 15 Feet of This Container.
PRINCIPAL RADIOACTIVE CONTENT
ACTIVITY OF CONTENTS
RADIATION UNITS FROM PACKAGE No.
Not more than 40 Units shall be loaded in one car or one motor vehicle or held at one location.

FIG. 2.

the regulations for shipment of radio-isotopes by air. The final draft is being completed at present by H. S. Youngs of the Air Transport Association.[3] The United States Coast Guard is responsible for the transportation of radioactive materials by water, and the regulations it establishes must not conflict with the Interstate Commerce Commission's regulations when shipments are transferred to rail or motor vehicle. It is to be hoped that if and when these three sets of regulations are adopted, there will be maintained a minimum of conflict so as to minimize confusion when shipments are transferred from air to rail or to water.

The regulations for the shipment of radioactive materials by rail and by highway have been prepared by this Shipping Committee of the National Research Council and submitted by the Bureau of Explosives to the Interstate Commerce Commission for final approval.[4] They can and should be amended from time to time when experience and further developments indicate the desirability of such changes. It would take a long time to give a complete discussion of these regulations, so they are outlined briefly below, with particular emphasis on those regulations that apply to the shipment of radio-isotopes for research use.

B. NEW REGULATIONS FOR THE SHIPMENT OF RADIO-ISOTOPES BY RAIL AND MOTOR VEHICLE

There are three groups of radioactive materials as follows:

Group I.—Radioactive materials that emit gamma-rays only or both gamma- and electrically charged corpuscular rays. The radiation from these packages must be limited to 10 units*** by the use of shileding and there must be no primary α- or β-radiation escaping from the shipping container.

Group II.—Radioactive materials that emit neutrons and either or both types of radiation characteristic of group I. In this group the radiation limits are:

1. γ-radiation of 10 units.
2. Electrically charged secondary corpuscular radiation that is the physical equivalent† of 10 units of γ-radia-

[3] This proposed Airline Tariff Rule for the Shipment of Radioactive Materials was distributed April 21, 1948 to the air carriers by Air Cargo, Inc. with the joint recommendation by the Air Transport Association of America that it be adopted. As soon as several air carriers have indicated approval, it will be submitted to the Civil Aeronautics Board as the official airlines tariff.

[4] These regulations were approved by the I.C.C. on October 24, 1947.

***1 unit = 1 mr/hr. at 1 meter for hard γ-radiation, or that amount of radiation which will have the same effect on sensitive film as 1 mr/hr. at a meter of hard γ from radium filtered through $\frac{1}{2}$ inch of lead.

† The physical equivalent of a roentgen is that amount of radiation that would be absorbed in tissue to the extent of 83 ergs per gram. It is sometimes called the "Roentgen equivalent physical" or abbreviated as "rep."

tion. None of the primary α- and β-radiation may escape from the package.

3. Neutron radiation which is physically equivalent of 2 units of gamma-radiation.
4. Combination of the above must not exceed the equivalent of paragraphs 1, 2, or 3.

Group III.—Radioactive materials that emit electrically charged corpuscular rays only, i.e., α or β, etc. None of the primary α- and β-radiation may escape from the package, and the secondary radiation must not exceed 10 mr/day at the surface of the package.

Some of the more important specific regulations are as follows:

a. If radioactive material of groups I, II, or III is liquid, it must be packaged with the use of a metal container and gaskets or with absorbent material so that none can leak to surface in case of an accident. (The former part of this rule is understood to apply also to radioactive gas.)
b. No loaded shipping container may have a γ-radiation exceeding 200 mr/hr. or equivalent at any point of the readily accessible surface.
c. The smallest permissible outside dimension of the shipping container is 4 inches.
d. All packing must be such that the degree of fogging of undeveloped film with a 24-hour exposure at 15 feet is not greater than that produced by 11.5 mr of γ from Ra filtered by $\frac{1}{2}$ inch of Pb. (The energy of such filtered Ra gamma is about 1.8 Mev.)
e. Not more than 2 curies of Ra, Po, Pu, or other members of the heavy radio active series, or more of other materials which emit greater than 10^{11} dis/sec., may be shipped in a single package.

TABLE I.

Total number of units*	Minimum distance in feet to nearest undeveloped film	Distance in feet to area that may be continuously occupied up to 8 hrs. by passengers or employees.	Distance in feet to area that may be continuously occupied over 8 hrs. by passengers or employees.
1 to 10	15	3	5
11 to 20	20	4	7
21 to 30	25	5	9
31 to 40	30	6	10

* See reference †††.

f. The package must have no significant†† surface contamination, and the shipping container must be of sturdy construction which meets certain specifications of the Bureau of Explosives.
g. Packages are exempt from these regulations provided they meet the following specifications:
   (1) There can be no leakage of radioactive material from the package.
   (2) The package does not contain more than 0.1 mc of Ra, Po, Pu, or 5×10^6 d/sec. of Sr^{89}, Sr^{90}, and Ba^{140}, or 50×10^6 d/sec. of other less harmful radio-isotopes.
   (3) There is no α, β, or neutron radiation reaching the surface of the package, and the γ-radiation is less than 10 mr/day at the surface.

   Note: Empty shipping containers must conform to item f and to the three regulations above.

   (4) The packages contain manufactured articles, other than liquids, such as clock dials that are properly packed, and the radiation at the surface of the package is less than 10 mr/day.

   Special regulations are set up for the shipment of ores. They are exempt from these regulations, provided they are of low activity and are securely packed in leak-proof containers for rail freight shipment. The gamma-radiation must not exceed 10 mr/hr. at a distance of 5 ft. from any surface of the freight car.
h. Materials that tend to remain fixed in the human body are classed as *especially hazardous*. Examples are Ra, Pu, Sr^{89}, etc. These materials must be packed in special inside

TABLE II.*

Potential (Mev)	Multiplication factor (K)	Potential (Mev)	Multiplication factor (K)
0.035	21	0.090	6
0.040	20	0.10	3.5
0.045	20	0.15	1.5
0.050	20	0.20	1.1
0.060	16	0.3	1
0.070	12	0.5	1
0.080	9	2.0	1

* The values were obtained by R. B. Wilsey of Eastman Kodak Company, and are probably the best available at present.

†† "No significant" contamination is defined as <500 d/min. measured over 100 cm² of surface for α and <0.1 mr/hr. of γ, or 0.1 mrep/hr. for β.

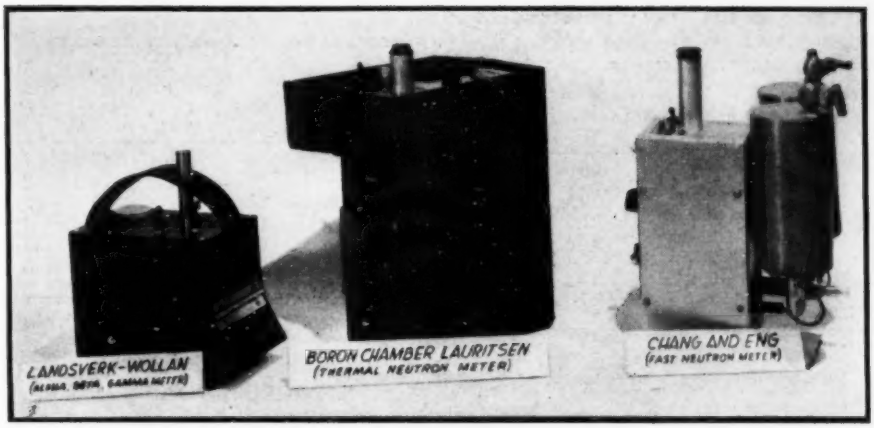

FIG. 3.

metal containers or other containers approved by the Bureau of Explosives (as required by paragraph a).

i. In case of fire, wreck, or breakage, great care should be taken to prevent radioactive materials from getting on or inside the body. The Bureau of Explosives must be notified immediately.

j. Special labels as obtainable from the Bureau of Explosives and shown in Figs. 1 and 2 must be properly filled in and placed on the outside of the package. The label in Fig. 1 is printed in red and the one in Fig. 2 is printed in blue.

k. Table I indicates the minimum distances of radioactive materials permitted to films and *persons* for shipment by motor vehicle. In case of rail shipments, column 4 in Table I is omitted and column 3 is applied to distances from the dividing partition of a combination car as well as to distances to passengers and employees. The distance in Table I must be measured from the nearest point of the radioactive container or containers. Not more than forty units††† of radioactive material (red label) shall be transported in any car or stored in a depot at one time. If for any reason a package containing radioactive material (red label) remains in the same building for a period longer than 24 hours, it must be moved to a different location after each 24 hours.

††† 1 unit = 1 milliroentgen per hour at one meter for hard gamma-radiation, or that amount of radiation which will have the same effect on film as 1 milliroentgen per hour at one meter of gamma-radiation from radium filtered through $\frac{1}{2}$ inch of lead.

Experimentally, there is no perfect instrument for making these measurements. The Landsverk-Wollan electrometer shown in Fig. 3 is the best available in that it has the necessary sensitivity, it is not very energy dependent, and it will measure α-, β-, and γ-radiation. The *unit* of radiation may be determined by making a measurement in mr/hr. at a meter from the nearest surface of the shipping box and then

$$\text{units of radiation} = K \times (\text{mr/hr. at 1 meter})$$

in which K is given approximately for gamma-radiation in Table II. The value of K is unity for neutron and beta ray shipments.

In spite of the large values of K in Table II for low energies, it is of interest to note that one need not use more than a $\frac{1}{16}$-in. sheet of lead to ship 2000 mc if the energy is less than 0.1 Mev because of the large coefficient of absorption of lead for this energy. In other words, Table II and the constant K can be ignored if one will always use a small amount of lead shielding for low energy sources.

Table III for cobalt and radium was prepared by J. H. Roberson of Oak Ridge National Laboratories from experimental data he has collected and is typical of those tables being used for the shipment of radio-isotopes. This table is for cylindrical lead containers with a cylindrical cavity having a diameter equal to the height for holding the radio-isotope. The corners of the cylinders were rounded off to reduce the weight.

The shield thickness required for beta-emitting radio-isotopes is given approximately by the

TABLE III. Wall thickness and weight of lead containers for shipment of radium and cobalt^{60}.

Wall thickness (inches)	Maximum millicures		Weight of lead container (lbs) diameter of cavity (inches)		
	Co^{60}	Ra in 0.5 mm Pt.	½	1	2
0.01	7.7	12	0.005	0.019	0.077
0.1	8.5	14	0.066	0.22	0.83
0.25	10	18	0.25	0.71	2.34
0.5	13	26	0.86	1.98	5.65
1.0	25	50	3.8	6.88	15.8
1.5	48	92	10.1	15.9	31.8
2.0	104	165	21.0	30.4	54.9

equation $X=(0.21E_m-0.065)/d$, in which X = thickness of material in inches to stop all β-rays, Em = maximum energy or β-rays in Mev, d = density relative to water (=g/cc).

This equation cannot be used for energies less than 0.3 Mev, but in this case, as with α-emitting substances, a few layers of tin foil are sufficient. In shielding large β-ray sources, low atomic number material should be used for the inner wrapper to reduce bremsstrahlen.

Neutron sources should be shielded with material containing hydrogen (and perhaps iron and boron). Paraffin and water are not very satisfactory for shields because of their liquid state. No completely satisfactory meter is available for these neutron measurements, but the double ionization chamber called Chang and Eng is best for fast neutron measurements and the boron lined electroscope is suitable for thermal neutron measurements. Figure 3 shows three instruments that might be recommended.

All the above regulations for shipment by rail apply equally as well to motor vehicles. In addition, motor vehicles carrying radioactive material must be marked with a placard reading "Dangerous—radioactive material." Also, no radioactive material may be carried on a bus when passengers are being transported unless no other practicable means of transportation is available.

TABLE IV.

Total No. of units	Minimum distance to films* (feet)			Minimum distance to humans (feet)		
	under 6 hr.	6 to 12 hr.	over 12 hr.	under 6 hr.	6 to 12 hr.	continuous exposure
Up to 2	3	5	7	1	2	3
3 to 5	5	8	10	2	3	4
6 to 10	8	10	15	3	4	6
11 to 20	10	15	20	4	6	8
21 to 30	13	18	25	5	7	9
31 to 40	15	20	30	6	8	11

* "Films" is interpreted to include mail, baggage and unidentified cargo.

C. PROPOSED REGULATIONS FOR THE SHIPMENT OF RADIO-ISOTOPES BY AIR

These proposed regulations are very similar to those given above for shipments by rail and motor vehicle. There are a few differences as follows:

a. The limits for especially hazardous materials unless packaged so they cannot spill in case of an accident are:
   1. 100 mc of Ra as a soluble salt or 300 mc when hermetically sealed in a small metallic capsul,
   2. 100 mc of Pu, Po, and similar hazardous α-emitters,
   3. Quantities of Sr^{89}, Sr^{90}, Ba^{140}, etc. that emit 4×10^9 d/sec.

b. The limit of radiation exposure to animals is 100 mrep/day.

c. No photographic film should be shipped on planes carrying plane-load cargoes of radioactive materials. In any case, the exposure to films should be limited to 11.5 mr (or equivalent) total exposure.‡

d. The gauge pressure of any gaseous shipment must not exceed 25 lbs. per square inch at 70°F.

e. A different distance table is used for air shipments and is shown in Table IV.

‡ It should be noted that no provision is made to protect film shipments that will be en route by plane, rail, or motor express for periods exceeding 24 hours. When such film shipments are to be made, special labels should be placed on the film package requesting that it not be in shipment with radioactive material.

Contributed Original Research

Irradiation of Biological Materials by High Energy Roentgen Rays and Cathode Rays

J. G. TRUMP, *Electrical Engineering Department*, AND R. J. VAN DE GRAAFF, *Physics Department*,
Massachusetts Institute of Technology, Cambridge, Massachusetts

(Received February 16, 1948)

In this work roentgen rays and cathode rays of several million-volts energy have been applied to an investigation of their biological, photo-chemical, and germicidal effects, particularly as they are related to the processing of foods and biological materials. A constant-potential electrostatic generator, together with an acceleration tube, was used to produce continuous streams of electrons with homogeneous and controllable energy. [R. J. Van de Graaff, K. T. Compton, and L. C. Van Atta, Phys. Rev. **43**, 149 (1943).] These high energy electrons were utilized both for the production of penetrating roentgen rays and for the direct irradiation of materials. The mechanism of the biological action of both roentgen rays and cathode rays is discussed, as well as the energy considerations in their application to various absorbers. The companion paper [C. G. Dunn, W. L. Campbell, H. Fram, and A. Hutchins, J. App. Phys. **19**, 605 (1948)] reports on measurements of the lethal action of these radiations on a wide variety of micro-organisms and also on the effect of the radiations on enzymes, vitamins, and certain whole food products. Both investigations have been conducted cooperatively by the Departments of Electrical Engineering and Food Technology at the Massachusetts Institute of Technology.

The systematic and quantitative study of the effects of roentgen and cathode rays on various elementary forms of living matter is regarded as an essential prelude to their possible widespread application to the preservation of foods and the sterilization of various biological materials. It was realized that the mechanisms of biological action of high energy roentgen rays and cathode rays are similar and depend closely upon the ionization energy absorbed per gram of material. The studies were begun with roentgen rays since these were immediately available and permitted quantitative measurement of the energy absorbed in the biological materials. Later, the water-cooled gold x-ray target was replaced with an aluminum cathode-ray window, and corresponding studies were begun on the direct application of high energy electrons to these materials. During the period of these biological studies the x-ray source was also used in a daily clinical program of deep cancer therapy under the medical direction of Dr. Richard Dresser and also in the investigation of the physical properties of high energy radiations. [R. Dresser, *Radiology*, in publication.]

ELECTROSTATIC SOURCE OF IONIZING RADIATIONS

THE source of high energy radiation was a pressure-insulated electrostatic generator of the belt type at the Massachusetts Institute of Technology rated at 3-million volts constant potential.[1] This generator, shown in Fig. 1, is completely contained in a steel pressure tank $4\frac{1}{2}$ feet in inside diameter and about 12 feet high, containing air at 13 atmospheres pressure.

The high voltage terminal of the generator is a stainless steel hemispherical spinning about 24 inches in diameter supported by an 88-inch high insulating column of metallic equipotential members separated by glass spacers. A single 3-ply butyl rubber cotton fabric belt 12 inches wide travels at 4000 feet per minute within the column and transfers negative electric charge continuously from ground to terminal. Although both sides may be utilized, it has been more convenient to spray charge merely on the upward run of belt. Under these conditions the continuous current available for the acceleration tube has been about 500 microamperes at full voltage.

The generated voltage may be controlled from values of a few hundred thousand volts to a maximum of about 4 million by regulating the amount of charge sprayed on the belt for a given fixed setting of the electron current in the tube. The negative voltage of the terminal is divided uniformly lengthwise the column by means of a variable corona gap between each of the separated equipotential planes.

The acceleration tube is mounted within the generator column and in a position parallel to the charge conveyor belt. The source of electrons is

[1] J. G. Trump and R. W. Cloud, Am. J. Roentgenology and Rad. Therapy **49**, 531 (1943).

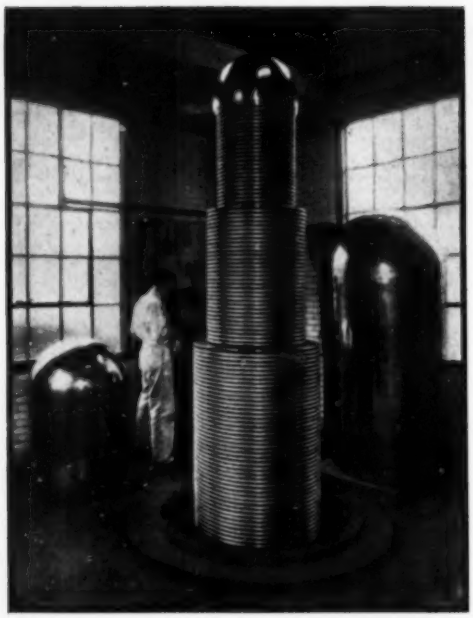

FIG. 1. 3-million volt pressure-insulated electrostatic accelerator with tank removed.

a hot tungsten filament supplied with power from a small permanent-magnet generator contained within the high voltage terminal and driven by the upper pulley. The insulating column of the tube is a rigid self-supporting structure made of alternate glass rings and flat stainless steel disks sealed together by a thermoplastic-film technique developed in this laboratory. Each disk has an axial 3-inch diameter hole and is electrically connected to the equipotential plane of the generator column at that level. The electrons are thus progressively accelerated as they pass from the filament axially downward through the planes of the diaphragms. The ground potential end of the tube extends on through the tank base into the room below and terminates in the target arrangement shown in Fig. 2. X-rays are produced when the electrons impinge on the water-cooled gold disk, which is 0.25 inch thick. The electrostatic focusing action of the tube diaphragms brings the electrons to the target in a focal spot about 10 millimeters in diameter. This may be brought to less than 0.25 millimeter by passing d.c. current through an axial magnet coil at the grounded end of the tube. By withdrawal of the gold disk from the path of the stream the electrons may be allowed to pass through the 0.002-inch aluminum window into the atmosphere as a high energy cathode-ray stream, as shown in Fig. 3. This target arrangement has permitted great flexibility in working alternately with x-rays and cathode rays since it eliminates the necessity for breaking the vacuum and thereafter reconditioning the electrode surfaces. The acceleration tube is continuously evacuated by a mercury diffusion pumping system.

In the roentgen-ray studies the biological material was placed in a thin metal or glass container located an average distance of 3 centimeters below the x-ray source. The dosage rate at this position could be adjusted to a maximum of about 5000 roentgens per second. A small special ionization chamber was mounted directly under the sample and connected to an integrating circuit to measure the total ionization dose received by the material. The total doses applied to samples ranged from 10-thousand to 2-million roentgens, a roentgen being defined as that amount of radiant energy which, when passing through 1 cubic centimeter of air at standard temperature and pressure, will release 1 electrostatic unit of charge. Figure 4 shows containers of 0.005-inch aluminum and 0.01-inch stainless steel used in this work, together with the carrier for sample and ionization chamber which could be automatically moved into or out of the beam of radiant energy.

NATURE OF THE BIOLOGICAL REACTION TO RADIATION

The photo-chemical and biological reactions produced by the absorption of x-rays and cathode rays are similar in their physical nature and require closely equivalent energies. When matter is traversed by x-rays, energy is absorbed from the x-ray photons by the photoelectric, Compton scattering, or pair-production mechanisms, and electrons are accelerated with related amounts of energy. These energetic secondary electrons excite and ionize many other atoms in their path and may thereby produce low energy tertiary electrons still capable of excitation and ionization. Chemical changes in an absorber are brought about primarily by the ionization and to a lesser extent by the excitation of the constituent atoms. These higher energy states generally favor the dissociation of complex molecules, though

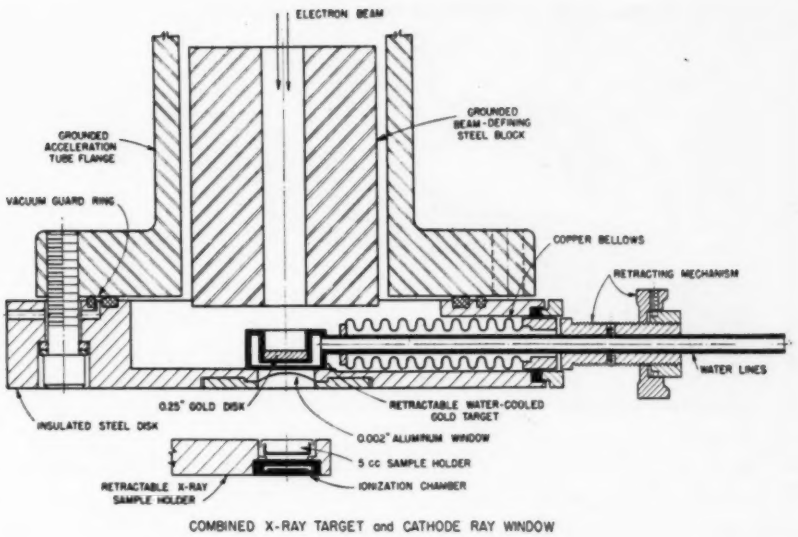

FIG. 2. Combined x-ray target and cathode-ray window.

combination is also often made possible, as in the formation of hydrogen peroxide by the irradiation of water. The ionizing energy is imparted so directly to the absorber that profound chemical changes may often be accomplished with negligible gross heating effects. In the case of living tissue, injury—and in the limit death—of a cell is the result of physiochemical changes brought about by direct absorption of ionizing energy or indirectly by the reaction of surrounding irradiated tissue. Much is now known concerning the influence of dosage rate, the linear ion density along the track of the high energy particle, and the influence of the surrounding medium on the complex response to radiation of molecules, cells, and microorganisms. Ultimately, the physiochemical and biological reactions depend on the number of ionizing electrons produced in the passage of the radiation through the material.

In cathode-ray irradiation electrons are directly projected into the material and produce ionization similar in its general characteristics to that produced by x-rays. Each high energy electron in the cathode-ray stream proceeds into the material, losing energy by collision and causing the excitation or ionization of thousands of atoms in its path. These primary electrons thus distribute the energy of the cathode-ray stream through the volume of the absorber. Many of the secondary electrons produced in these encounters may themselves possess sufficient energy to act as biological agents by the ionization of other atoms. The biological effects are produced by these excitation and ionization events.

In general the primary difference between the action of supervoltage x-rays and cathode rays on

FIG. 3. 3-million volt cathode-ray beam.

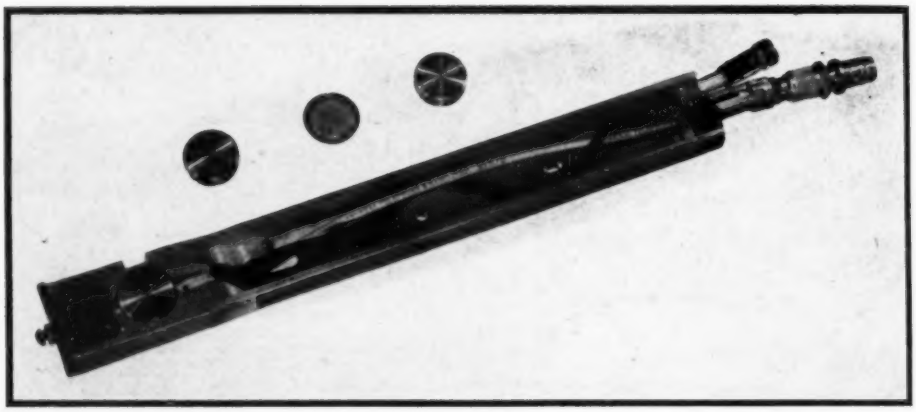

FIG. 4. Retractable carriage with ionization chamber and sample holders for x-irradiation.

living matter is in the gross distribution of the ionization energy within the absorber. Whereas cathode rays may penetrate into water a maximum distance of about 1 centimeter for each 2-million volts of energy and produce no effect beyond this maximum range, x-rays are relatively penetrating and diminish exponentially in passing through an absorber. Thus the intensity of a 2-million volt roentgen-ray beam diminishes almost one-half for each 10 centimeters of water through which it passes.[2] In the case of initially parallel cathode rays of homogeneous energy, the maximum ionization density produced in an absorber occurs at about one-third the maximum range.[3] This location of the region of maximum ionization toward the forward part of the maximum range for any given voltage is due to the naturally high scattering tendencies of electrons and would be accentuated if the cathode-ray beam were accelerated by pulsed or varying voltages. The insert of Fig. 5 compares the gross distribution of ionization produced by a beam of 3-million volt x-rays traversing water with that produced by cathode rays passing through the same material.

ENERGY ABSORBED AND TEMPERATURE RISE OF IRRADIATED MATERIAL

The amount of energy absorbed in a gram of air when 1 million roentgens of x-radiation pass through it can be measured and calculated. Irradiation of air with a dose of 1 million roentgens is equivalent to the absorption of 8.5 joules of ionizing energy per gram of the absorber.[4] Over a wide range of wave-lengths this relation between energy absorbed per gram and x-ray dose in roentgens also holds fairly closely for water which has constituents of atomic number close to those of air. Dependence upon the atomic number of the absorber becomes pronounced for radiation of less than 100 kilovolts energy because of the photoelectric absorption process and above several million volts where pair production becomes an influential absorption mechanism. For the energy region between, in which the Compton scattering process predominates, the energy absorption per gram is nearly independent of atomic number.

In another investigation[3] we have found, as might be expected, that this relation likewise holds when cathode rays are directed at an absorber. In our physical measurements close equivalence has been found between the number of ion pairs produced by the absorption of a given amount of roentgen-ray energy and the same amount of cathode-ray energy. It is therefore reasonable to expect that experimental studies of the biological and photo-chemical effects of x-rays conducted under conditions of high physical control can usually be correlated to closely corresponding effects obtained with equal amounts of cathode-ray energy.

The energy absorbed by the passage of roentgen-ray or cathode-ray energy through a material ultimately appears as heat and is manifested by a corresponding temperature rise. The temperature rise in water produced by an x-ray dose of 1 million roentgens or by the absorption

[2] D. E. Lea, *Actions of Radiations on Living Cells*, The Macmillan Company, New York, 1947).

[3] J. G. Trump, R. J. Van de Graaff, and R. W. Cloud, Am. J. Roentgenology and Rad. Therapy **43**, 728 (1940).

[4] L. H. Gray, Proc. Roy. Soc. **A156**, 578 (1936).

of 8.5 joules per gram is 2.04°C. This temperature rise is directly proportional to the x-ray dose and inversely proportional to the specific heat of the absorbing material. Since 6000 roentgens is a high cancericidal dose and 1 million roentgens is a 100 percent bactericidal dose, it is evident that pronounced biological and photo-chemical effects are realized with amounts of radiation which produce a relatively unimportant temperature rise in the absorbing material. The energy of these penetrating radiations is not expended directly in raising the average thermal energy of the molecules as in the case of heat sterilization, but is used more efficiently to induce by the process of excitation and ionization discrete changes in the atomic and molecular structure of the irradiated material.

CHARACTERISTICS OF CATHODE RAYS FOR IRRADIATION

The advantage of cathode rays over x-rays in the irradiation of living materials lies primarily in the high inherent efficiency of this process and in the controllability of the cathode-ray dosage under proper conditions. The efficiency of utilizing the electron beam energy can ordinarily be several hundred times higher in cathode-ray irradiation than when x-rays are used. In utilization of the cathode rays accelerated in a constant-potential vacuum tube, an over-all efficiency approaching 100 percent is realizable. All of the emergent cathode-ray beam energy may be directed into the absorber and expended in ionization processes within the well defined maximum electron range, which increases linearly with voltage. The efficiency and controllability of the electrostatic cathode-ray process makes possible the continuous delivery of ionization doses equivalent to millions of roentgens in a small fraction of a second.

With x-radiation, on the other hand, most of the kinetic energy of the electrons within the acceleration tube is lost as heat at the target. At 100 kilovolts only 0.2 percent of the energy of the electron stream is converted into x-radiation. At 2-million volts about 5 percent is transferred into radiant energy. Moreover, since x-rays are penetrating and proceed in all directions, only a small fraction of the x-ray energy can readily be absorbed uniformly within the desired volume of the selected absorber.[5]

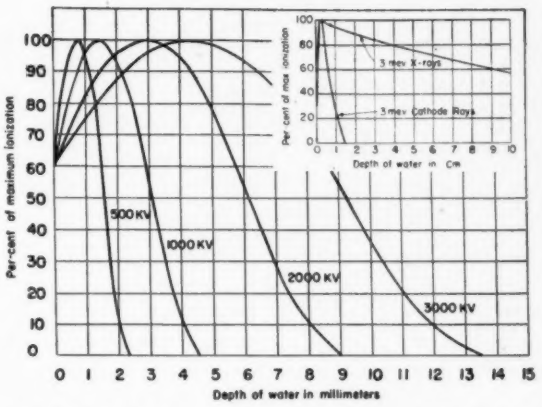

FIG. 5. Distribution of ionization in water by 0.5-, 1-, 2-, and 3-million volt cathode rays and by 3-million volt x-rays.

The cathode-ray dosage falling on an absorber can be completely specified with great exactness as it is determined by the number of impinging electrons per second and their accelerating voltage. With the constant-potential electrostatic

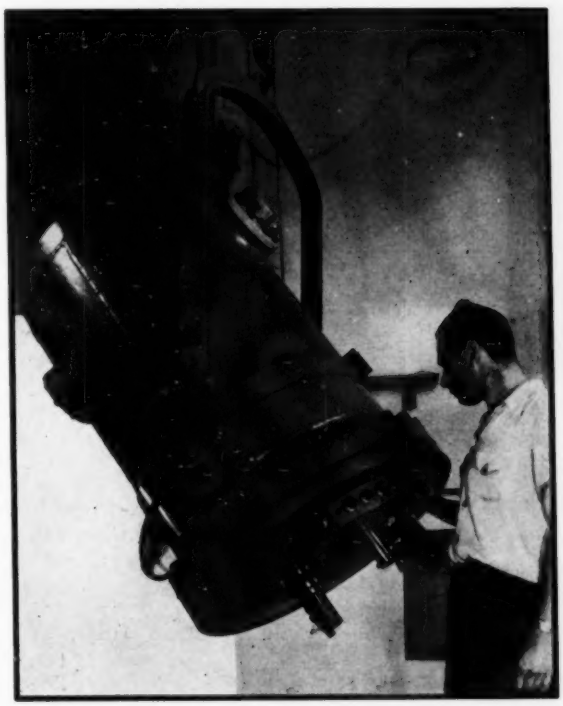

FIG. 6. Compact 2-million volt x-ray or cathode-ray source using pressure-insulated electrostatic generator.

[5] J. G. Trump, C. R. Moster, and R. W. Cloud, Am. J. Roentgenology and Rad. Therapy **57**, 703 (1947).

TABLE I.

Rate per	10^6r dose (0.85 joules/gram)	10^6r dose (8.5 joules/gram)
Second	500 grams	50 grams
Minute	30 kilograms	3 kilograms
Hour	1800 kilograms	180 kilograms
Day	43,000 kilograms	4300 kilograms
300 24-hr. days	13,000,000 kilograms	1,300,000 kilograms

accelerator the ionizing power of the incident cathode rays can be accurately determined by direct measurement of the voltage and current. Thus the ionizing power of the compact 2-million volt generator shown in Fig. 6 operating with an electron beam current of 250 microamperes is 500 joules per second, or 500 watts. Applied to the sterilization of water-equivalent materials, such a cathode-ray source can produce a sterilizing dose of 8.5 joules per gram (equivalent to 1 million roentgens) in about 50 grams of material per second. Table I gives the calculated sterilizing rate in continuous-processing applications for the cathode-ray source shown in Fig. 6 and operating with 500 watts output.

The distribution of ionization produced in water by a cathode-ray beam of 1-, 2-, and 3-million volt energy is shown in Fig. 5. For the 2-million volt electrons, for example, the maximum range in water is seen to be close to 10 millimeters, and the maximum ionization density occurs in a broad-thickness region centering at a depth of 3 millimeters. For many continuous processes a 2-million volt stream of cathode rays would be capable of irradiating effectively a stream thickness of about 6 millimeters. Two such cathode-ray sources irradiating from opposite sides would deliver a fairly uniform dose to approximately twice this thickness. Correspondingly higher voltages would be required for the irradiation of greater thicknesses, and allowance must be made for absorption by an intervening wall materials.

When the cathode-ray beam emerges into the atmosphere from the acceleration tube, some divergence of the beam results from the normal scattering by the window diaphragm. Hence the area which is irradiated by the beam increases with distance from the cathode-ray window. The cathode-ray stream may also be magnetically diverged. Thus the depth of penetration of cathode rays is determined by the voltage and the density of the absorbing material, while the area which is irradiated can be controlled by selection of window-absorber distances, by magnetic deflection, and by suitable scattering arrangements.

CONCLUSION

High energy cathode rays and x-rays now offer a new and effective means of producing biological, bactericidal, and even chemical changes on a practical scale. These changes are brought about by excitation and ionization of constituent atoms of the absorber and need relatively small amounts of ionizing energy. Cathode rays produce similar reactions and can be utilized with several hundred times the efficiency of x-rays. The temperature rise evoked by cancericidal doses of these radiations is about 0.01°C, while complete sterilization of bacteria can be accomplished with ionization doses resulting in a 2°C rise. The constant-potential output of electrostatic accelerators is well suited to quantitative radiation studies and to large-scale sterilization and inactivation processes.

ACKNOWLEDGMENTS

The authors wish to acknowledge the able assistance of R. W. Cloud and A. M. Clarke of the High Voltage Research Laboratory and of Professor W. L. Campbell and Professor C. G. Dunn of the Department of Food Technology. Appreciation is also expressed to the Godfrey M. Hyams Trust, whose generous grants have made possible the construction and improvement of the supervoltage radiation source for medical purposes. This work was supported in part by the Office of Naval Research.

Biological and Photo-Chemical Effects of High Energy, Electrostatically Produced Roentgen Rays and Cathode Rays

CECIL G. DUNN, WILLIAM L. CAMPBELL, HARVEY FRAM, AND ARDELIA HUTCHINS
Department of Food Technology, Massachusetts Institute of Technology, Cambridge, Massachusetts
(Received February 16, 1948)

INTRODUCTION

IN a companion article by Trump and Van de Graaff the physical characteristics of electrostatic accelerators for the production of high energy roentgen rays and electrons are discussed, together with factors influencing their application to the irradiation of biological materials. The principal portion of the research reported herein is concerned with the lethal action of x-rays produced at high voltages on pure cultures of microorganisms and those found in spices, apple juice, milk, soil, water, and catgut sutures. Some preliminary data on cathode rays are included.

MICROBIOLOGICAL INVESTIGATIONS WITH X-RAYS

Literature

A number of scientists have studied the lethal and sublethal effects of x-rays (particularly those produced at low or comparatively low voltages) on microorganisms. References to some of the more important of these papers are given at the end of this report.

Proctor, Van de Graaff, and Fram (1942) carried out research concerning the action of x-rays produced at high voltage on finely ground beef and observed that the bacterial counts were considerably reduced as a result of the irradiation. The present research was suggested as a result of these findings.

Microorganisms Used

Of microorganisms investigated to date the main emphasis has been on bacteria. Those examined consisted of food spoilage, heat-resistant, Gram-positive, Gram-negative, spore forming, non-spore forming, and pathogenic organisms. The yeasts included both active and dormant cultures; the molds, two of the more commonly occurring species.

The microorganisms used were obtained from the stock collection of the Department of Food Technology, M.I.T.; the American Can Company; and the National Canners' Association.

Procedure

The lethal effects of high voltage x-rays on pure cultures of microorganisms were determined essentially as follows. The organism was grown in a medium (liquid or solid) and at a temperature conducive to the development of a large number of cells or spores. A uniform suspension of the organism was prepared either in a broth medium or in sterile distilled water. When necessary, the culture was shaken with sterile glass beads in order to obtain a uniform suspension. Occasionally the supernatant portion of the suspension was transferred aseptically to a second sterile tube before use. The suspension thus prepared was pipetted into the sterile glass or stainless steel containers which were used for irradiation purposes. The containers with their contents were placed successively in the x-ray field and subjected to various roentgen doses, varying from as low as 10,000 to as high as 8,000,000 roentgens. At the time of irradiation, data were recorded concerning the dosage in roentgens, the voltage in megavolts, the electron beam current in microamperes, and the exposure time in seconds or minutes. The irradiated samples were immediately plated in a solid medium suitable for the growth of the organism. The plates were incubated at temperatures favorable for the growth of the survivors and the visible colonies were counted with a Quebec Colony counter after a suitable incubation period. Details concerning some of the experimental data are presented in Table I of this report.

Suspensions containing viable bacterial spores were prepared by heating suspensions of the organisms being investigated at 80°C for 10 minutes or at the boiling temperature for five or more minutes. The suspensions thus contained the viable bacterial spores and the heat-destroyed vegetative cells and weaker spores.

The spices examined were purchased on the open market. One-gram samples were used for irradiation purposes. Control and irradiated samples of the spices were shaken with sterile distilled water in wide-mouth glass bottles containing sterile glass beads and dilutions prepared therefrom. Aliquot portions of various dilutions were plated in duplicate in Bacto nutrient agar and incubated at 30°C for three to six days before final observations were made.

TABLE I. Some experimental data.

Culture	Source of culture	Medium in which grown	Temperature at which grown, °C	Age of culture (in days)[f]	Composition of irradiation container	Medium in which bacteria suspended for irradiation	Plating medium	Incubation temperature °C	Incubation period (in days)
Aerobacter aerogenes	Stock collection[a]	Bacto nutrient broth	37	1	Glass	Nutrient broth	Bacto nutrient agar	37	1
Escherichia coli	Stock collection	Bacto nutrient broth	37	1	Glass	Nutrient broth	Bacto nutrient agar	37	1
Pseudomonas aeruginosa	Stock collection	Bacto nutrient broth	37	2[b] 3	Stainless steel	Nutrient broth	Bacto nutrient agar	37	2
Pseudomonas fluorescens	Stock collection	Bacto nutrient broth	24–26	1[b] 3	Stainless steel	Nutrient broth	Bacto nutrient agar	24–26	3–4[d]
Serratia marcescens	Stock collection	Bacto nutrient agar	30	2	Stainless steel	Nutrient broth	Bacto nutrient agar	26	2
Sarcina flava	Stock collection	Bacto nutrient broth	30	1[b] 2	Stainless steel	Nutrient broth	Bacto nutrient agar	30	4.5
Staphylococcus aureus	Stock collection	Bacto nutrient broth	37	1	Glass	Nutrient broth	Bacto nutrient agar	37	1
Bacillus mesentericus, strain	Manioca sirup	Bacto nutrient broth			Stainless steel	Nutrient broth	Bacto nutrient agar	26	3
B. sterothermophilus	American Can Company	Dextrose tryptone broth	55	1	Stainless steel	Dextrose tryptone broth	Bacto dextrose tryptone agar	55	2
B. thermoacidurans (No. 43-P)	National Canners Association	Special proteose peptone agar[c]	37	5[b] 7	Glass	Distilled water	Special proteose peptone agar[c]	52–54	1–4[d]
Canco 6B	American Can Company	Bacto nutrient agar	37	3[b] 5	Glass	Distilled water Nutrient broth	Bacto nutrient agar	37	2
Flat sour (No. 1518)	National Canners Association	Bacto dextrose tryptone agar	53	3 4	Glass	Distilled water	Bacto dextrose tryptone agar	53	3–4[d]
Spore former	Catgut suture	Bacto nutrient agar	37	2[e] 4	Stainless steel	Nutrient broth	Bacto nutrient agar	37	3

[a] Department of Food Technology, Massachusetts Institute of Technology.
[b] Some tests carried out using cultures of one age, some using cultures of another age.
[c] Refer to Food Research 7, 186 (1942).
[d] The incubation period varied between these limits, depending on the test.
[e] Held at room temperature for several days in addition.
[f] At time of irradiation.

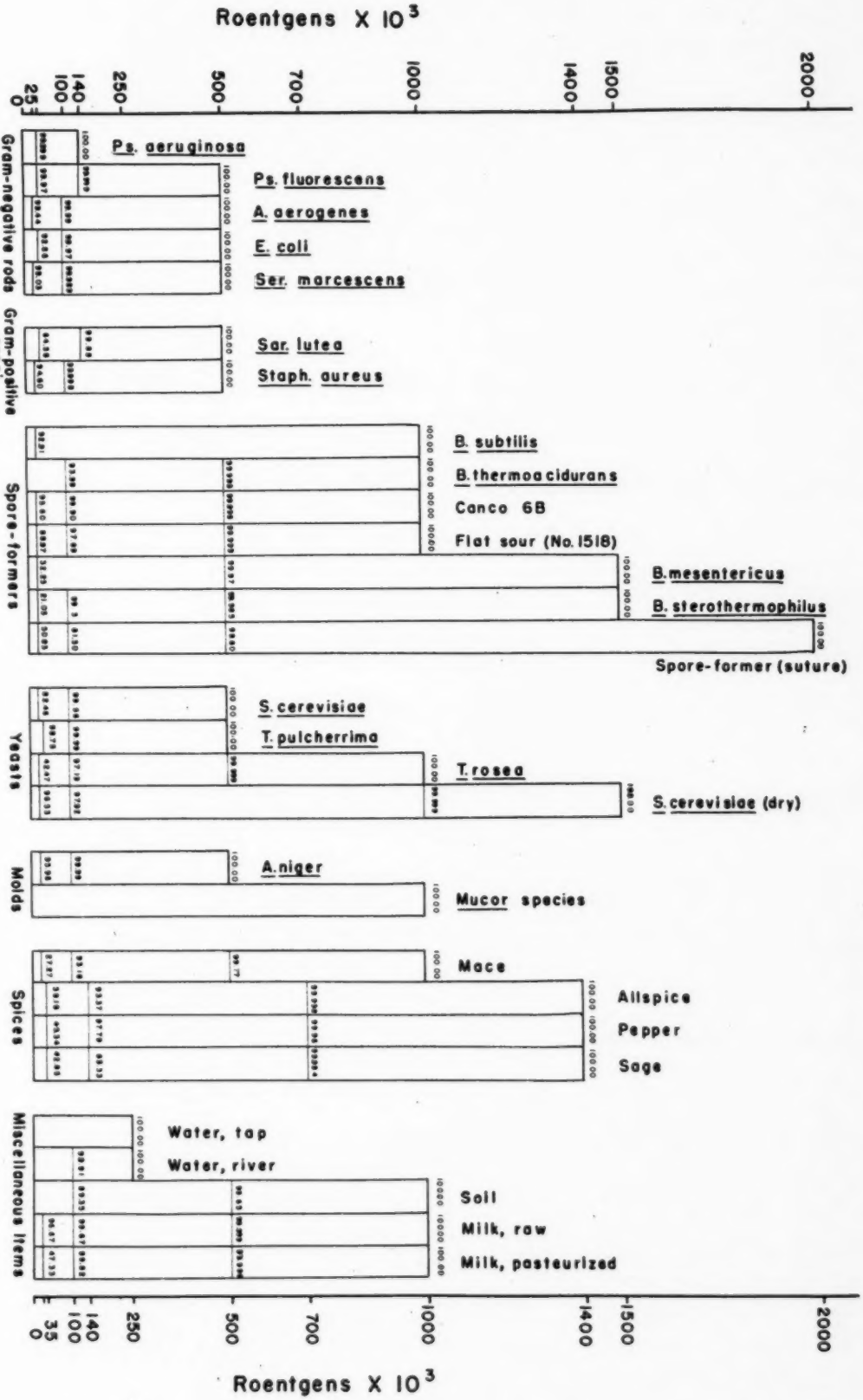

Fig. 1. Lethal effects of x-rays on microorganisms. (Roentgen doses *versus* percentages destroyed.)

TABLE II. Summary of data on lethal

Organism	Morphology	Gram reaction	Relation to oxygen	Sporulation	Pathogenicity	Number of organisms per ml	Percentage destroyed by 25,000 roentgens	Percentage destroyed by 35,000 roentgens
Aerobacter aerogenes	Rods	Negative	Aerobic, facultative	None	None	238,000,000	99.44	——
Escherichia coli	Rods	Negative	Aerobic, facultative	None	None	700,000,000	——	92.86+
Pseudomonas aeruginosa	Rods	Negative	Aerobic, facultative	None	Pathogenic to some small animals	760,000,000	——	99.999+
						400,000,000	——	99.999+
Pseudomonas fluorescens	Rods	Negative	Aerobic	None	None	2,090,000,000	——	99.97
						337,000,000	99.999+	——
Serratia marcescens	Rods	Negative	Aerobic facultative	None	None	990,000,000	99.39	——
						380,000,000	98.68	——
Sarcina flava	Cocci	Positive	Aerobic	None	None	2,400,000	——	64.58
Staphylococcus aureus	Cocci	Positive	Aerobic facultative	None	Pathogenic	1,000,000,000	94.60+	——
Bacillus mesentericus, strain	Rods	Positive	Aerobic facultative	Spores	None	6,200,000[a]	32.25	——
Bacillus sterothermophilus	Rods	Negative	Aerobic facultative	Spores	None	65,000,000	15.4	——
						75,000,000	26.7	——
Bacillus subtilis	Rods	Positive	Aerobic facultative	Spores	None	4,800,000[b]	92.91	——
Bacillus thermoacidurans	Rods	Positive	Aerobic facultative	Spores	None	240,000,000[b]	——	——
						44,500,000[c]	——	——
Canco No. 6B	Rods	Positive	Aerobic, facultative	Spores	None	400,000,000[b]	——	——
						420,000,000[b]	95.60	——
Flat sour (No. 1518)	Rods	Positive	Aerobic, facultative	Spores	None	2,200[b]	81.8	——
						1,100,000[b]	96.15	——
Spore former from catgut suture	Rods	Positive	Aerobic, facultative	Spores	None	22,000,000[b]	46.4	——
						13,000,000[b]	55.3	——

[a] The sample contained 40.32 percent of spores.
[b] A mixture of spores and vegetative cells.

effects of x-rays on selected bacteria.

Percentage destroyed by 100,000 roentgens	Percentage destroyed by 140,000 roentgens	Percentage destroyed by 500,000 roentgens	Percentage destroyed by 700,000 roentgens	Number of roentgens required for destruction	Age of culture	Special comments
99.99	——	100.00	100.00	Less than 250,000 but more than 100,000	1 day	
99.97+	——	100.00	100.00	Less than 150,000 but more than 90,000	1 day	Of sanitary significance
——	100.00	100.00	100.00	Less than 140,000 but more than 35,000	2 days	Produces Fluorescence
——	100.00	100.00	100.00	Less than 140,000 but more than 35,000	3 days	
——	99.999+	——	100.00	Less than 350,000 but more than 140,000	1 day	Produces Fluorescence
100.00	——	100.00	100.00	Less than 100,000 but more than 25,000	3 days	
99.98+	——	99.999+[d]	——	——	2 days	Produces red pigment
99.999+	——	100.00	100.00	Less than 500,000 but more than 250,000	1 day	
——	99.88+	——	100.00	Less than 350,000 but more than 140,000	2 days	Produces yellow pigment
99.998	——	100.00	100.00	Less than 250,000 but more than 100,000	1 day	Produces orange pigment
——	——	99.97	——	Less than 1,500,000 but more than 1,000,000	——	Strain especially resistant to heat; isolated from manioca starch
99.0	——	99.99	——	Not destroyed by 1,000,000		
99.6	——	99.98	——	Destroyed by 1,500,000 but not by 1,000,000		
——	——	——	——	Less than 1,000,000	1 day	
95.41	——	99.997+	——	Less than 1,000,000 but more than 500,000	7 days	Produces flat-sour spoilage of tomato juice
92.58	——	99.999+	——	Less than 1,000,000 but more than 500,000	7 days	
98.1	——	99.996	——	Not destroyed by 500,000	3 days	Causes spoilage of canned foods
99.90	——	99.999+	——	Less than 1,000,000 but more than 500,000	5 days	Source—American Can Company
95.41	——	100.00	100.00	Less than 500,000 but more than 250,000	4 days	Causes flat sour spoilage
99.97	——	99.999+	——	Less than 1,000,000 but more than 500,000	3+ days	Source—National Canners Association
71.0	——	98.0	——	Not destroyed by 1,500,000	4 days	Resistant organism isolated from catgut suture
91.6	——	99.6	——	Less than 2,000,000 but more than 1,500,000	5+ days	

[c] All spores—no viable vegetative cells.
[d] Only one organism survived. In three other tests, the organism failed to survive the application of 500,000 roentgens.

TABLE III. Summary of data concerning lethal effects of x-rays on yeasts.

Designation of yeast	Percentages of yeasts destroyed by 25,000 roentgens	100,000 roentgens	250,000 roentgens	500,000 roentgens	1,000,000 roentgens	1,500,000 roentgens	Number of roentgens required for destruction
Saccharomyces cerevisiae strain 1	85.70	99.98+	99.999+	100.00	100.00		Less than 500,000 but more than 250,000
S. cerevisiae strain 2	86.20	98.62	99.966	100.00	100.00		Less than 500,000 but more than 250,000
S. cerevisiae strain 3	58.98	99.45	99.998+	100.00	100.00		Less than 500,000 but more than 250,000
S. cerevisiae strain 4	93.75	99.82+	99.998+	100.00	100.00		Less than 500,000 but more than 250,000
S. cerevisiae strain 5	87.70	99 95	99.997	99.999+	100.00		Less than 1,000,000 but more than 500,000
S. cerevisiae (dry state) strain 4	96.53	97.92			99.999+	100.00	Less than 1,500,000 but more than 1,000,000
Torulopsis pulcherrima	98.75[a]	99.99+	99.999+	100.00	100.00		Less than 500,000 but more than 250,000
Torulopsis rosea	67.30	97.98	99.90	99.999			More than 500,000
	17.64	96.41	99.95	99.999+	100.00		Less than 1,000,000 but more than 500,000

[a] Received 28,500 roentgens.

Irradiated and control samples of raw and pasteurized milks, apple juice, soil, and waters, after appropriate dilution with sterile distilled water, were plated in Bacto nutrient agar and incubated at approximately 25°C for two to five days before making final observations.

Vials containing catgut sutures rolled on a spindle and partly submerged in liquid were subjected to irradiation by the high voltage x-rays. The tubes were dipped in alcohol and flamed following irradiation and broken at scored points. The catgut sutures were removed aseptically and placed in large culture tubes containing nutrient broth enriched by the addition of 0.5 percent sodium chloride and 0.1 percent of dextrose.

TABLE IV. Lethal effects of x-rays on Aspergillus niger.[a]

Dose in roentgens	Average percentage destruction of molds	Range of percentage destruction of molds
25,000	95.96	91.29 to 98.25
50,000	99.63	98.93 to 99.96
100,000	99.98	99.954 to 99.999
250,000	99.999	99.999 to 100.00
500,000	100.00	100.00 to 100.00

[a] The results are based on a minimum of five separate tests. The ages of the cultures irradiated varied from 2 to 28 days. The molds were grown on Bacto Sabouraud's dextrose agar and suspended in Bacto malt extract broth for irradiation.

Observations were made after incubation for one week at 37°C.

Observations and Results

Many of the observations and results concerning the lethal effects of x-rays produced at high voltage are summarized in Tables II to VI, inclusive, and in Fig. 1.

Discussion of Results

An examination of Table II reveals a number of interesting facts. The non-spore forming bacteria, both Gram-negative and Gram-positive, were destroyed by doses of less than 500,000 roentgens and from 64.5 to 99.999 percent of them were destroyed by 35,000 roentgens. *Pseudomonas aeruginosa* and *Ps. fluorescens* were particularly susceptible to the lethal action of x-rays, the former being destroyed by less than 140,000 roentgens. Bacterial spores, however, were considerably more resistant to the action of x-rays produced at high voltage than the vegetative cells and generally required more than 500,000 roentgens for destruction of all cells. The most resistant spore-former investigated required more than 1,500,000 but less than 2,000,000 roentgens for destruction. However, under the conditions of the tests, most spores were destroyed by the

TABLE V. Summary of data concerning lethal effects of x-rays on the microorganisms in some spices.

Spice	Number of organisms per gram	Percentage destroyed by 35,000 roentgens	140,000 roentgens	350,000 roentgens	700,000 roentgens	1,400,000 roentgens	Number of roentgens required for destruction
Allspice, ground	740,000	39.18	93.37	99.45	99.998	100.00	Less than 1,400,000 but more than 700,000
Pepper, white, ground	8,600	45.34	97.79	99.88	99.96	100.00	Less than 1,400,000 but more than 700,000
Sage, ground	84,000	42.85	83.33	99.70	99.994	100.00	Less than 1,400,000 but more than 700,000
		Percentage destroyed by 25,000 roentgens	100,000 roentgens	250,000 roentgens	500,000 roentgens	1,000,000 roentgens	
Mace	2,200	27.27	93.18	97.72	99.77	100.00	Less than 1,000,000 but more than 500,000

application of less than 1,000,000 roentgens and from 15 to 96 percent were destroyed by 25,000 roentgens.

The yeasts (Table III) examined appeared to be slightly more resistant on the average to x-radiation than the average non-spore forming bacteria. Destruction of all cells of four strains of *Saccharomyces cerevisiae* occurred with the application of less than 500,000 roentgens and from 58.9 to 93.7 percent of the cells of five strains of *S. cerevisiae* were destroyed by 25,000 roentgens. It required more than 500,000 but less than 1,000,000 roentgens to effect complete destruction of a strain of *S. cerevisiae* in the dry state. Two species of *Torulopsis* were destroyed by less than 1,000,000 roentgens. *T. rosea* appeared to be somewhat more resistant to x-rays than *T. pulcherrima*.

Research carried out on two species of molds indicated that considerable variation in susceptibility to x-rays may be expected amongst different species. In four out of five tests (Table IV), *A. niger* was destroyed by the application of 250,000 roentgens. Both the youngest (2 days old) and the oldest (28 days old) cultures of *A. niger* were destroyed by this dosage. In five tests carried out with a mold of a species of the genus *Mucor*, using essentially similar procedures as for *A. niger*, a dose of 1,000,000 roentgens destroyed all of the individual molds, whereas 500,000 roentgens destroyed over 99 percent of them. The species of *Mucor* was thus considerably more resistant to x-rays produced at high voltage than the strain of *A. niger* used.

The microorganisms associated with ground allspice, mace, white pepper, and sage (Table V)

TABLE VI. Summary of data concerning lethal effects of x-rays on microorganisms found in miscellaneous items.

Item	Number of organisms per ml or per gram of unirradiated sample	Percentage destroyed by 25,000 roentgens	100,000 roentgens	250,000 roentgens	500,000 roentgens	1,000,000 roentgens	Number of roentgens required for destruction
Apple juice	440,000[a]			99.47	99.96	99.999+	
Milk, raw	1,550,000	96.67	99.67	99.998	99.999+	100.00	Less than 1,000,000 but more than 500,000
Milk, pasteurized	15,000	47.33	99.82	99.98	99.986	100.00	Less than 1,000,000 but more than 500,000
Soil	8,000,000[b]		91.7	98.9	99.4	100.00	Less than 1,000,000 but more than 500,000
	14,000,000[b]		87.0	98.0	99.9	100 00	
Water, tap	146			100.00			Less than 250,000
Water, river	12,000		99.91	100.00	100.00	100.00	Less than 250,000 but more than 100,000

[a] The apple juice contained 200,000 molds per ml and 240,000 bacteria and yeasts per ml. No molds survived the application of 1,000,000 roentgens.
[b] Organisms per gram of sample.

TABLE VII. Summary of data concerning the lethal effects on some microorganisms of cathode rays produced at high voltage.

Culture	Medium in which grown[a]	Temperature at which grown, °C	Age of culture (in days)[a]	Plating medium	Number of organisms per ml[a]	Equivalent roentgen value required for destruction	Time required for destruction (in seconds)
Staphylococcus aureus	Bacto nutrient agar	37	1	Bacto nutrient agar	56,000,000	1,400,000	Less than 5
Escherichia coli	Bacto nutrient agar	37	1	Bacto nutrient agar	381,000,000	1,000,000	Less than 5
Bacillus cereus	Bacto nutrient agar	37	5	Bacto nutrient agar	28,000,000	1,900,000	Less than 20
Serratia marcescens	Bacto nutrient agar	30	1	Bacto nutrient agar	480,000,000	275,000	Less than 6
Torulopsis rosea	Bacto malt extract agar	30	1	Bacto malt extract agar	7,800,000	610,000	Less than 29
Saccharomyces cerevisiae	Malt extract broth	30	1	Bacto Wort agar	19,700,000	[b]	[c]
Aspergillus niger	Sabouraud's dextrose agar	30		Bacto Sabouraud's dextrose agar	52,000	52,000	Less than 3

[a] Prior to irradiation.
[b] Survived equivalent of 180,000 roentgens, the largest dose used.
[c] Maximum period used was 5 seconds.

were destroyed by doses of less than 1,400,000 roentgens, but in all cases there were survivors after the application of 500,000 roentgens. From 27 to 45 percent of the organisms were destroyed by 35,000 roentgens, which indicates that destruction was less rapid during the initial stages than when pure cultures of microorganisms were irradiated.

Preliminary tests carried out with raw and pasteurized milks, soil, and waters (Table VI) indicate that sterilization may be accomplished by doses of less than 1,000,000 roentgens. It required less than 250,000 roentgens to destroy the organisms associated with the tap and river waters. Apple juice was not rendered sterile by the use of 1,000,000 roentgens, although over 99.999 percent of the microorganisms were destroyed by this dosage (based on one experiment only).

BIOCHEMICAL INVESTIGATIONS WITH X-RAYS

A limited number of preliminary tests have been carried out to determine the effects of x-rays produced at high voltages on fats, vitamins, and enzymes.

Fats

Butter and olive oil were subjected to roentgen doses varying from 0 to 1,000,000 roentgens and their peroxide oxygen values determined by the method described by Lea.[35] There were slight increases in the peroxide oxygen values (ml 0.002*N* thiosulphate per g of fat) for both the butter and olive oil. The rate of increase did not appear to be linear. It was observed that the orange yellow color of the butter was progressively destroyed with increased radiation.

Vitamins

Preliminary tests were carried out to determine the effect of x-rays produced at high voltage on ascorbic acid in pure solution and in fresh fruit juices. The ascorbic acid used was U.S.P. Reference Standard Ascorbic Acid (20 mg made up to 100 ml with 0.5 percent oxalic acid). The fruit juices were grapefruit and orange juices, freshly

expressed and strained through several layers of cotton gauze. Two-milliliter amounts were placed in each of the stainless steel dishes for irradiation. The x-ray doses were varied from 10,000 to 500,000 roentgens. Reduced and total ascorbic acids on control and irradiated samples were determined by the Indophenol Colorometric Method.[4]

The application of 500,000 roentgens resulted in rather high losses in the reduced ascorbic acid contents of the pure ascorbic acid solution and the fruit juices. However, the losses in total ascorbic acid were considerably less—23.4 and 18 percent for the ascorbic acid solution and the orange juice, respectively.

Enzymes

Preliminary tests were carried out to determine whether x-rays produced at high voltage had the ability to destroy or inactivate those enxymes in vegetables which may be inactivated by the heat process known as blanching. The tests commonly used to check the efficacy of heat blanching by steam or hot water were used as an index of the value of x-rays as a blanching agent. Tincture guaiacum (1 percent in ethyl alcohol) and tincture benzidine (1 percent in 50 percent ethyl alcohol) were used to determine the presence of peroxidase in $\frac{3}{8}$-inch slices of white potatoes, before and after irradiation. Hydrogen peroxide (1 percent) was used to accelerate the tests and to detect the presence of catalase.

The slices of potato showed positive tests for peroxidase and catalase even after the application of 8,000,000 roentgens.

Treatment of comminuted pieces of chicken liver with as high as 5,000,000 roentgens (which required 25 minutes) failed to destroy all of the catalase in the liver, although boiling for six minutes in water accomplished destruction of this enzyme.

Preliminary qualitative tests indicated that x-rays produced at high voltage destroyed or inactivated much of the amylolytic activity of the enzymes in dilute (1 to 10 percent) malt syrup preparations when applied in doses of 1,500,000 to 3,000,000 roentgens.

The actions of x-rays produced at several million volts on crude enzyme preparations appear to be in agreement with those found by other investigators when using x-rays produced at low or comparatively low voltages. Scott[56] reported that enzymes are inactivated by x-rays only after enormous doses. Dale,[11] as a result of researches with hard x-rays on crystalline carboxypeptidase and partly purified polyphenoloxidase, showed that the percentage inactivation of both enzymes was a function of its concentration for a given dose of radiation and also that the rate of inactivation of the enzyme preparation depended on its purity. Similar findings were made by Tytell and Kersten[59] while investigating the effects of soft x-rays on catalase and urease. They demonstrated that crude preparations of catalase did not show inactivation in dilute or concentrated solution after long irradiation. However, they showed that crystalline preparations were partially inactivated by large doses of soft x-rays. Forssberg[18,19] showed that catalase was extremely radioresistant *in vivo*, whereas dilute water solutions of the pure enzyme proved to be rather sensitive. Catalase appeared to be highly protected from roentgen rays when in its natural cell environment.

MICROBIOLOGICAL STUDIES WITH CATHODE RAYS

Only a limited number of tests have been carried out on the uses of cathode rays produced at high voltages. The results of a few such tests are shown in Table VII.

THE TREATMENT OF CONTINUOUSLY FLOWING RAW MILK WITH CATHODE RAYS

The effect of cathode rays produced at high voltage on raw milk continuously passing through the irradiation field was determined.

The raw milk was allowed to flow by gravity from a glass carboy reservoir through the irradiation field to a receiving glass carboy through glass tubing with rubber connectors. The carboy reservoir, located on the floor of the room directly above the irradiation room, was equipped with inlet and outlet tubes. The inlet tube, which was plugged with cotton, entered the top of the carboy through a rubber stopper. Its purpose was to allow sterilized air to enter the carboy to replace milk withdrawn. A glass outlet tube, located at the bottom of the carboy, led to the exterior of the container through a rubber stopper

to a short length of rubber tubing. A screw clamp was attached to the rubber tubing and was used to regulate the flow of milk through the field of irradiation.

Glass tubing, with an external diameter of six mm and an internal diameter of about four mm, was used as the means of conducting the milk through the field of irradiation. The area occupied by the wound portion of tubing exposed to irradiation (3.5 turns) was about four inches square. This portion of the tubing, which was to receive the irradiation, was coated with graphite to prevent damage by static effects to the glass during the irradiation.

Below the irradiation unit was another short piece of rubber tubing which served as a connection between the former and a piece of glass tubing which led through a rubber stopper to approximately the middle of the receiving glass carboy. The carboy was also provided with an air-inlet tube which allowed air to be displaced aseptically as the irradiated milk was collected.

Before initial use, both carboys and all of the tubing and connections were sterilized in a steam autoclave.

The raw milk was irradiated with cathode rays produced at 2,000,000 volts.

Bacterial counts were made on the raw and cathode ray treated samples of milk, using Bacto nutrient agar as the plating medium and incubation for 2 days at 30°C. There were 37,000,000 bacteria per ml in the raw milk and two bacteria per ml in the irradiated milk.

Cottage cheese was prepared from the raw milk and from the milk treated with cathode rays, using lactic acid "starters" obtained from a local source. Outside of the fact that the raw milk appeared to curd a little more rapidly (undoubtedly associated with the large number of viable bacteria present before inoculation with the starter), there appeared to be no important organoleptic differences between the cheeses produced from the raw and cathode ray treated milks.

CONCLUSIONS

1. X-rays produced at high voltage (approximately 3 megavolts) readily destroyed bacteria, yeasts, and molds in massive concentrations in pure culture and when associated with liquid or solid substrates such as milk, water, apple juice, ground spices, soil, and catgut sutures.

2. Spoilage types, spore formers, non-spore formers, Gram-positive and Gram-negative, pigmented and fluorescent bacteria were destroyed by high voltage x-rays. The spore formers were most resistant and the fluorescent bacteria the least resistant of the bacteria examined to date.

3. The application of 25,000 roentgens destroyed from 94 to 99.999 percent of the non-spore forming bacteria. However, it occasionally required 10 to 20 times as many roentgens to achieve complete destruction of the residual bacteria.

4. Doses of 500,000 roentgens usually destroyed all non-spore formers and 99.9 percent or more of the spore formers.

5. In only one case did a spore former survive the application of 1,500,000 roentgens. Some spore formers were destroyed by 1,000,000 roentgens.

6. The dose required to destroy bacteria with cathode rays appears to be similar to that necessary with x-rays. However, it was possible to obtain the result with cathode rays much more rapidly than with x-rays because the available output in roentgens per minute of cathode rays is much greater than when using the same equipment for x-rays. Preliminary tests indicate the possibility of sterilizing fluids by a continuous process.

7. Potatoes cannot be blanched successfully with x-rays, although preliminary investigations have shown that there is some destruction of oxidative and amylolytic enzymes, especially on prolonged radiation.

8. The peroxide oxygen values of butter and olive oil are increased slightly by x-radiation.

9. Preliminary tests indicate there is a gradual decrease in the reduced form of ascorbic acid with increasing doses of x-rays, especially when a pure solution (in oxalic acid) of the acid is irradiated. Similar trends, but at a slower rate, were shown when orange and grapefruit juices were x-radiated. However, it was indicated that most of the ascorbic acid was oxidized only to the dehydroascorbic acid stage.

ACKNOWLEDGMENT

The authors gratefully acknowledge: the helpful suggestions of Dr. Trump, Dr. Van de Graaff,

and Dr. Proctor; the technical assistance of Mr. Arthur Clarke and Mr. Robert W. Cloud; and the participation of the American Can Company, the Dow Chemical Company, Nestle's Milk Products, Inc., Pillsbury Mills, Standard Brands, and Wilson and Company.

REFERENCES

(1) E. Beltran, "Estado actual de nuestros conocimientos acera del *Plasmodium gallinaceum* Brumpt (1935)," Rev. Inst. Salub. y Enf. Trop. **2**, 95–113 (1941).

(2) B. E. Bennison and G. R. Coatney, "Inactivation of malarial parasites by x-rays," Reprint No. 2602 from Pub. Health Reports 60 (No. 5), 127–132 (1945).

(3) M. Bertrand and A. Marin, "A Study of the Effects of Long Wave X-rays on the *Staphylococcus aureus* and on the *Microsporon audouini*," Can. Med. Assoc. J. **20**, 496 (1929).

(4) A. O. Bessy, "A method for the determination of small quantities of ascorbic acid and dehydroascorbic acid in turbid solutions and colored substances in the presence of other reducing substances," J. Biol. Chem. **126**, 771–784 (1938).

(5) I. H. Blank and H. Kersten, "Inhibition of growth of *Bacillus subtilis* on modified extract agar by x-radiation of the medium." J. Bact. **20**, 21–32 (1935).

(6) M. G. Brown, J. M. Luck, G. Sheets, and C. V. Taylor, "The action of x-rays on Euplotes taylori and associated bacteria," J. Gen. Physiol. **16**, No. 3, 397–406 (1933).

(7) R. Bruynoghe and W. Mund, "L'action du radium sur les microbes," Comptes rendus Soc. Biol., Paris **92**, 211–213 (1925).

(8) G. N. Burger, "The lethal action of soft x-rays on microorganisms," Bull. Basic Sci. Res. **3**, No. 2, 71–81 (1931).

(9) G. L. Clark, "The effects of x-radiation on cell structure and growth. A general survey of radiobiology," Cold Spring Harbor Symposia Quant. Biol. **2**, 249–263 (1934).

(10) W. D. Claus, "Enhanced lethal effects of x-rays on *Bacillus coli* in the presence of inorganic salts," J. Exper. Med. **57**, 335–347 (1933).

(11) W. M. Dale, "The effect of x-rays on enzymes," Biochem. J. **34**, 1367–1373 (1940).

(12) Dall 'Acqua and De Antoni, "Vittirio, Richerche sperimentali sull' azione baltercida delle radiazione di diversa lunghezza d'ona," Radiol. med. **18**, 869 (1931).

(13) W. F. Drea, "The attenuation by x-rays of the virulence of human tubercle bacilli," Am. Rev. Tuberc. **38**, 205–228 (1938).

(14) W. F. Drea, "Attenuation of human tubercle bacilli," Am. Rev. Tuberc. **41**, 507–511 (1940).

(15) B. M. Duggar, *Biological Effects of Radiation* (McGraw-Hill Book Company, Inc., New York, 1936).

(16) P. Ellinger and E. Gruhn, "Über biologische Röntgenstrahlen Wirkung. IV. Mitteilung. Über die Verstarkung der Röntgenstrahlenwirkung durch Sekundärstrahlung," Strahlen-Therapie **38**, 58–97 (1930).

(17) E. Forfota and A. Hamori, "Ueber die Wirkung harter Röntgenstrahlen auf Typhusbazillen," Zentr. Bakt. Parasitenk., I, Orig. **139**, 163–167 (1937).

(18) A. Forssberg, "Action of x-rays on catalase and its biological significance," Archiv. For Kemi, Mineralogi o. geologi **21A**, No. 7, 1–15 (1945).

(19) A. Forssberg, "The action of roentgen rays on the enzyme catalase," Acta Radiol. **27**, No. 157–158, 281–293 (1946).

(20) A. Forssberg, "Mechanism of the action of x-rays on enzymes in water-solution," Nature **159**, 308 (1947).

(21) T. H. Grainger, Jr., "The effects of x-rays on a strain of *Eberthella Typhosa*," J. Bact. **53**, No. 2, 165–172 (1947).

(22) H. F. O. Haberland and K. Klein, "Die Wirkung der Röntgenstrahlen auf Tuberkelbazillen (Typ. humanus, 'Chelonin,' Friedmann-Stamm), Munch. med. Wochschr. **68**, 1049–1050 (1921).

(23) S. Haberman and L. D. Ellsworth, "Lethal and dissociative effects of x-rays on bacteria," J. Bact. **40**, 483–503 (1940).

(24) S. Haberman, "Dissociation of staphylococci by x-rays, J. Bact. **42**, 148–149 (1941).

(25) L. Halberstaedter, "The effect of x-rays on trypanosomes," Brit. J. Radiology **11**, 267–270 (1938).

(26) L. Halberstaedter and J. Leibowitz, "Haemolysis and fixation of erythrocytes by x-rays," Biochem. J. **41**, No. 2, 235–239 (1947).

(27) G. Hevesy, "On the effect of roentgen rays on cellular division," Rev. Mod. Phys. **17**, 102–111 (1945).

(28) M. Hochberg, D. Melnick, and B. L. Oser, "Photometric determination of reduced and total ascorbic acid," Ind. Eng. Chem. Anal. Ed. **15**, 182–188 (1943).

(29) F. Holweck, "Production de rayons X monochromatiques de grande longueur d'onde. Action quantique sur les microbes," Comptes rendus Acad. Sci. **188**, 197–199 (1929).

(30) F. Holweck, Étude energétique de l'action biologique de diverses radiations," Comptes rendus Acad. Sci. **190**, 527–529 (1930).

(31) H. Klövekorn, "Die Einwirkung der Röntgenstrahlen auf Bacterien," Strahlentherapie **20**, 354–477 (1925).

(32) A. Lacassagne, "Action des rayons X de grande longueur d'onde sur les microbes. Établissement de statistiques précises de la mortalité des bactéries irradiées," Comptes rendus Acad. Sci. **188**, 200–202 (1929).

(33) A. Lacassagne, "Difference de l'action biologique provoquée dans les levures par diverses radiations," Comptes rendus Acad. Sci. **190**, 524–526 (1930).

(34) L. Lange and M. Fraenkel, "Die Wirkung von Rönt-

genstrahlen auf Tuberkelbacillen," Klin. Wochschr. **2**, 1161–1162 (1923).

(35) C. H. Lea, "Rancidity in edible fats," Dept. Sci. and Ind. Res., Food Investigation, Special Report No. 46, His Majesty's Stationery Office, London, 1938.

(36) D. E. Lea, "The action of radiations on viruses and bacteria," Brit. Med. Bull., Radiobiology: Exper. and App. **4** (No. 1), 24–26 (1946).

(37) D. E. Lea, *Actions of radiations on living cells* (The Macmillan Company, New York, 1947).

(38) D. E. Lea and R. B. Haines, "The bactericidal action of ultraviolet light," J. Hyg., Camb. **40**, 162–171 (1940).

(39) D. E. Lea, R. B. Haines, and E. Bretscher, "The bactericidal action of x-rays, neutrons and radioactive radiations," J. Hyg., Camb. **41** (No. 4), 1–16 (1941).

(40) D. E. Lea, R. B. Haines, and C. A. Coulson, "Mechanism of the bactericidal action of radioactive radiations," Proc. Roy. Soc. **B120**, 47–76 (1936).

(41) D. E. Lea, R. B. Haines, and C. A. Coulson, "The action of radiations on bacteria," Proc. Roy. Soc. **B123**, 1–21 (1937).

(42) B. S. Levin and I. Lominski, "Action des rayons X mous sur les microbes," Comptes rendus Acad. Sci., Paris **200**, 863–865 (1935).

(43) K. P. Lorenz and P. S. Henshaw, "Radiobiologic action and the killing effects of x-rays on *Achromobacter fischeri*," Radiology **36**, 471–481 (1941).

(44) S. Luria, "Action des radiations sur le Bacterium coli," Comptes rendus Acad. Sci. **209**, 604–606 (1939).

(45) S. E. Luria and F. M. Exner, "The inactivation of bacteriophages by x-rays—Influence of the medium," Proc. Nat. Acad. Sci. **27**, 370–375 (1941).

(46) E. C. McCulloch, *Disinfection and Sterilization* (Lea and Febiger, Philadelphia, 1945), 2d Ed.

(47) E. McDonald, "Annual report of the Biochemical Research Foundation of the Franklin Institute (1945)," J. Franklin Inst. **241** (No. 1), 23–29 (1946).

(48) E. McDonald, "Progress of the Biochemical Research Foundation (1946)," J. Franklin Inst. **242** (No. 6), 435–448 (1946).

(49) F. Minch, "Zur Frage über die Einwirkung der Röntgenschen Strahlen auf Bakterien und ihre eventuelle therapeutische Verwendbarkeit," Münch. med. Wochschr. **5**, 101–102 (1896).

(50) W. E. Pauli and E. Sulger, "Über die baktericide Wirkung der Röntgenstrahlen," Strahlentherapie **32**, 761–768 (1929).

(51) J. R. Porter, *Bacterial Chemistry and Physiology* (John Wiley & Sons, Inc., New York, 1946).

(52) B. E. Proctor and H. Fram, "Effect of x-ray irradiation on the bacterial count of ground meat," Research Reports on Quartermaster Contract Projects from July 1, 1942, to June 30, 1943, by the Food Technology Laboratories, Massachusetts Institute of Technology, p. 217.

(53) A. T. Pugsley, T. H. Oddie, and C. E. Eddy, "The action of x-rays on certain bacteria," Proc. Roy. Soc. **B118**, 276–298 (1935).

(54) W. Schepmann and H. Flecke, "Über die Einwirkung 'überweicher' Röntgenstrahlen auf Bakterien," Klin. Wochschr. **5**, 1608–1611 (1926).

(55) E. Schneider, "Worauf Beruht die geringe biologische Wirkung der Röntgenstrahlen auf einzellize Lebewesen," Klin. Wochschr. **5**, 97–99 (1926).

(56) C. M. Scott, "Some quantitative aspects of the biological action of x- and γ-rays," Great Britain Med. Res. Council, Special Report Series, No. 223, 99 (1937).

(57) R. M. Stern, C. P. Hegarty, and O. B. Williams, "Detection of *Bacillus thermoacidurans* (Berry) in tomato juice, and successful cultivation of the organism in the laboratory," Food Res. **7**, 186–191 (1942).

(58) C. V. Taylor, J. O. Thomas, and M. G. Brown, "Studies on protozoa, IV: Lethal effects of the x-radiation of a sterile culture medium for *Colpidium campylum*," Physiol. Zool. **6** (No. 4), 467–492 (1933).

(59) A. A. Tytell and H. Kersten, "Effects of soft x-rays on urease and catalase," Proc. Soc. Exper. Biol. and Med. **48**, 521–525 (1941).

(60) R. W. G. Wyckoff, "The killing of certain bacteria by x-rays," J. Exper. Med. **52**, 435–446 (1930).

(61) R. W. G. Wyckoff, "The killing of colon bacilli by x-rays of different wave lengths," J. Exper. Med. **52**, 769–780 (1930).

(62) R. W. G. Wyckoff and B. J. Luyet, "The effects of x-rays, cathode rays, and ultra-violet rays on yeast," Radiology **17**, 1171–1175 (1931).

(63) R. W. G. Wyckoff and T. M. Rivers, "The effect of cathode rays upon certain bacteria," J. Exper. Med. (N. Y.) **51**, 921–932 (1930).

(64) H. Zain and A. Wolf, "Einfluss der Röntgen-Strahlen auf die Entwicklung der Endothelstadien der Vogelmalaria (Plasmodium gallinaceum)," Dtsch. Tropenmed. Z. **47**, 68–71 (1943).

(65) H. Zeller, "Wirkung von Arzneimitteln und Strahlen auf Hefe. II. Mitteilung: Nachweis der Wirkung von Röntgenstrahlen auf Substanzen durch Hefe," Biochem. Zeits. **172**, 105–125 (1926).

(66) R. E. Zirkle, "The radiobiological importance of the energy distribution along ionization tracks," J. Cell. and Comp. Physiol. **16**, No. 2, 221–235 (1940).

The Analysis of Retarded Control Systems

LOUIS A. PIPES
Department of Engineering, University of California, Los Angeles, California
(Received November 17, 1947)

This paper presents a mathematical discussion of retarded control systems. The analysis presented is applicable to general control systems and is based on the solution of a linear differential equation of infinite order. The mathematical investigation is performed by operational methods, and the question of stability is studied by the use of the complex variable.

INTRODUCTION

THE development of modern electronic apparatus has increased the range of application of control devices to industrial processes and military equipment. The mathematical analysis of control problems has received considerable attention in the last few years.[1–4] It has been found that the methods of electrical circuit synthesis and analysis are very useful in the design and the study of stability of linear control systems.[4, 5]

In the general literature of control systems[6–8] the effect of the retarded action of the controller is discussed. A critical analysis of the effect of time lag in control systems reveals the fact that erroneous conclusions may sometimes be reached if the problem is not analyzed from a rigorous mathematical point of view.

It is the purpose of this discussion to analyze the effects of time lags in simple control systems by the use of the modern operational or Laplacian transform theory that is now used so extensively in electrical circuit analysis and synthesis.[9, 10] The analysis is extended to a discussion of some simple non-linear servomechanisms.

I. FUNDAMENTAL EQUATION OF SIMPLE CONTROLLED SYSTEMS

In the usual control problem, a certain quantity, $\phi(t)$, a function of the time t, is a measure of the departure of the system from a preselected state which may be designated as $\phi=0$. The quantity that $\phi(t)$ denotes varies in various types of control problems.

For example, the function $\phi(t)$ may represent the following typical quantities:

$\phi(t)$ = the angular deviation of a ship or an airplane from its predetermined value which the control system is supposed to maintain, or

$\phi(t)$ = the deviation of the angular velocity of an engine from a certain desired angular velocity.

$\phi(t)$ = the deviation of pressure or temperature from a predetermined value in a pressure or thermal control system.

In general, most control systems deal with motions of a system in the vicinity of an equilibrium position. The stability and general behavior of such systems may be studied by the application of the principles of the theory of small oscillations. This method of analysis leads to linear differential equations with constant coefficients. The justification of such a procedure is based on the fact that if the small oscillation analysis shows that the small deviation from the

[1] H. L. Hazen, "Theory of servomechanisms," J. Frank. Inst. **218**, No. 3, 279–331, 534–580 (1934).
[2] N. Minorsky, "Directional stability of automatically steered bodies," J. Am. Soc. Naval Eng. **34**, 280 (1922).
[3] L. A. MacColl, *Fundamental Theory of Servomechanisms* (D. Van Nostrand Company, Inc., New York, 1945), contains an excellent bibliography.
[4] A. C. Hall, *The Analysis and Synthesis of Linear Servomechanisms* (The Technology Press M. I. T., Cambridge, 1943), contains an excellent bibliography.
[5] H. W. Bode, *Network Analysis and Feedback Amplifier Design* (D. Van Nostrand Company, Inc., New York, 1945).
[6] S. D. Mitereff, "Principles underlying the rational solution of automatic control problems," Trans. A.S.M.E. **57**, 156 (1935).
[7] Callender, Hartree, and Porter, "Time lag in a control system," Phil. Trans. Roy. Soc. **235A**, 415 (1936).
[8] N. Minorsky, "Control problems," J. Frank. Inst. **232**, 451, 519 (1941).
[9] M. F. Gardner and J. L. Barnes, *Transients in Linear Systems* (John Wiley and Sons, Inc., New York, 1942), Vol. I.
[10] L. A. Pipes, *Applied Mathematics for Engineers and Physicists* (McGraw-Hill Book Company, Inc., New York, 1946).

predetermined value vanishes as time increases, then the use of this analysis is justified and stability of the system is assured.

The analysis of most dynamical systems that contain inertia terms leads, in general, to linear equations of the second order with constant coefficients. If the purpose of the system is to control temperature, pressure, degree of illumination, etc., the differential equation of the system is usually one of the first order.

It is possible, of course, that the control system may be a "coupled" system; in this case its analysis leads to a system of linear differential equations with constant coefficients. Elimination between the system of equations leads to a linear equation with constant coefficients of higher order than the second. In this paper only systems whose equations is of the second order will be considered. The analysis developed is applicable to more complicated control systems.

The analysis of most controlled dynamical systems may be based on the following equation:

$$A\ddot{\phi}(t)+B\dot{\phi}(t)+C\phi(t)=F_d(t)-F_c(t), \qquad (1.1)$$

where $\phi(t)$ = the departure of the system from the preselected state; A, B, C = constant coefficients determined by the nature of the system; $F_d(t)$ = the external "disturbing" force; $F_c(t)$ = the "control action" of the system.

II. RETARDED CONTROL ACTION

Let us consider Eq. (1.1) in the case where the external disturbing force, $F_d(t)=0$. In this case the equation reduces to

$$A\ddot{\phi}(t)+B\dot{\phi}(t)+C\phi(t)=-F_c(t). \qquad (2.1)$$

In order for the control system to be analyzed it is necessary to specify the functional form of the "control action" of the system, $F_c(t)$. From a theoretical standpoint, there are an endless number of possible specifications for $F_c(t)$. One of the simplest forms that the control action may be given is the following one:

$$F_c(t)=n_0\phi(t)+n_1\dot{\phi}(t)+n_2\ddot{\phi}(t), \qquad (2.2)$$

where n_0, n_1 and n_2 are constants. It is possible to realize this type of control practically. However, in any control system, whether electrical, mechanical, or thermal, there are always time lags in the action of the system so that the control action takes place at a retarded time.

For simplicity, let the time lag for all the three types of control terms of Eq. (2.2) be T. Then instead of the various terms in (2.2) being evaluated at the instant of time, t, they must be evaluated at a past instant, $t-T$, so that we must write:

$$F_c(t)=n_0\phi(t-T)+n_1\dot{\phi}(t-T)+n_2\ddot{\phi}(t-T). \qquad (2.3)$$

If we now substitute $F_c(t)$ into (2.1), we obtain:

$$A\ddot{\phi}(t)+B\dot{\phi}(t)+C\phi(t)+n_0\phi(t-T)+n_1\dot{\phi}(t-T)+n_2\ddot{\phi}(t-T)=0. \qquad (2.4)$$

This is the equation of the controlled system in the absence of an external disturbing function. Equation (2.4) is a mixed difference-differential equation. It may be reduced to a differential equation by the use of the following symbolic form of Taylor's expansion:[10]

$$e^{-TD}\phi(t)=\phi(t-T), \qquad (2.5)$$

where D is the derivative operator d/dt and e is the base of natural logarithms. Hence we may also write:

$$\dot{\phi}(t-T)=De^{-TD}\phi(t), \qquad (2.6)$$

and

$$\ddot{\phi}(t-T)=D^2e^{-TD}\phi(t). \qquad (2.7)$$

Substituting these expressions in (2.4), we

$$[AD^2+BD+C+n_0e^{-TD}+n_1De^{-TD}+n_2D^2e^{-TD}]\phi(t)=0. \qquad (2.8)$$

This is a linear differential equation of infinite order with constant coefficients. In the mathematical literature it is designated as a "hystero-differential" equation.[11] This equation arises in the study of dynamical systems whose behavior depends on the past history of the system and also in certain mathematical investigations in economics.[12]

The characteristic equation of the differential equation (2.8) is given by

$$(AZ^2+BZ+C)+e^{-TD}(n_2Z^2+n_1Z+n_0)=0=F(Z). \qquad (2.9)$$

[11] L. Silberstein, "On a hystero-differential equation arising in a probability problem," Phil. Mag. May 29 (1940).

[12] H. T. Davis, *The Theory of Linear Operators* (The Principia Press, 1936), Chapter VI, contains an excellent bibliography.

Stability of the system is assured if Eq. (2.9) has no roots with positive real parts. An approximate analysis of stability may be based on the expansion

$$e^{-TD}=1-TZ/1!+T^2Z^2/2!-T^3Z^3/3!+\cdots. \quad (2.10)$$

If the time lag is small, then an approximate analysis of stability can be carried out by neglecting the T^2 term in the expansion (2.10), so that Eq. (2.9) becomes

$$(AZ^2+BZ+C)+[1-(TZ/1!)] \times(n_2Z^2+n_1Z+n_0)=0, \quad (2.11)$$

or

$$-Tn_0Z^3+Z^2(n_2+A-n_1T) +Z(n_1+B-n_0T)+(C+n_0)=0. \quad (2.12)$$

This cubic equation is of the form

$$A_0Z^3+A_1Z^2+A_2Z+A_3=0. \quad (2.13)$$

The Hurwitzian criteria of stability[13] are

$$A_0>0, \quad A_1>0, \quad A_2>0, \quad A_3>0 \quad (2.14)$$

and

$$A_1A_2>A_0A_3.$$

It must be noticed that if more terms of the expansion (2.10) are taken, the Hurwitzian criteria of stability are not satisfied. This indicates the need of checking the approximate theory by exact analysis, since the results of the approximate theory are inconclusive and hence of no value.

III. OPERATIONAL ANALYSIS OF RETARDED CONTROL ACTION

The physical significance of retarded control action may be seen if Eq. (2.4) is analyzed by the modern operational or Laplace transform method.[9,10] Let us consider Eq. (2.4) that includes the effect of the retarded control action and also an external disturbing function of the "unit function" type which will be designated by the symbol $1(t)$ and defined by

$$1(t)=\begin{cases}0 \text{ for } t<0\\ 1 \text{ for } t>0\end{cases} \quad (3.1)$$

In this case, the hystero-difference equation

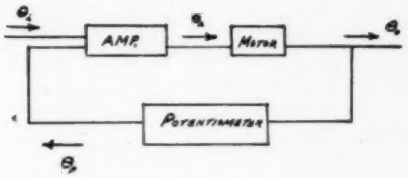

FIG. 1.

(2.4) may be written in the form

$$A\ddot{\phi}(t)+B\dot{\phi}(t)+\phi(t)+n_0\phi(t-T) +n_1\dot{\phi}(t-T)+n_2\ddot{\phi}(t-T)=1(t). \quad (3.2)$$

Following the usual method used in solving differential equations with constant coefficients by the Laplacian transformation,[9,10] we introduce the Laplace transform

$$L\phi(t)=\theta(p). \quad (3.3)$$

The system will be supposed to be at rest at $t=0$ so that $\phi(t)$ and its first derivative $\dot{\phi}(t)$ are both zero at $t=0$. We then have from the theory of the Laplacian transformation,[9,10]

$$L\dot{\phi}(t)=p\theta, \quad (3.4)$$

$$L\ddot{\phi}(t)=p^2\theta, \quad (3.5)$$

$$L\phi(t-T)=e^{-Tp}\theta, \quad (3.6)$$

$$L\dot{\phi}(t-T)=pe^{-Tp}\theta, \quad (3.7)$$

$$L\ddot{\phi}(t-T)=p^2e^{-Tp}\theta, \quad (3.8)$$

$$L1(t)=1. \quad (3.9)$$

As a consequence of these transforms, Eq. (3.2) transforms into the equation

$$(Ap^2+Bp+C)\theta+e^{-Tp}(n_2p^2+n_1p+n_0)\theta=1. \quad (3.3)$$

If we solve for θ, we have

$$\theta=\frac{1}{(Ap^2+Bp+C)+e^{-Tp}(n_2p^2+n_1p+n_0)}. \quad (3.4)$$

Now let

$$Z_0(p)=(Ap^2+Bp+C) \quad (3.5)$$

and

$$Z_1(p)=(n_2p^2+n_1p+n_0), \quad (3.6)$$

then (3.4) may be written in the form:

$$\theta=\frac{1}{Z_0(p)+e^{-Tp}Z_1(p)} =\frac{1}{Z_0(p)\{1+e^{-Tp}(Z_1/Z_0)\}}. \quad (3.7)$$

[13] A. Hurwitz, "Ueber die Bedingungen unter welchen eine Gleichung nur Wurzulen mir negativen rellen Theilen besitzt," Math. Ann. 46, 273 (1895).

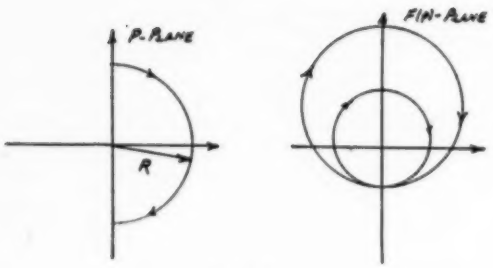

FIG. 2.

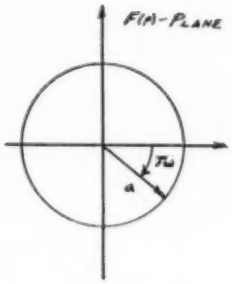

FIG. 3.

As in the usual method used in the study of wave propagation by the Laplacian transformation, we expand the term in braces in the following manner:

$$\frac{1}{\{1+e^{-Tp}(Z_1/Z_0)\}}=1-e^{-Tp}\frac{Z_1}{Z_0}+e^{-2Tp}\left(\frac{Z_1}{Z_0}\right)^2-e^{-3Tp}\left(\frac{Z_1}{Z_0}\right)^3+\cdots. \quad (3.8)$$

Hence (3.7) becomes,

$$\theta=\frac{1}{Z_0(p)}-e^{-Tp}\frac{Z_1}{Z_0^2}+e^{-2Tp}\frac{Z_1^2}{Z_0^3}-e^{-3Tp}\frac{Z_1^3}{Z_0^4}+\cdots. \quad (3.9)$$

The series may be shown to be uniformly convergent. Now, the required deviation of the system is given by

$$\phi(t)=L^{-1}\theta(p), \quad (3.10)$$

the inverse transform of $\theta(p)$. The physical significance of the various terms of Eq. (3.9) are evident. In the range of time between $0<t<T$ the inverse transform of the second term is zero, so that the first term gives the response of the system to the external disturbing force before the controller has had time to act. In the range $T<t<2T$ the controller has acted on the system, and the value of $\phi(t)$ is obtained by taking the inverse transforms of the first two terms of (3.9) since the inverse transform of the third term is zero until $t=2T$ and the controller has acted again. Each succeeding transform is of increasing complexity.

As a simple example of this method of solution, consider a system with no appreciable inertia (such as a thermal control system) so that $A=0$, and let the control action be given by

$$F_0=n_1p, \quad (3.11)$$

so that we have derivative control. In this case, the functions Z_0 and Z_1 reduce to

$$Z_0=Bp+C=B[p+(C/B)] \quad (3.12)$$

and

$$Z_1=n_1p. \quad (3.13)$$

To simplify the writing, let

$$C/B=a. \quad (3.14)$$

For this case, the general series (3.9) reduces to

$$\theta(p)=\frac{1}{B(p+a)}-e^{-Tp}\frac{n_1p}{B^2(p+a)^2}+e^{-2Tp}\frac{n_1^2p^2}{B^3(p+a)^3}-e^{-3Tp}\frac{n_1^3p^3}{B^4(p+a)^4}+\cdots. \quad (3.15)$$

$\phi(t)$ may now be calculated by calculating the individual transforms of (3.15). We thus obtain

$$\phi(t)=1/C(1-e^{-at}) \quad 0<t<T, \quad (3.16)$$

$$\phi(t)=1/C(1-e^{-at})-n_1/B^2(t-T)e^{-a(t-T)} \quad T<t<2T, \quad (3.17)$$

$$\phi(t)=1/C(1-e^{-at})-n_1/B^2(t-T)e^{-a(t-T)}+n_1^2/2B^3\{2(t-2T)e^{-a(t-2T)}-(t-2T)^2ae^{-a(t-2T)}\} \quad 2T<t<3T. \quad (3.18)$$

If the time lag, T, is large, the method of solution based on Eq. (3.9), although laborious, may be carried out as many terms as desired. In this manner the behavior of the system may be studied for as long a value of time as is required.

The usual approximate theory valid for small time lags may be based on Eq. (3.7). The function e^{-Tp} may be expanded in a power series in

the form

$$e^{-Tp}=1-Tp/1!+T^2p^2/2!-T^3p^3/3!+\cdots, \quad (3.8)$$

and as many terms retained as is desired. The characteristic equation of the system is

$$F(p)=Z_0(p)+e^{-Tp}Z_1(p)=0. \quad (3.9)$$

If its roots are known, then the inverse transform of $\theta(p)$ may be completed by the theory of residues or an application of the Heaviside expansion theorem. This procedure is, however, most laborious and does not give a closed form solution.

IV. TIME LAG IN A SIMPLE SERVOMECHANISM

As a simple application of the general theory discussed above, consider the system of Fig. 1. Let the following notation be introduced:

$\theta_i(p)$ = the Laplace transform of the input electromotive force impressed on the amplifier.

$\theta_0(p)$ = the Laplace transform of the angular displacement of the motor shaft.

$\theta_A(p)$ = the Laplace transform of the output potential of the output of the amplifier.

$\theta_p(p)$ = the Laplace transform of the output potential of the potentiometer.

In order not to obscure the analysis, and to illustrate the salient features of time lag, the amplifier will be supposed ideal, the inertia of the rotating parts of the motor will be assumed negligible, and the potentiometer action will be supposed to be ideal but will be assumed to introduce a time lag of magnitude T. As a consequence of the above assumptions, we will suppose that the component parts of the system will have the following transfer functions:

$P_A=\mu$ = the transfer function of the amplifier. (4.1)

$P_M=G/Rp$ = the transfer function of the motor, where G is a positive constant and R is a positive constant that is a measure of the friction of the rotating parts of the motor. (4.2)

$Q=k_0e^{-Tp}$ = the transfer function of the potentiometer feed-back loop where k_0 is a positive constant and T is a measure of the time lag of the feed-back loop. (4.3)

Hence the transfer function of the forward loop is given by

$$P=P_AP_M=\mu G/Rp. \quad (4.4)$$

The relation between θ_0 and θ_i is given by the usual equation

$$\theta_0=[P/(1-PQ)]\theta_i, \quad (4.5)$$

and in this case this becomes

$$\theta_0=\frac{\mu G}{Rp+\mu Gk_0e^{-Tp}}=\frac{\mu G}{Rp}\,\frac{1}{\left[1+\dfrac{\mu G}{Rp}k_0e^{-Tp}\right]}. \quad (4.6)$$

If we let

$$b=\mu G/R, \quad (4.7)$$

Eq. (4.6) may be expanded in the following series form:

$$\theta_0=\frac{b}{p}-\frac{b^2}{p^2}k_0e^{-Tp}+\frac{b^3}{p^3}k_0^2e^{-2Tp}-\frac{b^4}{p^4}k_0^3e^{-3Tp}+\cdots. \quad (4.8)$$

The angular displacement of the motor shaft, $\theta_0(t)$, is the inverse transform of θ_0 and is given by

$$\begin{aligned}&\phi_0(t)=bt \quad \text{for} \quad 0<t<T,\\ &\phi_0(t)=bt-(b^2k_0/2)(t-T)^2 \quad \text{for} \quad T<t<2T,\\ &\phi_0(t)=bt-b^2k_0/2(t-T)^2\\ &\qquad+(b^3k_0^2/6)(t-T)^3 \quad \text{for} \quad 2T<t<3T. \quad (4.9)\end{aligned}$$

As many terms may be computed as desired. This method gives a closed form solution for any value of time. An alternative method of determining the inverse transform of 0_0 depends on the determination of the roots of the characteristic equations of the system.[14] This equation may be written in the following form:

$$F(p)=p-ae^{-Tp}=0, \quad (4.10)$$

where

$$a=\mu Gk_0/R. \quad (4.10a)$$

If $T=0$, then $p=-a$ is solution of the system and $\phi_0(t)$ is given by

$$\phi_0(t)=1/k_0(1-e^{-at}). \quad (4.11)$$

In this case the angular displacement of the motor follows the unit input signal rapidly, and

[14] N. Minorsky, "Self excited oscillations in dynamical systems possessing retarded action," Trans. A.S.M.E. **64**, A65–A71 (1942).

the system is stable. An approximate analysis that given qualitative results for small values of the time lag, T, is based on approximating the exponential function e^{-Tp} by the first three terms of its Maclaurin series expansion in the form:

$$F(p)=p+a[1-Tp+(T^2p^2/2)]=0. \quad (4.12)$$

In this case the characteristic equation is

$$p^2+[2(1-aT)p/T^2a]+(2/T^2)=0. \quad (4.13)$$

To this degree of approximation it may be seen that if

$$T>1/a \quad (4.14)$$

the characteristic equation will have roots whose real parts are positive and the system will be unstable in that the effect of transient disturbances will be magnified indefinitely. If

$$T=1/a, \quad (4.15)$$

then

$$p=j(\sqrt{2}/T) \quad (4.16)$$

and the output will oscillate with an angular frequency of $\omega=\sqrt{2}/T$. A precise analysis requires an investigation of the roots of Eq. (4.10) by assuming a solution of the form

$$p=\alpha+j\omega, \quad (4.17)$$

where ω and α are real and are to be determined from Eq. (4.10). Substituting (4.17) into (4.10), we obtain

$$\tan\omega T=\omega/\alpha, \quad e^{2T\alpha}=a^2/(\alpha^2-\omega^2). \quad (4.18)$$

If we eliminate α between these two equations, we obtain

$$\exp\left[\frac{2T\omega}{\tan\omega T}\right]=\frac{1}{a^2}\frac{\omega^2}{\tan^2\omega T}+\omega^2. \quad (4.19)$$

This transcendental equation may be solved graphically for the possible values of ω if numerical values of T and a are given.

Having determined the values of ω, then the corresponding values of α may be determined by means of the equation

$$\alpha=-\omega/(\tan\omega T). \quad (4.20)$$

If the values of α and ω, and hence the zeros of $F(p)$ given by Eq. (4.10), have been determined, then the response of the system, $\phi_0(t)$, is given by[9,10]

$$\phi_0(t)=\text{residues of } (b/pF(p))e^{pt} \quad (4.21)$$

at the zeros of $F(p)$.

This procedure is extremely laborious. The wave solution of Eq. (4.9) is much simpler and has greater physical significance.

V. STABILITY ANALYSIS

If only a knowledge of the stability of the system is desired, then it is only necessary to investigate whether or not the function $F(p)$ has zeros in the positive half of the p-plane. This may be done by an application of the following well-known theorem of Cauchy.

"Given a function, $F(p)$, that is analytic except for pole singularities within a closed contour in the complex p-plane. If the point p traverses the given contour once in the clockwise direction, then the number of times that the representative point in the $F(p)$-plane encircles the origin in the clockwise sense is equal to (N_0-N_p), where N_0 is the number of zeros and N_p is the number of poles of the function $F(p)$ that are within the given contour."

A suitable contour that may be used to determine whether or not the function $F(p)$ has zeros in the positive half of the complex p-plane is shown in Fig. 2.

The radius of the circle R tends to infinity. In the case under consideration, $F(p)=p+ae^{-Tp}$. Now along the axis of imaginaries, let $p=j\omega$, and consider

$$F(j\omega)=j\omega+ae^{-Tj\omega}. \quad (5.1)$$

As ω runs from $-\infty$ to $+\infty$ the point p traverses the imaginary axis. The point 0 of the p-plane corresponds to the point a of the $F(p)$ plane; as ω increases, the plot of $ae^{-Tj\omega}$ in the $F(p)$ plane is a circle of radius a as shown in Fig. 3.

$F(j\omega)$ may be regarded as the addition of the vector $j\omega$ and the vector $ae^{-Tj\omega}$. As long as p continues to increase along the axis of imaginaries, the vector $ae^{-Tj\omega}$ revolves around the circle of Fig. 3. The plot of $F(j\omega)$ may be constructed graphically. Since limit $|F(p)|\to\infty$, the portion of the $F(p)$ plot corresponding to the infinite semicircle is of no concern. It is only necessary to plot $F(j\omega)$ for values of $0<\omega<\infty$,

since the plot for $-\infty<\omega<0$ may be obtained as the mirror image of the plot for positive frequencies. It will be seen that whether or not $F(j\omega)$ encloses the origin will depend on the relative magnitudes of a and T. If a and T are small, $F(j\omega)$ will not enclose the origin and the system will be stable. If T is large and $a\gg 1$, then the origin will be enclosed and the system will be unstable. This procedure may be applied to more complicated systems, and it is essentially an application of the familiar Nyquist criterion[5] to systems having time lag and whose characteristic equation is of the transcendental type.

In conclusion, it may be mentioned that in many control mechanisms certain component parts of the system are non-linear. However, in order to facilitate the analysis the effects of the non-linear components is regarded as introducing time lags. The more rigorous approach to problems of this type is to consider the actual non-linear differential equations of the system. This procedure has been carried out by Bugakov in a recent paper.[15]

[15] B. V. Bugakov, "The method of van der Pol and its application to non-linear control problems," J. Frank. Inst. **240**, 1 (1946).

Erratum: Response of Linear Resonant Systems to Excitation of a Frequency Varying Linearly with Time

[J. App. Phys. **19**, 242 (1948)]

GUNNAR HOK
*Wesleyan University, Middletown, Connecticut**

THE author is indebted to Mr. R. R. Bennett of the California Institute of Technology for pointing out some errors of sign in Eq. (39) in the Appendix to the above paper. Since the computations for the graphs provided a satisfactory check of the consistency of the numerical methods used, the errors have evidently crept in during the final arrangement of the subject matter for publication.

The correct form of the equation is:

$$Fr(\gamma)\cong\frac{1}{2\gamma}+j\frac{1}{4\gamma^3}-\frac{3}{8\gamma^5}-j\frac{3\cdot5}{16\gamma^7}+\frac{3\cdot5\cdot7}{32\gamma^9}+\cdots$$

$$\cong\frac{1}{2r}\cos\theta+\frac{1}{4r^3}\sin3\theta-\frac{3}{8r^5}\cos5\theta-\cdots$$

$$+j\left\{-\frac{1}{2r}\sin\theta+\frac{1}{4r^3}\cos3\theta+\frac{3}{8r^5}\sin5\theta-\cdots\right\}. \quad (39)$$

Furthermore, Eq. (35) should be replaced by the following expansion, also obtained by integration by parts:

$$e^{-\varphi}\int_{-\infty}^{t}e^{\varphi}dT$$

$$=\frac{1}{\varphi_1}+\frac{jf''(t)}{\varphi_1^3}-\frac{jf'''(t)}{\varphi_1^4}+\frac{jf^{iv}(t)-3[f''(t)]^2}{\varphi_1^5}$$

$$-\frac{jf^{v}(t)-10f'''(t)f''(t)}{\varphi_1^6}$$

$$+\frac{jf^{vi}(t)-15f^{iv}(t)f''(t)-10[f'''(t)]^2-15j[f''(t)]^3}{\varphi_1^7}$$

$$-\cdots \quad (35A)$$

where $\varphi_1=d\varphi/dt$. The asymptotic quasi steady-state solution for slow frequency modulation is obtained when all subsequent terms are negligible compared to the first one. (Compare Eq. (23).)

If $f(t)=\epsilon t^2$, $\omega_1=\omega_0$ and both members are multiplied by $je^{\frac{1}{2}}$, Eq. (35A) gives Eq. (39).

* Now at University of Michigan, Ann Arbor, Michigan.

Rising Sun Magnetrons with Large Numbers of Cavities*

A. V. Hollenberg,** N. Kroll, and S. Millman**
Columbia Radiation Laboratory, Columbia University, New York, New York
(Received February 2, 1948)

Studies of the rising sun design for magnetron oscillators have been extended to large numbers of cavity resonators. Successful operation of pulsed magnetrons having as many as 38 cavity resonators has been achieved in the 1.25-cm wave-length region. The open cavity resonators heretofore used in rising sun magnetrons were found unsuited for oscillators containing a large number of cavities. The extension to higher numbers was made possible by the use of closed-end resonators. This modification in cavity geometry produces a favorable redistribution of the spectrum of the resonant modes of the rising sun structure, thereby making possible the operation of the magnetron in the desired π-mode without disturbance from other modes. The increase in the number of cavity resonators for magnetrons should serve to facilitate the extension of present magnetron techniques to the millimeter range and to increase the radiofrequency power obtainable from magnetrons at 1 cm and at longer wave-lengths.

I. INTRODUCTION

THE rising sun magnetron[1,2] was developed in the course of a search for stable magnetron operation at wave-lengths close to 1 cm. With this design, stable operation is achieved in the desirable π-mode without the use of straps. The resulting simplification in anode block construction, together with some electrical advantages, makes this type of magnetron particularly suitable for the generation of radiation in the short wave-length end of the microwave region. The early work[1,3] was confined almost entirely to the development of magnetrons having 18 cavity resonators in the anode block, a cross section of which is shown in Fig. 1. This number was quite adequate for the design of pulsed magnetrons in the neighborhood of 1.25 cm. With the development of interest in millimeter generators, however, it was realized that a larger number of resonators would be required. This is a direct consequence of the scaling laws in magnetrons[4] which require that if a scaled copy be made of a known workable magnetron by reducing all linear dimensions by a factor K without changing the number of resonators, the wave-length decreases by the same factor while the anode voltage and anode current remain unchanged despite the reduction in cathode area by a factor K^2. This imposes severe limitations on the cathode both with regard to electron emission and to heat dissipation. A similar need for a larger number of resonators arises when one wants to design a short wave-length *CW* magnetron from a known workable pulsed magnetron at the same wave-length. It was therefore considered desirable to attempt to extend the rising sun design to anode blocks having a number of resonators appreciably greater than 18.

In the following pages we shall first describe (Section II) some of the difficulties encountered in attempts to extend the rising sun design to anode blocks having a large number of cavity resonators. This will be followed (Section III) by a discussion of the use of closed-end cavity resonators, together with an explanation of how this modification in the anode block design helps to remove some of the difficulties encountered with magnetrons using open-end resonators. In Section IV some features incident to the construction of magnetrons having as many as 38 cavities will be discussed. In Section V a comparison will be given of the performance of the various tube types studied in these experiments. In the concluding section a general discussion of the results will be presented.

II. OPEN CAVITY RESONATORS

The early work consisted principally of attempts to develop rising sun magnetrons, for

* This paper is based on work done for the OSRD under Contract OEMsr-485.
** Now at Bell Telephone Laboratories, New York, New York.
[1] S. Millman and A. T. Nordsieck, J. App. Phys. **19**, 156 (1948).
[2] N. Kroll and W. E. Lamb, Jr., J. App. Phys. **19**, 166 (1948).
[3] NDRC Div. 14, Report No. 588.
[4] J. B. Fisk, H. D. Hagstrum, and P. L. Hartman, Bell Sys. Tech. J. **25**, 202 (1946).

pulsed operation in the 1.25-cm wave-length region, having anode blocks of the same general geometry as the satisfactory 18-vane magnetron, but with a larger number of cavity resonators. While no difficulty was experienced in constructing a successful oscillator having 22 cavity resonators,[3] considerable effort was expended in developing a moderately satisfactory 26-cavity magnetron for operation in about the same voltage range ($\sim$15 kv) as the 18-cavity magnetron. It was found that the performance of the 26-vane tubes was too readily affected by small changes in the value of r_1, the ratio of the resonator depths of the two different cavities (Fig. 1), and in the value of σ, the ratio of the cathode diameter (D_c) to the anode diameter (D_a). For the low values of r_1, mode competition was observed from the $n=12$ resonance, which is next to the π-mode ($n=13$) on the short wave-length side, with a mode separation of a few percent. For high values of r_1, the competing resonances were those members of the long wave-length multiplet[1] of the rising sun spectrum for which $n \gtreqless 3$, and operation in these unwanted modes occurred at nearly the same voltage as that for the π-mode.

Attempts to design an open cavity magnetron having 38 resonators have met with complete failure. No value of r_1 could be found which would eliminate the interference from both the $n=18$ mode and from some of the long wave-length resonances. The interference was so severe as to prevent any effective operation in the π-mode.

Similar mode competition was subsequently observed in 18-cavity magnetrons, except in much milder form. The performance of these was carefully studied[3] in the range of r_1 values from 1.35 to 2.40. It was found that for values of r_1 below 1.6 interference from the $n=8$ mode becomes troublesome, while for values above 2.0 competition is observed from members of the upper multiplet. In the range of r_1 values of 1.6 to 2.0, entirely satisfactory π-mode operation can be obtained.

From the results of the experiments with open-ended cavity magnetrons, the following conclusions were arrived at:

(a) When r_1 is too small, competition from the $n=[(N/2)-1]$ mode interferes with stable π-mode operation of the magnetrons.

(b) When r_1 is too large, mode competition from members of the long wave-length multiplet having $n \gtreqless 3$ prevents satisfactory operation.

(c) The range of satisfactory values of r_1 decreases as the number of resonators is increased. For magnetrons in the voltage range under discussion, satisfactory open-cavity vane type magnetrons with $N>26$ can probably not be designed.

In order to understand the nature of the mode competition we review the general features of a typical mode spectrum for the rising sun resonant system. These have been fully discussed in preceding papers.[1,2] In Fig. 2 is reproduced a plot of the computed values of the resonant wave-lengths of the various modes as a function of r_1 for $N=18$. The long wave-length multiplet includes the resonances with mode numbers 1 to 4. The mode spectrum for a resonant system with a larger number of cavities is similar to the one shown. The long wave-length multiplet contains additional resonances close to the $N=4$ mode with mode numbers up to $N/4$ or $(N-2)/4$, depending upon whether $N/2$ is even or odd. On the short wave-length side of the π-mode ($n=N/2$) there are the resonances with mode numbers $(N/2-1)$, $(N/2-2)$, $\cdots N/4$ or $(N-2)/4$ in order of decreasing wave-length. From the known principles of magnetron electronics the fact that the operating voltages for the competing resonances nearly coincided with that for the π-mode

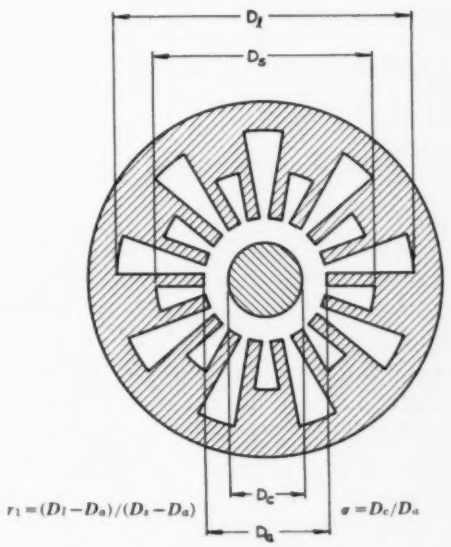

FIG. 1. Rising sun anode block and cathode.

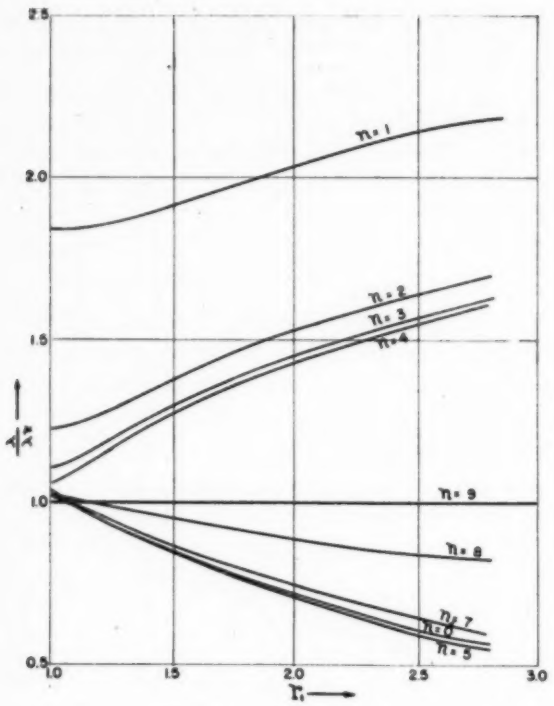

FIG. 2. Resonant wave-lengths of rising sun anode modes as a function of the ratio $r_1(N=18)$.

implied that

$$|\gamma|\lambda_n \cong \frac{N}{2}\lambda_\pi,$$

where λ_n is the wave-length of the competing resonance of mode number n, and γ is the effective mode number,*** defined by the relation

$\gamma = n + mN$ for a symmetrical anode block,

and by

$\gamma = n + m(N/2)$ for a rising sun resonant system,

with $m = 0, \pm 1 \pm 2 \cdots$.

From the measured values of λ_n and λ_π and the above relation it was apparent that the effective mode numbers for the competing long wave-length resonances did not correspond to $\gamma = n$ the fundamental, but to $\gamma = n - (N/2)$, one of the Hartree harmonics[4] of the mode number n. For the competing mode $n = [(N/2) - 1]$, however, the closeness of λ_n to λ_π makes it difficult to decide between $\gamma = n$ and $\gamma = (N - n)$ for the effective mode number of the competing resonance.

The general behavior of the spectrum as a function of r_1 leads one to conclude that competition from the $n = [(N/2) - 1]$ mode occurs when the separation between this mode and the π-mode $[n = (N/2)]$ becomes too small, while competition from members of the long wave-length multiplet occurs when its separation from the π-mode becomes too large. From the measured wave-lengths of competing modes it has been possible to show that the minimum separation permissible between the π and $[(N/2) - 1]$ modes does not change appreciably with N. On the other hand, the maximum allowable separation between the π-mode and the long wave-length multiplet decreases considerably as N increases. It is this latter circumstance which reduces the available range of r_1 as N is increased.

The decrease in maximum allowable separation between the π-mode and upper multiplet modes is readily understandable if one takes as a condition for mode free operation that the starting voltages for the members of the upper multiplet with $n \geq 3$ operating in the $[(N/2) - n]$ harmonics exceed the starting voltage of the π-mode. This leads to the condition† that $\lambda_3[(N/2) - 3] \leq (N/2)\lambda\pi$ or $\lambda_3 \leqslant \lambda\pi[N/(N-6)]$.

The above observations suggest that a modification of the resonant system which would depress the long wave-length multiplet relative to the π-mode might eliminate mode competition from the upper multiplet. Of course such a modification would elevate the starting voltages of the harmonics of the $n = 1$ and $n = 2$ modes into the neighborhood of the π-mode. Since, however, the open-end 18-resonator magnetrons had operated satisfactorily with such a distribution of starting voltages, one might hope that this would not be a source of trouble.

III. CLOSED-ENDED RESONATORS

One method of depressing the long wave-length multiplet consists of brazing cover plates to the end surfaces of the anode block, as shown in Fig. 3. The closing of the resonators depresses the

*** γ as used here has the same meaning as the symbol k in reference 4.

† This condition is somewhat stronger than necessary as the $n = 3$ mode becomes a progressively weaker competitor as N is increased. Some reasons for this will be given later.

wave-length of each mode in accordance with the approximate formula

$$\frac{1}{\lambda^2 \text{ closed}} = \frac{1}{\lambda^2 \text{ open}} + \frac{1}{(2h)^2},$$ ††

where h is the anode block height. The resultant depression of the long wave-length modes relative to the rest of the spectrum is exhibited in Fig. 4 for the case $N=18$, from which it is clear that for a given separation between the π-mode and the $n=8$ mode the separation between the π-mode and the upper multiplet resonances is considerably less for the closed-end anode blocks.

To test this idea a magnetron having 26 closed-end cavities was constructed. The anode and cathode diameters were approximately the same as the corresponding diameters in the open cavity 26-vane tube. The height of the anode block had to be increased to exceed one half-wave-length. The resonator depths were also increased so as to compensate for the wave-length shortening effects of closing the ends. It was observed that competition from the upper multiplet modes could be entirely eliminated, even in tubes with an r_1 value as large as 3.3. These encouraging results were followed up by the construction of 38-cavity closed-end magnetrons, where r_1 values as large as 2.7 were used, without any appreciable competition from the long wave-length resonant modes. The value of r_1 below which competition from the shorter wave-length $(N/2)-1$ mode begins to appear is greater for the closed-end anode blocks. Since, however, the upper multiplet moding problem is eliminated, there remains no objection to large values of r_1.

No competition has been observed from the harmonics of the $n=1$ and $n=2$ resonances even though the operating voltages for these harmonics are considerably lower than that for the π-mode and therefore are passed through in every application of the voltage pulse to the magnetron. Furthermore, the competition from the $n=3$ mode has been rather light, particularly for magnetrons with the larger number of resonators in which the operating voltage for the $[(N/2)-3]$ harmonic has been quite close to that of the π-mode. These observations imply that conditions are unfavorable for the starting of harmonics of low number modes even though the voltage satisfies the resonance condition for operation.

A partial explanation for the absence of interference from harmonics of low number modes may be derived from a study of the dependence of the tangential and radial components of the r-f electric field on the radial coordinate for the various Hartree harmonics. Approximate expressions for these are:[2]

$$E_\phi \sim \left(\frac{2r}{D_a}\right)^{|\gamma|-1} \frac{\sin\gamma\theta}{\gamma\theta} \frac{\{1-(D_c/2r)^{2|\gamma|}\}}{\{1-(D_c/D_a)^{2|\gamma|}\}},$$

$$E_r \sim \left(\frac{2r}{D_a}\right)^{|\gamma|-1} \frac{\sin\gamma\theta}{\gamma\theta} \frac{\{1+(D_c/2r)^{2|\gamma|}\}}{\{1-(D_c/D_a)^{2|\gamma|}\}},$$

where θ is half the angle subtended at the origin by the mouth of the resonant cavity. These approximations improve with increasing values of $|\gamma|$.

It may be seen from the above expressions that the field amplitude falls off rapidly as r decreases from $D_a/2$ to $D_c/2$, with the rate of decrease increasing with $|\gamma|$. Thus near the cathode surface the low $|\gamma|$ components, and in particular the fundamental, generally predominate. In considering the possibility of a given mode competing with the π-mode it seems reasonable to suppose that the chance of π-mode operation improves as $|\gamma|$ increases. For as $|\gamma|$ increases the field amplitude near the cathode becomes weaker and it becomes more difficult for the oscillation in the competing mode to build up. In the case that the

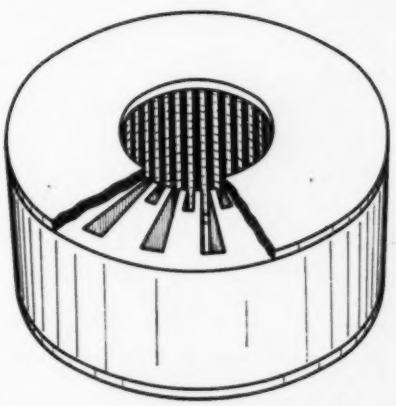

FIG. 3. Rising sun anode block with cover plates.

†† This expression is based on the assumption that the open cavity wave-length corresponds to an infinite anode height and that the brazed-on covers include the interaction space region.

competing mode is being driven by a harmonic one must further consider the effect of the fundamental component, which in general will be much stronger than the harmonic in question near the cathode. The disparity in strength will increase with increasing $|\gamma|-n$, which in the case $|\gamma|=[(N/2)-n]$ is $[(N/2)-2n]$. The main effect of the presence of the fundamental probably consists of distorting the electron orbits and thus preventing proper coupling with the harmonic and thereby improving the probability of starting in the π-mode.

According to the above considerations one would expect the lower n members of the upper multiplet to be the weaker competitors, a conclusion which is consistent with the observed non-interference from the $(n=1)$ and $(n=2)$ modes. The fact that the $n=3$ component becomes a weaker competitor as N increases is consistent with the facts that (a) the disparity between the $[(N/2)-3]$ and $N/2$ components decreases as N is increased due to the increased value of D_c/D_a which always accompanies an increase in N, and (b) the disparity between the $\gamma=3$ (fundamental) component and the $|\gamma|=(N/2)-3$ increases as N increases, which increase is only partially compensated by the increase in D_c/D_a.

The above considerations can also be applied directly to the question of the effect of the ratio D_c/D_a upon moding. It has been quite generally observed that increases in D_c/D_a always reduce competition from the long wave-length multiplet. This would follow from the fact that any such increase increases the $N/2$ component amplitude relative to that of the competing $|\gamma|$ component.

We now examine the effect produced by the closing of the resonator ends on the zero component contamination of the π-mode interaction field.[2] Within fairly wide limits this contamination has very little effect on the moding situation, but it affects the operating efficiency of the magnetron for some region of magnetic field. It is worth noticing, however, that the situation is no worse for the closed-end resonant system than for the open-end cavity magnetrons. This is illustrated in Fig. 5 in which the ratio of zero to $N/2$ component amplitudes at the anode surface is plotted as a function of λ_π/λ_8 for the same two anode blocks used in Fig. 4.

IV. CONSTRUCTION

In this section we shall review briefly some of the features of construction of the magnetrons discussed above, emphasizing some of the problems that arose in connection with an increased number of resonators. The study of the variation of the performance with the ratio of resonator depths required the construction of one or more magnetrons for each value of r_1. The effect of varying the ratio of cathode-to-anode diameters could frequently be accomplished by replacing cathodes of different diameters in the same tube. Counting each cathode replacement as leading to a new magnetron, over 90 magnetrons were built in the course of these experiments.

The construction of these magnetrons was similar to that of 18-vane, 1.25-cm rising sun

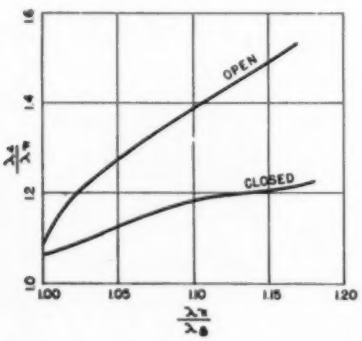

FIG. 4. Ratio of wave-length of the lowest member of the upper multiplet to that of the π-mode as a function of the ratio of the wave-length of the π-mode to that of the highest member of the lower multiplet, for open- and closed-end anodes $(N=18)$.

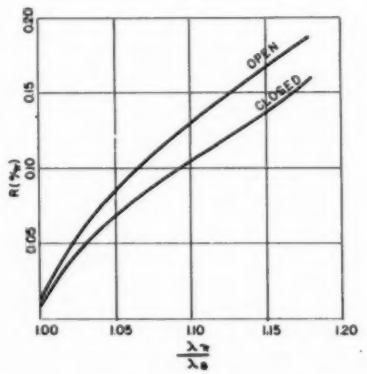

FIG. 5. Ratio of zero mode to π-mode amplitude at the anode surface as a function of the ratio of the wave-length of the π-mode to that of the highest member of the lower multiplet for open- and closed-end anodes $(N=18)$.

magnetrons which were, during the period of these experiments, in an advanced state of development in this laboratory and elsewhere.[3,4] While some of the tubes were made with radially mounted cathodes, more attention was paid to the tube design in which the cathode is mounted axially and pole pieces are built into the vacuum envelope. The latter design yields a more efficient magnetic circuit and greater accuracy in centering the cathode with respect to the anode. Both features are particularly desirable for short wavelengths. For these reasons it has seemed desirable to meet the problems which might arise in this design when the number of resonators is increased.

The essential features of a typical magnetron with inserted pole pieces and axially mounted cathode are shown in Fig. 6. The wave-guide output shown was used in all cases. Some variation in the dimensions of the output quarter-wave transformer was required in the various tube types.

In some of the closed-end anode blocks, steps were introduced at the ends of the cylindrical anode surface in order to provide adequate voltage clearance between the anode and the end hat of the cathode in scaled down versions of these designs. A sectional view of a portion of the cathode and anode block involved in this modification is shown in Fig. 7. Successful operation both with and without the step has been observed. The built-in pole pieces had cylindrical holes in the center, large enough to pass the end hats of the cathode. This design feature is used to facilitate the alignment of cathodes and their replacement. Since the end hats were only slightly smaller than the anode diameter, magnetrons with a large number of cavity resonators required large holes in the pole pieces with some resulting complications.

One consequence of the large holes in the pole pieces was an unfavorable distribution of magnetic field in the interaction space near the pole pieces, giving rise to excessive current leakage in some of the 38-vane magnetrons containing the large pole piece holes. Permendur††† cathode hats, shaped to produce uniform field throughout the interaction space, according to electrolytic

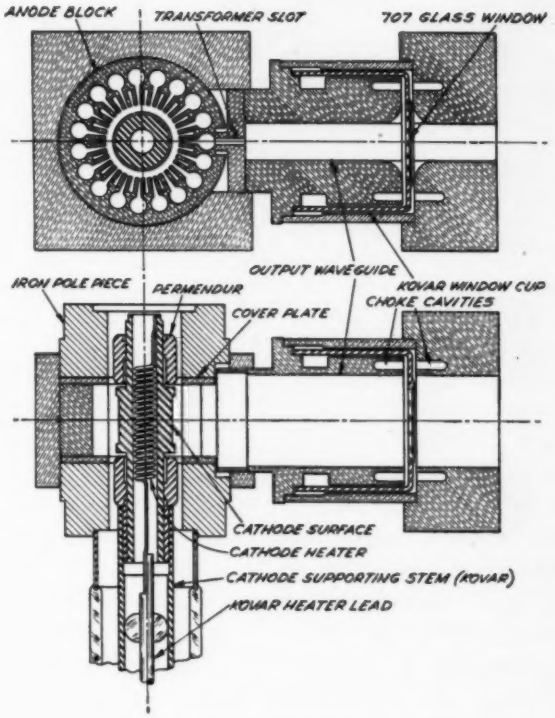

FIG. 6. Typical magnetron assembly.

bath model tests, were employed in a later design, and the current leakage was materially reduced, to an amount not appreciably more than is observed with magnetrons having no holes in the pole pieces.

Another consequence of the large pole piece hole was serious leakage of power out of the magnetron through the coaxial transmission line formed by the cathode mounting stem in this hole. A number of facts concerning the leakage have been observed, and will be listed in the next paragraph. This will be followed by the interpretation of the observed behavior and by suggestions for the elimination of the leakage without introducing any further complication in mode competition.

The most obvious manifestation of the leakage was the lighting up of a neon bulb placed near the hole in either pole piece, with an intensity in some cases comparable to that obtained by placing the bulb directly in front of the wave-guide output. A second manifestation was that abnormally low values for the unloaded Q of a leaky magnetron were obtained in "cold" measurements in which power was fed into the magnetron from an ex-

††† Reference 4, p. 328.

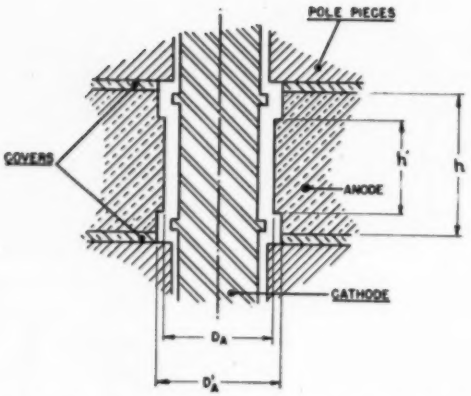

FIG. 7. Step modification at ends of anode block.

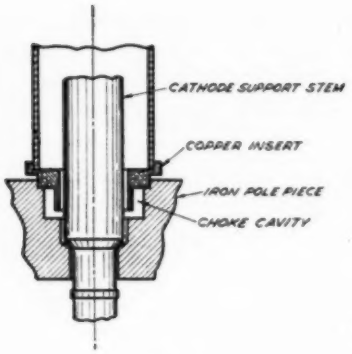

FIG. 8.

ternal source. Moreover, bringing metallic objects into the neighborhood of the pole piece holes affected the measured values of the Q's. Power leakage of this magnitude was not observed from the 18-vane magnetrons. It varied in amount from tube to tube in the 26- and 38-vane magnetrons. Very bad leakage was observed in one 38-vane tube in which the $[(N/2)-1]$ mode was nearly coincident with the π-mode, but was not observed in the same tube when a cathode of slightly smaller diameter was used. In the latter case the two modes were more definitely separated.

A comparison of pole piece hole and cathode stem dimensions for the 18-vane tube with those of the 26- and 38-vane tubes shows that only principal coaxial mode propagation is possible with the first set of dimensions, whereas second coaxial mode propagation as well is permitted by the dimensions in the 26- and 38-vane tubes. This indication that the leakage occurs because of second coaxial mode propagation appears to have been confirmed by the fact that it was eliminated, on the cathode support end, by the use of a choke structure (Fig. 8) whose dimensions were based on the assumption of second coaxial mode propagation. Furthermore, the leakage was eliminated on the opposite end by a reduction, below the cut-off value for the second coaxial mode, of the diameters of the pole piece hole and of the heat conducting stem which protruded from the cathode. The diameter of the hole in the iron was the same in both pole pieces. The reduction at one end was made by the insertion of non-magnetic material in order to preserve symmetry in the magnetic field.

While the evidence is strong that the leakage was due to second coaxial mode propagation, the fact that it did not invariably occur when the dimensions permitted requires further explanation. This may be obtained by comparing the radiofrequency field patterns in the interaction space, for the π- and $[(N/2)-1]$ modes with those of the first and second coaxial modes in the cathode support line. For the principal coaxial mode, no strong coupling to any of the modes of the resonant system is apparent, even when the possibility of asymmetries is taken into account. For the second coaxial mode, there is obviously a strong coupling between the cathode support line and the $n=1$ component of the $[(N/2)-1]$ mode, but there should be no coupling to this transmission line either by the π-mode or by the zero component contamination present in it, under symmetrical conditions. Some coupling of the second coaxial mode to the π-mode may, however, be expected under asymmetrical conditions, the coupling being stronger the smaller the separation between the π- and $[(N/2)-1]$ modes. The amount of leakage present may therefore be expected to be related to accidental asymmetry in cathode location and on the degree of excitation of the $[(N/2)-1]$ mode. Both of these may vary from tube to tube.

If the coupling to the $[(N/2)-1]$ mode is much stronger than to the π-mode, as suggested above, the insertion of a choke in the cathode support line has, for the $[(N/2)-1]$ mode, the effect of connecting the interaction space to a short circuited section of transmission line, in which case the frequency of this mode alone

should be appreciably affected by the position of the choke. Such a selective dependence of the $[(N/2)-1]$ mode frequency on choke position has been observed in experiments with a movable choke. These results have been reported in detail by one of us.[5] It will be necessary, therefore, to use some care in the location of a choke introduced for the purpose of eliminating leakage, in order to avoid an unnecessary reduction in mode separation.

Another consequence of the increase in the number of cavity resonators is the introduction of new problems in anode block construction. The technique of hobbing[3] had been very successful in forming 18-cavity anode blocks and the construction of blocks with the larger number of resonators by the same method was attempted. The vane thickness and the smallest space between vanes was nearly the same as at 18 vanes. The latter dimension is of significance because it is the smallest dimension of the hob sector which forms the resonant cavity in the anode block, and is therefore important in determining the strength of the hob. The important differences between the 18 and larger N anode blocks are that the large anode diameter requires the displacement of a much greater volume of copper in the center, and that in the case of the closed-end anode blocks, larger cavities are required. 26-vane blocks were hobbed with some success, but at 38 vanes, hob failure occurred on the second or third, if not on the first, use of the hob. This circumstance led to the use of the cavity structure shown in Fig. 9. The sector structure could

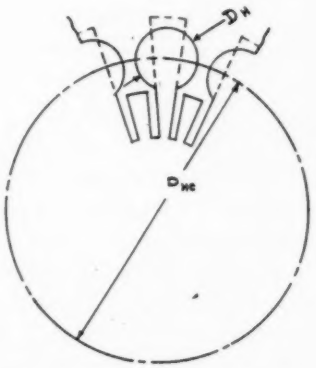

FIG. 9. Hole and vane construction of anode block.

[5] Columbia Radiation Laboratory Progress Report, October 1, 1946.

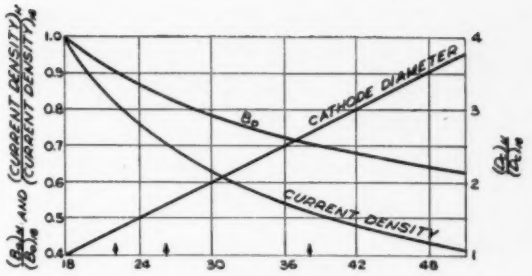

FIG. 10. Ratios of cathode diameter, current density, and B_0 for N resonators to corresponding values for 18 resonators. Arrows indicate N values studied.

be produced by hobbing because of the absence of the long sectors of large area. The holes joined onto alternate sectors were bored after the hobbing operation. Recently it has been found possible to produce the complete anode block by the hot hobbing technique.[6] In hot hobbing the maintenance of the copper in an annealed condition greatly reduces the forces which tend to break the hob.

V. DESIGN AND PERFORMANCE

In this section we summarize the essential design principles and the bases for comparison used in evaluating the performance of the various tube types. Performance charts and some tube dimensions are presented for the more successful magnetrons.

In designing magnetrons of N greater than 18, in predicting their advantages, and in evaluating their performance, a scaling procedure taking into account the change of N and the accompanying change in σ was employed, using the extensively studied 18-vane design as a starting point. The system of reduced variables formulated by Slater[7] was used for this purpose. The coordinates V_0 and B_0 of the point of tangency of the Hartree line for the operating mode to the cut-off parabola, and the anode current I_0 for this point, form the basis of the system of reduced variables. Performance charts for two properly operating magnetrons are essentially the same, neglecting differences in circuit losses, when plotted in terms of V/V_0, B/B_0, and I/I_0, even though they differ in wave-length, number of

[6] Columbia Radiation Laboratory Progress Report, January 1, 1947.

[7] G. B. Collins, *Microwave Magnetrons* (McGraw-Hill Book Company, Inc., New York, 1948) p. 416.

resonators, and operating voltage range. For the voltage at which operation in a mode just begins, the quantities V/V_0 and B/B_0 are connected by Hartree's equation

$$V/V_0 = 2(B/B_0) - 1.$$

The beginning of oscillation is obscured by effects which spoil the operation at very small currents. Since, however, the dynamic impedance of magnetrons is small, the above relation can be taken to hold approximately for the operating voltages. The quantities V_0, B_0, and I_0 are related to the dimensions and the wave-length of the magnetron as follows:

$$V_0 = 2.52\times 10^6 (D_a/n\lambda)^2 \text{ volts},$$

$$B_0 = \frac{21{,}400}{(1-\sigma^2)n\lambda} \text{ gauss, when } \lambda \text{ is in cm},$$

$$I_0 = \frac{5.23\times 10^5}{(1-\sigma^2)^2\left(\frac{1}{\sigma}+1\right)} a_1 \left(\frac{D_a}{n\lambda}\right)^3 \left(\frac{h}{D_a}\right) \text{ amp.},$$

where h is the anode length‡ and a_1 is a function of σ, nearly equal to unity in the range of σ of interest here. A plot of a_1 as a function of σ is given by Slater.[7]

All of the magnetrons constructed and tested in these experiments were designed for the same values of λ and V_0. Small variations in λ and V_0 resulted from errors in resonator dimensions arising from the use of approximate calculations and from errors in construction. Operation in the π-mode ($n = N/2$) was the objective in all cases. Other values of n enter into the problem when the possibility of competition from other modes is considered.

The initial values of σ chosen for magnetrons with an untried number of resonators was based on Slater's semi-empirical formula $\sigma = (n-2)/(n+2)$. After experimentation it was found that the best compromise between efficiency and stability occurred very nearly at $\sigma = 0.94[(n-2)/(n+2)]$ in all cases.

The possible advantages that can be derived from the use of a large number of resonators assuming the above design relationship to hold are shown in Fig. 10, where the quantities B_0, D_c and cathode current density are plotted as a function of N for magnetrons of the same λ, V_0, and h and operating at equal values of I/I_0. N values which have been actually used are indicated. The increase in cathode size and the reduction in current density resulting from large N should help to extend practical limits on scaling down in wavelength, on reducing operating voltage, or on operating at higher power input. In the latter connection it is of interest that one form of 38-vane 1.25-cm magnetron has been driven to 90-amperes pulsed current, yielding 300 kw of pulsed power output for a brief period.

To evaluate the performance of each of the magnetrons tested, an extensive program of measurements was carried out. Since the major problem was that of obtaining stable π-mode operation, a large part of these measurements was concerned with mapping out the regions of the performance chart in which such operation occurred, and the regions in which disturbances appeared. Wave-length measurements on the competing modes were made for identification purposes. While the unwanted modes made their presence known in different ways, depending upon particular tube design and on circumstances of operation, their most persistent manifestation in these experiments was in the form of pulse-to-pulse mode shifting. Here operation occurs in the π-mode for the duration of some pulses, and in the unwanted mode during other pulses, the shifting occurring apparently at random. Observed symptoms of this kind of mode shifting were: (a) the appearance of apparently simultaneous traces on an oscilloscope which records current pulses, indicating distinctly different values of pulsed current for each mode, (b) the random appearance and disappearance of lines in the presentation of the π-mode spectrum on the screen of a spectrum analyzer, and (c) two distinct responses on the wave meter, one for the π-mode and one for the unwanted mode. The term "mode competition," used in Sections II and III fits this situation particularly well. The competition occurs in the starting of every pulse, the outcome being in doubt until the pulse is well established. Since the rate of build-up of the

‡ An effective value of h is used in the computation of I_0 for closed-end tubes, in which the r-f electric field intensity varies sinusoidally along the length of the anode. The complication of the step construction in some of the tube types has also been included in the effective values.

π-mode, for which the output circuit of the magnetron is designed, depends upon the external loading, the stability of π-mode operation is dependent on the external loading as well as upon applied voltage and magnetic field. The operation over a reasonable range, in magnitude and phase, of external load impedance was therefore investigated for stability.

The experimental observations on the magnetrons constructed show that the mode competition can be eliminated, by proper design, for values of N as great as 38, and there is no indication that this is an upper limit. For $N=38$ this was accomplished only with the closed-end design. For 26 vanes stable operation with open ends was observed for one particular set of dimensions, but the closed-end design allows more latitude in the choice of design parameters, and is therefore to be preferred.

The elimination of mode competition alone

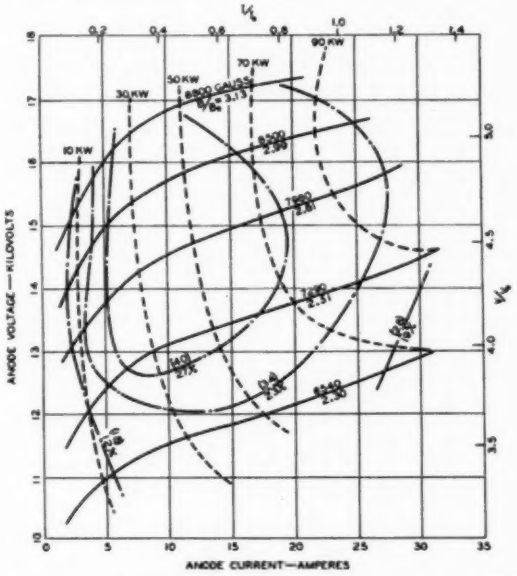

(a) 18-vane magnetron: pulse duration—0.3 μsec.; duty cycle—0.0003; wave-length—1.29 cm.

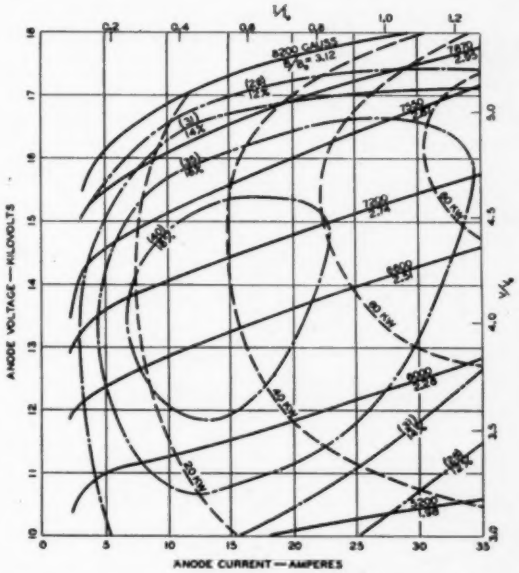

(b) 26-vane magnetron: pulse duration—0.2 μsec.; duty cycle—0.0002 (closed ends); wave-length—1.26 cm.

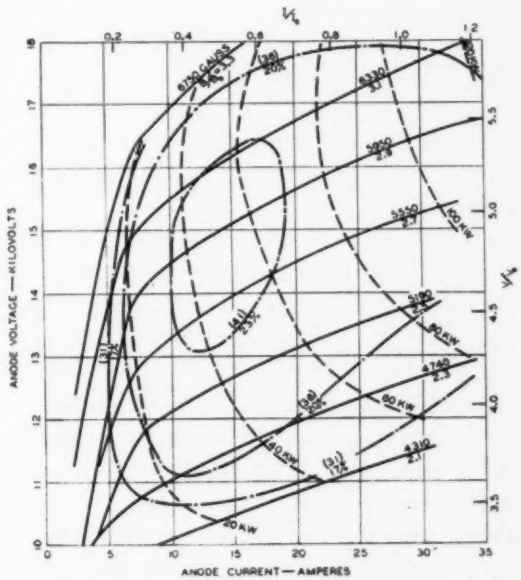

(c) 38-vane magnetron: pulse duration—0.2 μsec.; duty cycle—0.0002; wave-length—1.3 cm.

FIG. 11. Comparison of performance of 18-, 26-, and 38-vane rising sun magnetrons. (Electronic efficiencies are given in parentheses above the over-all efficiencies.)

TABLE I. Design and operating data for best 22-, 26-, and 38-vane, 1.25-cm magnetrons, with good 18-vane tube for comparison.

Number of resonators resonator ends cath. mount	18 Open axial	22 Open radial	26 Open radial	26 Closed axial	38 Closed axial
D_a (in.)	0.165	0.181	0.218	0.234	0.339
*D_a' (in.)				0.270	0.381
h (in.)	0.190	0.170	0.170	0.309	0.350
*h' (in.)				0.220	0.272
D_i (in.)	0.403	0.410	0.457	**	**
D_s (in.)	0.300	0.311	0.349	0.386	0.479
r_1	1.76	1.76	1.82	2.6	2.68
σ	0.59	0.64	0.70	0.71	0.76
V_0 (volts)	3280	3030	3020	3350	3050
B_0 (gauss)	2840	2780	2620	2630	2060
I_0 (amps.)	24	23	27	28	29
λ_π (cm)	1.290	1.207	1.230	1.257	1.300
External Q	350	500	340	1030	800
Unloaded Q	750	710	600	860	1000
Performance at maximum efficiency					
Electronic eff. (percent)	43	43	43	44	43
I (amp.)	11	9	17	12	12
V/V_0	4.5	5.0	4.9	4.2	4.8
B/B_0	2.8	3.1	2.8	2.7	2.9
I/I_0	0.47	0.40	0.63	0.44	0.42

* Step dimensions, see Fig. 7.
** See Fig. 9. 26-vane tube has $D_H = 0.096$ and $D_{HC} = 0.490$; 38-vane tube has $D_H = 0.079$ and $D_{HC} = 0.586$.

may not be sufficient to make available the advantages which have been predicted for large N. That these are indeed available may be demonstrated by a comparison, in terms of reduced variables, of performance charts of the large N magnetrons with those of the 18-vane magnetron.

A typical good 18-vane tube and best individual specimens of the 26- and 38-vane tubes are compared on the above basis in the performance charts in Fig. 11. Reduced variable scales, as well as the ordinary scales appear in the charts, and electronic efficiencies as well as ordinary efficiencies are given.

Electronic efficiencies are given for comparison in the performance charts because of the complication arising from variations in loading. Most of the effect of this variation on the observed efficiency may be removed by comparing electronic efficiencies rather than over-all efficiencies. The electronic efficiency also varies with the loading, but slowly enough that uncorrected values of this quantity serve for a fair comparison. It may be seen that the three performance charts are quite similar, particularly in terms of the reduced variables and the electronic efficiency. There is, in fact, no more variation among them than is found among samples of presumably identical magnetrons at this frequency. It may be concluded, therefore, that all expectations have been fulfilled in this scaling operation, and that operation at N values up to 38 can be as good as at $N = 18$.

A criterion of performance that is of special interest in connection with scaling to short wavelengths is the low field behavior, since at very short wave-lengths the lower values of B/B_0 may be the only ones within reach. It may be seen from the performance charts that, in this respect, the 26- and 38-vane magnetrons are, if anything, slightly better than the 18-vane magnetron.

Table I gives design and operating data for these three magnetrons and also for open-end 22-vane and open-end 26-vane magnetrons. The performance of the magnetrons in the table for which performance charts are not given is well represented by the maximum electronic efficiency and the coordinates at which it appears on the performance chart. In all cases operation was stable π-mode operation with good spectrum over the region covered by the performance charts shown.

VI. CONCLUSION

From the results of the experiments reported here we may conclude that the rising sun design can be applied to the construction of magnetrons with a number of cavities considerably greater than 18. Successful operation for open cavity resonant systems has thus far been limited to magnetrons with 26 resonators in the voltage range in use for pulsed magnetrons, and can perhaps be extended to 30 resonators for low voltage CW magnetrons. When closed-end cavity resonators are used the number of cavities can be increased to at least 38, and there is no reason to believe that this number constitutes an upper limit.

The advantages derived from the use of a large number of cavities are principally in the increase in cathode size and in some reduction in the required magnetic field for magnetron operation. These advantages are, of course, very attractive when one is concerned with the design of high frequency generators in the millimeter range. It should be pointed out, however, that serious

difficulties remain in realizing satisfactory magnetron operation in the millimeter range. In addition to the increase in constructional difficulties there is the problem of decreasing distance between cathode and anode for constant voltage difference, as the wave-length is decreased. Moreover, the anomalously poor operation of the magnetron in the low current region may be aggravated by the high space charge densities that are expected with increasing magnetic field. It is hoped, however, that the use of a larger number of resonators for magnetrons will facilitate the extension of the present magnetron techniques to wave-lengths of a few millimeters. The increase in the number of resonators can certainly lead to increased output power at 1 cm or longer wave-lengths in situations where the output power is limited by the cathode area.

ACKNOWLEDGMENTS

This research was carried out under Contract OEMsr-485 of OSRD with Columbia University. The authors wish to acknowledge the participation of the Columbia Radiation Laboratory staff in the experiments performed. The authors are especially grateful for the contributions made by Mr. C. Dechert and Mr. M. Bernstein in the construction of the magnetrons.

Calendar of Meetings

July

21–23 American Society of Civil Engineers (Convention), Seattle, Washington

28–August 3 International Union of Crystallography (First General Assembly and International Congress), Cambridge, Massachusetts

29–31 Second Symposium on Applied Mathematics, American Mathematical Society (Cosponsorship of American Institute of Physics), Cambridge, Massachusetts

August

18–20 Society of Automotive Engineers (West Coast Meeting), San Francisco, California

19–28 International Union of Geophysics, Oslo, Norway

24–27 American Institute of Electrical Engineers (Pacific General Meeting), Spokane, Washington

30–September 4 American Chemical Society (Eastern Session), Washington, D. C.

September

6–7 Mathematical Association of America, Madison, Wisconsin

6–10 American Chemical Society (Midwest Session), St. Louis, Missouri

7–10 American Mathematical Society, Madison, Wisconsin

8–9 Society of Automotive Engineers (National Tractor Meeting), Milwaukee, Wisconsin

13–17 Instrument Society of America, Philadelphia, Pennsylvania

13–17 American Chemical Society (Western Session), Portland, Oregon

13–17 American Association for the Advancement of Science, Washington, D. C.

15–17 American Institute of Chemical Engineers, French Lick, Indiana

19–23 Illuminating Engineering Society, French Lick, Indiana

20–24 Illuminating Engineering Society (National Technical Conference), Boston, Massachusetts

21–24 International Rheological Congress, Scheveningen, Holland

27–29 Technical Association for the Pulp and Paper Industry, Poland Spring, Maine

30–October 3 Institute of Radio Engineers (West Coast Convention), Los Angeles, California

October

5–7 American Institute of Electrical Engineers, Washington, D. C.

6–9 Society of Automotive Engineers (National Aeronautic Meeting and Aircraft Engineering Display), Los Angeles, California

13–15 American Society of Civil Engineers (Fall Meeting), Boston, Massachusetts

13–16 Electrochemical Society, New York, New York

18–22 American Institute of Electrical Engineers (Midwest General Meeting), Milwaukee, Wisconsin

21–23 Optical Society of America, Detroit, Michigan

25–28 Technical Association of the Pulp and Paper Industry, Buffalo, New York

25–29 American Society for Metals, Philadelphia, Pennsylvania

25–29 Society of Motion Picture Engineers, Washington, D. C.

30 American Mathematical Society, New York, New York

Transmission Losses in 2n-Terminal Networks

VITOLD BELEVITCH
Bell Telephone Manufacturing Company, Antwerp, Belgium
(Received October 23, 1947)

The semipositive character of the dissipation function of any physical 2n-terminal network imposes some restrictions on the realizability of prescribed transmission losses between the various pairs of terminals when they are connected to given impedances. These restrictions are most easily expressed in terms of elements of the efficiency matrix of the network, which is defined in the first part of this paper. Discussions of the application of matrix calculus to the solution of reactive and resistive, transformer-type, and general 2n-terminal networks are presented.

A very useful tool in solving telephone transmission problems is the conventional theory of 4-terminal transducers, often called 4-pole networks. Although this theory is sufficient for the study of most circuits, some problems involve networks with a larger number of terminals, which are often referred to as 2n-terminal, or 2n-pole networks. This paper is a contribution to their theory.

The particular point that will be considered in this paper is the restriction imposed by physical realizability on the arbitrary choice of transmission losses between various pairs of terminals connected to a given set of terminating (generator or receiver) impedances.

THIS theory was suggested by an old paper by Campbell and Foster,[1] and a part of the following theorems is an extension of their results in modern notation using matrix calculus.

I. DEFINITION OF TRANSMISSION LOSSES

Assume a 2n-pole network with terminal pairs numbered (1,1′), (2,2′), $\cdots$, (n,n′). Any pair (p,p′) will be across a generator or a receiver impedance R_p, presumed, as is usual in transmission theory, to be a pure resistance. The network is thus associated with a given set of terminating resistances.

Suppose that a generator of voltage V_p be connected in series with resistance R_p, producing a current I_q through resistance R_q, when all other terminal pairs are across their respective resistances. We shall let S_{qp} be the square root of the ratio between the complex power $R_qI_q^2$ delivered to the receiver, and the maximum power $V_p^2/4R_p$ available from the generator. Thus

$$S_{qp}=[2(R_pR_q)^{\frac{1}{2}}I_q/V_p]. \tag{1}$$

The usual definitions of the effective loss A_{qp} in nepers, and of *phase shift* B_{qp} in radians are

$$A_{qp}+jB_{qp}=-\log_eS_{qp}. \tag{2}$$

In the following we shall use instead the expression S_{qp}, and call it the *complex efficiency factor* between terminals p and q.

[1] G. A. Campbell and R. M. Foster, "Maximum output networks for telephone substation and repeater circuits," Trans. A.I.E.E. (February, 1920).

It will also be convenient to introduce a factor S_{pp}, which will be defined as the *reflection coefficient* at the terminal pair (p,p′);

$$S_{pp}=(R_p-\zeta_p/R_p+\zeta_p), \tag{3}$$

where ζ_p is the impedance measured between the terminals (p,p′), with all other terminal pairs closed on their associated resistances. By writing

$$A_{pp}+jB_{pp}=-\log_eS_{pp}, \tag{4}$$

the usual definitions of the *return loss* and *phase* are obtained. The factor S_{pp} is thus the square root of the complex ratio of reflected power to maximum power. The condition $S_{pp}=0$ expresses an impedance match at terminals (p,p′).

The matrix S, composed of elements S_{pq}, will be termed the *efficiency matrix* of the 2n-pole network associated with a given set of terminating resistances. If the main diagonal of this matrix is zero, the network is simultaneously matched at all its terminal pairs.

A simultaneous multiplication of the pth row and of the pth column by -1 is irrelevant, because it merely interchanges the terminals p and p'.

II. CALCULATION OF EFFICIENCY MATRIX

We start from the usual set of equations of a 2n-pole network in terms of the self and transfer impedances;

$$V_p-R_pI_q=Z_{p1}I_1+Z_{p2}I_2+\cdots+Z_{pn}I_n, \tag{5}$$

where $p=1, 2, \cdots, n$. In (5), for the sake of

generality, it is supposed that generators were present in any terminal pair.

Introducing *normalized* currents, voltages, and impedances by writing

$$I_p' = (R_p)^{\frac{1}{2}} I_p, \quad V_p' = V_p/(R_p)^{\frac{1}{2}}, \quad Z_{pq}' = Z_{pq}/(R_p R_q)^{\frac{1}{2}}, \tag{6}$$

the system of equations in (5) becomes

$$V_p' - I_p' = Z_{p1}' I_1' + Z_{p2}' I_2' + \cdots + Z_{pn}' I_n'. \tag{7}$$

Since we will always consider normalized quantities in the following equations, we may drop the primes and write (7) in matrix form:

$$V - I = ZI, \tag{8}$$

where V and I are one-column matrices, and Z is the usual normalized impedance matrix of the network.

Introducing the unit-matrix E, (8) may be written

$$V = (Z+E)I. \tag{9}$$

Solving for I,

$$I = QV, \tag{10}$$

where Q is the inverse matrix of $Z+E$;

$$Q = (Z+E)^{-1}. \tag{11}$$

A generator V_p, acting alone in the terminal pair p, produces in the terminal pair q a current $I_q = Q_{qp} V_p$. Since normalized expressions are equivalent to making the terminating resistances equal to unity, (1) is reduced to

$$S_{qp} = 2Q_{qp}. \tag{12}$$

Similarly, Q_{pp} is the normalized driving-point admittance of mesh p. If we denote by ζ_p' the normalized impedance ζ_p/R_p, (3) becomes

$$S_{pp} = (1-\zeta_p')/(1+\zeta_p'). \tag{13}$$

But, by Thévenin's theorem,

$$Q_{pp} = 1/(1+\zeta_p'), \tag{14}$$

and, from (13) and (14),

$$S_{pp} = 2Q_{pp} - 1. \tag{15}$$

Equations (12) and (15) may be combined in matrix form:

$$S = 2Q - E = 2(Z+E)^{-1} - E, \tag{16}$$

which may also be written

$$S = (E-Z)(E+Z)^{-1}. \tag{17}$$

This is a formal extension of (13).

In this calculation, we assumed that both matrices Z and Q exist, but this is not necessarily true. The degenerate cases will be examined later on.

It is shown in (17) that the matrix S is symmetrical, as is Z (reciprocity theorem). By replacing Z with Z^{-1} (or taking the inverse network), S is simply changed into $-S$, and this is a form of the duality principle. Inverse networks give the same transmission losses.

III. REACTIVE 2N-POLE NETWORKS

In the case of a network composed of only reactive elements, the matrix Z is purely imaginary. Taking the complex conjugate $\bar{S}$, Z is simply changed into $-Z$;

$$\bar{S} = (E+Z)(E-Z)^{-1}. \tag{18}$$

By multiplying (17) and (18),

$$S\bar{S} = E, \tag{19}$$

and *the efficiency matrix of a reactive 2n-pole network is therefore a complex orthogonal matrix.* The diagonal terms of (19), written explicitly, are

$$\exp(-2A_{p1} + \exp(-2A_{p2}) + \cdots + \exp(-2A_{pn}) = 1, \tag{20}$$

where $p = 1, 2, \cdots, n$. This demonstrates that no power can be consumed in a reactive network; it is an extension of a familiar relation first established by Feldtkeller for reactive 4-pole networks.

IV. RESISTIVE 2N-POLE NETWORKS

In the case of a purely resistive network, the matrix Z is real. It is easily shown that Z and S may be simultaneously reduced to diagonal matrices (respectively, $\hat{Z}$ and $\hat{S}$) by means of a non-singular linear orthogonal transformation. Equation (17) is then transformed into

$$\hat{S}_{pp} = (1-\hat{Z}_{pp})/(1+\hat{Z}_{pp}). \tag{21}$$

The expression for the power consumed in a passive network is known to be of a semipositive quadratic form; when the quadratic form is transformed into a sum of squares, the coeffi-

cients are $\hat{Z}_{pp}$ and must be positive or zero. We thus have

$$-1 \leqslant \hat{S}_{pp} \leqslant 1. \tag{22}$$

The case of a degenerate network having no impedance matrix may be considered as being the limiting case of a network for which at least one of the numbers $\hat{Z}_{pp}$ becomes infinite, so that (22) must be extended:

$$-1 \leqslant \hat{S}_{pp} \leqslant 1. \tag{23}$$

In this last form the condition obviously expresses the fact that both matrices $E+S$ and $E-S$ are semipositive. This can be written explicitly in the usual way in terms of principal minors.

As an example, we will consider the case of a hexapole simultaneously matched at all its terminal pairs. The efficiency matrix is

$$S = \begin{Vmatrix} 0 & S_{12} & S_{13} \\ S_{12} & 0 & S_{23} \\ S_{13} & S_{23} & 0 \end{Vmatrix}.$$

By noting that the determinants of $E+S$ are non-negative, one obtains the two non-trivial conditions

$$1 \pm 2S_{12}S_{23}S_{13} - S_{13}^2 - S_{23}^2 - S_{12}^2 \geqslant 0. \tag{24}$$

If the hexapole has the same losses between all terminal pairs, i.e., if

$$|S_{12}| = |S_{13}| = |S_{23}| = s,$$

one of these conditions gives

$$1 - 3s^2 - 2s^3 = (1+s)^2(1-2s) \geqslant 0,$$

the other one being trivial. Thus

$$s \leqslant \tfrac{1}{2},$$

and the minimum value of the loss is 0.69 neper $=6$ decibels, or twice as great as could be expected from the division of the input energy between the two output resistances. Actually, a 3-decibel loss is obtained in a hybrid coil, but it is not symmetrical with respect to all terminal pairs.

V. IDEAL TRANSFORMERS

A network composed of only ideal transformers may be considered as being the limiting case either of a reactive or of a resistive network. As its efficiency matrix is real, (19) becomes

$$S^2 = E. \tag{25}$$

For an orthogonal symmetric matrix, the numbers $\hat{S}_{pp}$ are either $+1$ or -1. Since the sum of these numbers is equal to the sum of the main diagonal elements of S, the sum must be zero for a network simultaneously matched at all of its terminals, which is obviously impossible if the order of the matrix is odd. As a consequence, a network matching an odd number of terminal pairs and composed only of ideal transformers that match an odd number of terminal pairs does not exist.

VI. GENERAL $2n$-POLE NETWORKS

The restrictions imposed on the efficiency matrix of a general $2n$-pole network are obtained by stating that the real part Z_{real} of the impedance matrix is semipositive. From (16) or (17),

$$Z = (E-S)(E+S)^{-1} = 2(E+S)^{-1} - E,$$

and

$$\begin{aligned} Z_{\text{real}} &= \tfrac{1}{2}(\bar{Z}+Z) = (E+\bar{S})^{-1} - E + (E+S)^{-1} \\ &= (E+\bar{S})^{-1}(E-S\bar{S})(E+S)^{-1}. \end{aligned}$$

Solving for $E-S\bar{S}$ and noting that (16) gives $E+S=2Q$, one obtains

$$E - S\bar{S} = 4\bar{Q}Z_{\text{real}}Q. \tag{26}$$

Consider now a semipositive quadratic form of matrix Z_{real} and apply to the variables the non-singular complex linear transformation defined by the matrix Q; the quadratic form becomes a Hermitian form in the new variables and has the transformed matrix (26). As the semipositive character is not changed by the transformation, the conditions of physical realizability can be obtained explicitly in terms of the efficiency factors by writing that the principal minors of $E-S\bar{S}$ must be positive or zero. The results previously obtained for reactive or resistive networks are particular cases of these conditions.

Transmission of Monoenergetic Slow Neutrons through Solid Solutions and Mechanical Mixtures of TiC and WC*

S. S. SIDHU**
Argonne National Laboratory, Chicago, Illinois
(Received December 9, 1947)

TiC and WC form continuous substitutional solid solutions at least up to 25 percent TiC+75 percent WC by weight when heated to 4000°F, TiC being the solvent and WC the solute. Total neutron scattering cross sections of a series of finely powdered solid solutions and corresponding mechanical mixtures of the two carbides were determined as a function of the mole percent of WC from the measured transmission of monoenergetic neutrons with energies 0.08138, 0.03479, 0.02056, and 0.01526 ev or wave-lengths $\lambda=1.004$A, $\lambda=1.536$A, $\lambda=1.998$A and $\lambda=2.319$A, respectively. The cross sections of both the solutions and the mixtures increase with increasing mole percent of WC. For mixtures they are the same as the additive cross sections, each constituent scattering independently of the other. They are analogous to x-ray scattering for the mixtures in which each constituent gives its own diffraction pattern and the patterns of the two constituents are superimposed. The neutron cross sections of solid solutions are lower than those of the mixtures at low percentages of WC but increase rapidly with the concentration of the solute molecules. They appear to be sensitive both to the structure of the solvent and the concentration of the substituting atoms.

1. INTRODUCTION

THE transmission of neutrons with wave-lengths comparable to the interplanar spacings in a crystalline substance has been shown[1–6] to be modified by the physical state of the substance. The scattering is due mainly to Bragg reflections from crystalline planes that satisfy the usual Bragg relation, $n\lambda=2d\sin\theta$. The scattering cross sections that are determined from the measured transmission would consequently vary with the number of Bragg reflections. Any factor which would tend to cause a change in the lattice of a crystalline material would also cause a change in its scattering cross section. Crystallinity, crystallization, grain size, order disorder, orientations, strain, presence of different phases, solute atoms in a solid solution, etc., would have a marked effect on the scattering cross sections of the material for slow neutrons. Therefore, the change in the scattering cross section may be used as a measure of the presence and the degree of such factors.

In the present investigation the transmission of monoenergetic slow neutrons through finely powdered solid solutions and mechanical mixtures of TiC and WC was measured and the total neutron scattering cross sections determined as a function of the mole percent of WC.

2. SAMPLES

The samples studied were titanium carbide, tungsten carbide, and a series of solid solutions and mechanical mixtures of the two carbides made in the following percentage by weight:

(1) 85 percent TiC+15 percent WC,
(2) 75 percent TiC+25 percent WC,
(3) 65 percent TiC+35 percent WC,
(4) 50 percent TiC+50 percent WC,
(5) 35 percent TiC+65 percent WC,
(6) 25 percent TiC+75 percent WC.

All the samples were as free from impurities and moisture as they could be made with usual care. They were ground to finer than 325 mesh and packed into standard cylindrical aluminum holders for cross-section measurements.

An x-ray diffraction pattern of a specimen obtained from each sample was made to determine

* This document is based on work performed under the auspices of the Atomic Energy Commission at the Argonne National Laboratory.
** On leave from the University of Pittsburgh.
[1] M. D. Whitaker and H. G. Beyer, Phys. Rev. **55**, 1101 (1939).
[2] H. G. Beyer and M. D. Whitaker, Phys. Rev. **57**, 976 (1940).
[3] Franco Rassetti, Phys. Rev. **58**, 321 (1940).
[4] F. C. Nix, H. G. Beyer, and J. R. Dunning, Phys. Rev. **58**, 1031 (1940).
[5] F. C. Nix and G. F. Clament, Phys. Rev. **68**, 159 (1945).
[6] E. Fermi, W. J. Sturm and R. G. Sachs, Phys. Rev. **71**, 589 (1947).

TABLE I. Total scattering cross sections for $\lambda = 1.004$A as a function of mole percent of WC in units of 10^{-24} cm^2/molecule.

Mole percent of WC	σ measured for solution	σ measured for mixture	Additive* cross section
5.1	13.1	14.5	14.1
9.3	13.3	14.7	14.3
14.1	13.4	14.8	14.6
23.4	14.9	15.1	15.1
36.2	16.4	16.0	15.9
47.8	17.6	16.3	16.6

* Additive values were computed from measured values of TiC and WC according to the proportion in which each compound was present.

the crystalline state of the material and also to differentiate between solid solutions and mechanical mixtures. The sample 25 percent TiC +75 percent WC, which contained the largest amount of WC was a complete solid solution and well within the limit of solid solubility of WC in TiC at 4000°F, the temperature used for making the solid solutions.

3. MEASUREMENT OF TOTAL NEUTRON CROSS SECTIONS

The method of measuring relative neutron transmission through the samples was essentially the same as used by Sturm,[7] and by Sawyer, Wollan, Bernstein, and Peterson.[8] The neutron flux from the heavy water moderated Argonne pile was diffracted from the (111) planes of a LiF single crystal, and the neutrons satisfying the Bragg relation, $n\lambda = 2d \sin\theta$, where $\lambda = h/mv$, with energies 0.08138, 0.03479, 0.02056, and 0.01526 electron volts or wave-lengths $\lambda = 1.004$A, $\lambda = 1.536$A, $\lambda = 1.998$A, and $\lambda = 2.319$A, respectively, were used. The transmission of the sample for neutrons of above wave-lengths was determined by setting the crystal at the glancing angle θ and the counter at an angle of 2θ to the incident beam. The counter used was a proportional counter filled with BF_3 enriched in the B^{10} isotope. The counting rates were measured with and without the sample in the path of the diffracted beam first at the glancing angle θ and second with the crystal rotated through 1°, while the position of the counter was kept fixed. The transmission was then calculated from the four measurements according to the relation

$$I/I_0 = (R_1 - r_1)/(R_2 - r_2), \quad (1)$$

in which R_1 is the counting rate of the beam transmitted through the sample and the sample container, R_2 the counting rate through the container only, and r_1 and r_2 the corresponding counting rates after the crystal was rotated through 1°. The values of r_1 and r_2 gave the background due to incoherent scattering which reached the counter through the sample. $(R_2 - r_2) = I_0$ was taken as the intensity of the incident beam and $(R_1 - r_1) = I$ as the intensity of the transmitted beam.

Total cross sections were calculated from the relation

$$I/I_0 = e^{-\sigma N}, \quad (2)$$

where σ is the total neutron cross section of sq. cm per molecule and N is the number in molecules per sq. cm of the sample. The value of N for a solid solution or a mechanical mixture was obtained from the formula

$$N = (\text{wt. percent/molecular wt. of TiC} + \text{wt. percent/molecular wt. of WC}) \times 6.023 \times 10^{23}/\text{surface area}, \quad (3)$$

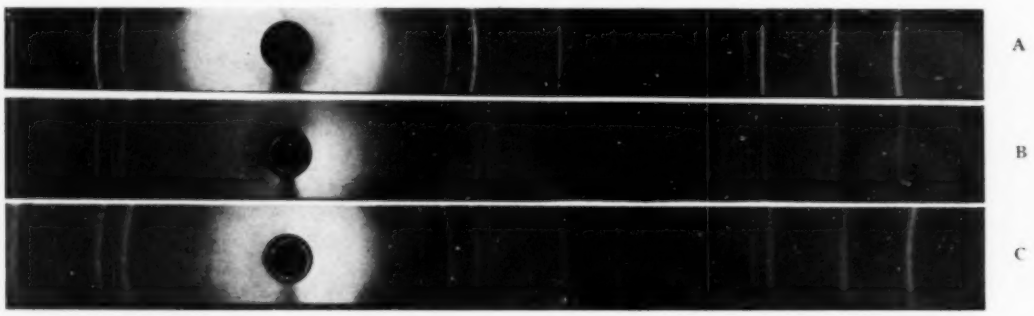

FIG. 1. X-ray diffraction photographs of TiC and solid solutions of TiC and WC. (A) TiC, (B) 50 percent TiC+50 percent WC, and (C) 25 percent TiC+75 percent WC.

[7] William J. Sturm, Phys. Rev. **71**, 757 (1947).
[8] R. B. Sawyer, E. O. Wollan, S. Bernstein, and K. C. Peterson, Phys. Rev. **72**, 109 (1947).

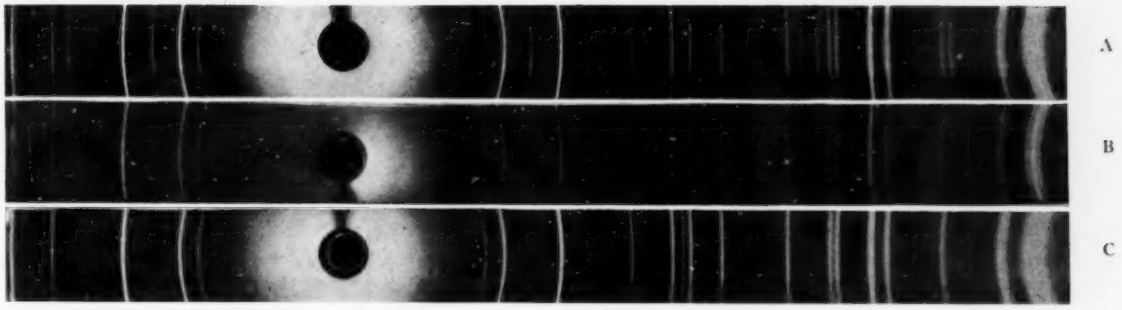

FIG. 2. X-ray diffraction photographs of mechanical mixtures of TiC and WC and WC. (A) 50 percent TiC+50 percent WC, (B) 25 percent TiC+75 percent WC, and (C) WC.

and of σ from:

$$\sigma = (1/N) \ln(I_0/I). \quad (4)$$

4. RESULTS

X-ray diffraction photographs of TiC and some of the solid solutions are given in Fig. 1, and those of the corresponding mechanical mixtures and WC are given in Fig. 2. The total cross sections of the solutions and the mixtures for $\lambda = 1.004$A, as a function of the mole percent of WC are given in Fig. 3. Similar curves were obtained for other wave-lengths used here. For comparison the measured and the additive cross sections are given in Table I.

5. DISCUSSION OF RESULTS

Both the x-ray diffraction patterns and the total scattering cross sections of the solid solutions and the mechanical mixtures show several points of interest. It is quite apparent from Fig. 1 that TiC is the solvent and WC the solute, and they form continuous substitutional solid solutions at least up to 25 percent TiC+75 percent WC when heated to 4000°F.

The measured cross sections of both the solutions and the mixtures, as shown in Fig. 3, increase with increasing mole percent of WC. For mixtures they are practically the same as the additive cross sections as shown in Table I. It is apparent that each constituent scatters independently of the other. This is quite analogous to x-ray scattering from the mixtures. As shown in Fig. 2 each constitutent gives its own diffraction pattern and the patterns of the two constitutents are superimposed.

The scattering cross sections of solid solutions are different from those of the mixtures or the additive cross sections. They are lower than those of the mixtures at low percentages of WC, but increase rapidly with the concentration of the solute molecules. This effect was observed for neutrons of all four wave-lengths used in this investigation. Since all solid solutions were heated to the same temperature and powdered to the same mesh this increase could not be ascribed to the grain size and the particle size of the material.

The measured scattering cross sections of TiC and WC for neutrons of $\lambda = 1.004$A were 13.8 and 19.6 barns, respectively. Since for low concentrations of WC in TiC the scattering cross sections are lower than those of the corresponding mixtures and increase rapidly with the solute

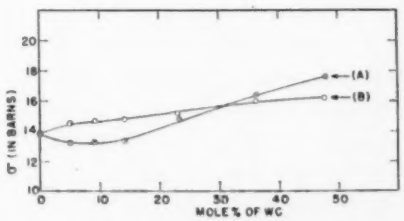

FIG. 3. Total cross sections of microcrystalline (A) solid solutions and (B) mechanical mixtures of TiC and WC as a function of mole percent of WC. Neutron energy 81.38 $\times 10^{-3}$ ev or wave-length 1.004A. σ in units of 10^{-24} cm^2 per molecule.

molecules, it appears that they are sensitive both to the structure of the solvent and the concentration of the substituting atoms. For a given structure, therefore, the scattering cross section may be used as a measure of the solubility of the solute.

Mr. David Meneghetti helped in taking some of the readings.

Experimental Results on Standing Wave Type Linear Accelerators for Electrons

ELLIOTT J. LAWTON AND W. C. HAHN
General Electric Research Laboratory, Schenectady, New York
(Received December 18, 1947)

The work that was done in this laboratory on the development of a resonant cavity type linear accelerator is briefly described. The experimental results demonstrate that electrons entering at low energies will accelerate to a higher energy in passing through a group of cavities of equal $\beta(\lambda_0/2)$ spacing and along which appears a standing wave field distribution. Starting at 57 kv, an energy of 0.345 Mev was attained with two cavities. An 8-cavity accelerator of cavity length corresponding to $\beta=0.75$ had a maximum output of 0.57 Mev. Experimentally determined energies were in fair agreement with theoretical values at equal axial gradients. Excitation power was found to be proportional to $[(\text{Mev})^2/\text{Length}](1/Q)\times$coupling coefficient. The power required for an axial gradient of 1 Mev/ft., even for the most favorable design, was high and would require the full output of one HK7 type magnetron for each foot of accelerator length. Energy spread in the accelerated beam was large for the two cavity tubes but small for the longer 8-cavity tube. It is believed that the apparent low energy spread observed in the 8-cavity case resulted from a limited range in entering angle brought about by the reduced axial gradient. There was little evidence of radial defocusing. A change in resonance wave-length amounting to +0.000225 cm per degree centigrade was observed. There was indication that the magnetron would follow a resonance change of approximately 5°C.

INTRODUCTION

THE advent of the high power r-f pulse type magnetron equipment and techniques developed during the war in the 2000- to 3000-megacycle range has been the cause for a renewed interest in the linear accelerator principle that was first tried by Wideroe[1] in Germany in 1928 and later in this country by Sloane and Lawrence[2] and Beams and Snoddy.[3] The peak power output of some of these new magnetrons is in the megawatt range and so made energies of the order of 1 Mev/ft. appear practical.

At these frequencies, instead of an individual accelerator gap being formed between the ends of two cylindrical electrodes, it becomes part of a cavity resonator. A series of such resonators joined together in line at $\beta(\lambda_0/2)$ interval form the accelerator. $\beta=V/C$, where V is the electron velocity for the given gap spacing and C the velocity of light. λ_0 is the resonance wave-length of the structure.

Operation depends on establishing a standing wave field distribution along the axis of the line of cavities such that a complete phase reversal takes place over each fundamental cavity length. An electron whose velocity matches the phase velocity of this wave will experience an accelerating force at each gap or cavity.

Electrons can be injected at practical velocities, $\beta=0.19$ to 0.41 corresponding to 10 to 50 kv, providing the spacing of the first few gaps is so adjusted that the electron receives a net accelerating force at each gap that tends to synchronize it with the phase velocity of the exciting wave. This spacing must be systematically increased until the electron has reached a nearly constant velocity approaching that of light. It is not necessary, however, to increase progressively the spacing of each individual gap, as there are strong-phase focusing forces in the beginning along a group of equally spaced gaps that tend to synchronize the velocity of the particle with the wave.

A theoretical study of this phase of the problem on the differential analyzer indicated that for an axial excitation field of 1 Mev/ft. three group spacing changes would be necessary to bring the electron up to approach the velocity of light; namely, spacings correspond to $\beta=0.75$, 0.96, and finally 1.0. Eight of the $\beta=0.75$ and 11 of the $\beta=0.96$ cavities were indicated to bring the electrons up to the approximately 2-Mev entering velocity for the $\beta=1.0$ final section. For phase focusing and bunching, the electron, on entering a given cavity, must be in advance of the peak accelerating field. Figure 1 shows some typical differential analyzer runs for these conditions

[1] Rolf Wideroe, Archiv. fur Electrotechnik **21**, 387–406 (1928).
[2] D. H. Sloan and E. O. Lawrence, Phys. Rev. **38**, 2031 (1931).
[3] J. W. Beams and L. B. Snoddy, Phys. Rev. **44**, 784 (1933) and **45**, 287(A) (1934).

with 1-Mev/ft. gradient and 50-kv injection. Curve A shows the variation of energy of the electron as it traverses the accelerator, for a time-entering angle 45° in advance of the peak of the a.c. gradient. Likewise B corresponds to 90° and C to 135° angular advance. From these it is seen that the stable phase position corresponds to an entering angle between 45° and 90°. A corresponding study for 0.763 Mev/ft. shows that there was no such stable entering angle.

The holes in the cavity washers set up radial components of the electric field, so that an electron on passing through the cavity will see a focusing field on entering and a defocusing field on leaving. Unfortunately, the condition that the particle be slightly in advance of the peak accelerating field for bunching results in its passing through a radial field on leaving the cavity that is larger than the entering focusing field. The conditions for phase focusing and bunching are therefore incompatible with those for radial focusing.

The associated magnetic field is of such a direction as to produce a focusing action during the phase focusing period and therefore counteracts the defocusing effect of the electric field. Whether the counteracting effect of the magnetic field would balance the defocusing effect of the electric field is problematical and would depend somewhat on the final configuration. The experimental evidence for the first eight cavities points to a favorable balance.

Since many mutually coupled resonant cavities are involved, there will be other undesirable modes of oscillation that must be avoided in order not to have interference between the operating and adjacent modes. This interference will set an upper limit to the length of the accelerator. It has been demonstrated[4] that the greatest mode separation is near the center $\pi/2$ mode of the over-all $n+1$ modes of the mode spectrum, making this mode best for operation. Mode separation can be further increased by symmetrical excitation at the center of an array of equal number of cavities where the field distribution is maximum for the center mode but zero for the two adjacent modes. Choice of the $\pi/2$ mode and a practical value of coupling $K=9.05$ percent and a $Q=9000$ leads to a limiting accelerator length of 10 to 20 ft. at 10.7-cm wave-length. This length could probably be extended in proportion to the square root of the wave-length through the use of a longer operating wave-length. The power, required to maintain a given axial gradient, however, would need be increased in proportion to the $(\lambda)^{\frac{1}{2}}$ because of the resultant lower Q.

[4] Elliott J. Lawton, J. of App. Phys. **19**, 534 (1948).

EXPERIMENTAL

The schematic arrangement of an 8-cavity accelerator tube and associated equipment are shown in Fig. 2. The photograph of Fig. 3 shows the experimental set-up with a 2-cavity accelerator section in the test position.

The resonant cavities of the accelerator are formed by joining together alternate thin copper washers W, and large diameter ring spacers S at regular $\beta(\lambda_0/2)$ interval (see Fig. 2). The number of washers W for each interval establishes the desired mode of oscillation while the dimension of washer and spacer determines the wave-length and coupling K between cavities. K is the wave-length difference between the lowest and highest modes expressed as a percentage of the wave-length of the lowest order mode. To establish the desired $\pi/2$ operating mode two partitions were necessary in each $\beta(\lambda_0/2)$ interval. Dimensions were usually determined experimentally and, because of the high Q's involved (9000), machining tolerances of the order of $\pm 0.0005''$ necessarily had to be maintained.

Electrons entered and left the accelerator through terminating cylinders of diameter less

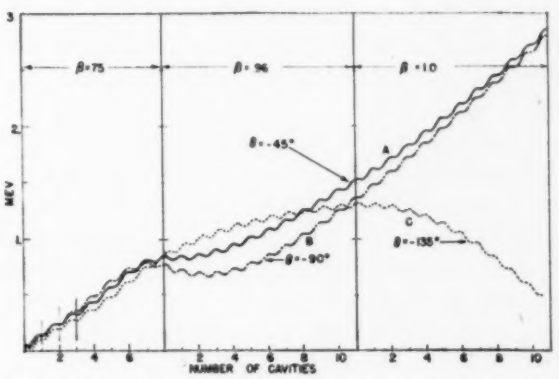

FIG. 1. Differential analyzer run for a 1-Mev/ft. gradient and 50-kv injection. θ = time entering angle.

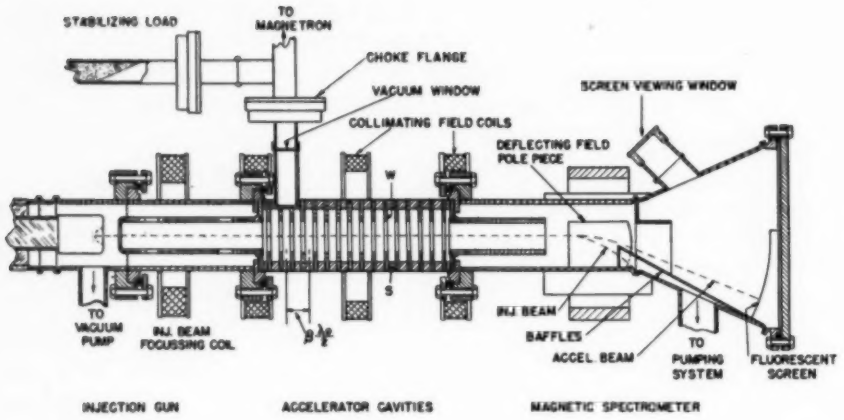

FIG. 2. Schematic diagram of an 8-cavity UHF linear accelerator for electrons.

than the "cut-off" diameter for the resonance wave-length. By adjusting the amount that the end of the terminating cylinder extended into the end cavities, the termination could be made to appear as a short circuit. The termination could be either at a mid-plane through the cavity between two partitions or through the partition proper. In the case of short tubes (two cavities) the partition termination resulted in a higher Q than the cavity type because of the one less partition required.

R-f power was supplied from a 1-megawatt pulse type HK7, 10-cm tuneable magnetron. A pulse width of 3.4μ seconds and at a repetition rate of 262 cycles per second was used. A minimum pulse width of 1.5μ second was found necessary to allow for the build-up time due to the high Q of the cavity and for the r-f field to become steady inside the cavity.

Power was transmitted from the magnetron to the accelerator through $1\frac{1}{2}''\times 3''$ wave guide. Excitation of the accelerator cavities was through a hole in the outer diameter of one of the cavities. The size of this hole was so adjusted that the unloaded Q_u equalled the external Q_{ext}, the condition for match.

The photographs of Figs. 4 and 5 show, respectively, a completed 2-cavity accelerator of the type terminated at a point midway between partitions and of coupling $K=17.75$ percent and a 2-cavity tube terminated at a partition and of coupling $K=9.05$ percent. The cavity length in both cases corresponds to $\beta=0.75$. In Fig. 5, the wave guide connection has been removed and shows the coupling hole, which in this case necessarily had to be centered about the partition for this type of feed and termination. In the case of the tube in Fig. 4, the coupling hole lies midway between the two partitions. Figure 4 also shows the wave guide connection to the tube and resonant type glass window used as the vacuum seal between the wave guide and the accelerator cavities.

For stable operation of the magnetron at the desired resonance wave-length, it was necessary to include a series impedance between magnetron and cavity (see Fig. 2). It was necessary to dissipate approximately 40 percent of the total magnetron power in this series load in order to destroy the condition for resonance at more than one wave-length between the two oscillating circuits, magnetron, and loaded transmission line.

The above duty cycle and the unavoidable amount of power that necessarily had to be dissipated in the series stabilizing load limited the useful power from the HK7 to approximately 0.3 megawatts at the tube.

Injection was with a standard x-ray tube type gun. Focusing of the injection beam was accomplished with an external magnetic field. A steady d.c. injection beam current of the order of 0.2 to 15 ma was used.

The energy of the accelerated beam was measured with a simple magnetic spectrometer. The deflection of the accelerated beam was determined by observing its position on a fluorescent screen. This also provided a means of determining energy spread in the accelerated beam. The spectrometer was calibrated with the d.c. injection beam. The screen was observed from a distance with a telescope because of the danger of x-rays.

The over-all tube including gun, accelerator, and spectrometer was evacuated to a pressure of the order of 2 to 5×10^{-5} mm of Hg with two oil diffusion pumps. No extensive preliminary outgassing was found necessary. The vacuum seal at the wave guide connection to the tube was with a resonant type glass-to-fernico seal window.[5] Mechanical alignment of gun, accelerator, and spectrometer was accomplished optically by sighting through sets of peepholes along the axis. Final electrical alignment, to compensate for stray magnetic fields which were quite objectionable, was taken care of by shifting the gun and associated focusing coil.

Surrounding the accelerator section were magnetic field coils for compensating for any radial defocusing.

EXPERIMENTAL RESULTS

The experimental results are confined to accelerator sections made up of cavities of length corresponding to $\beta<1$ and which represent the initial gun stages necessary to bring the electron up to the entering velocity of the final $\beta=1$ stages.

Four different accelerator sections based on the $\pi/2$ mode design were tested, namely: No. 1, an eight-cavity tube of cavity length corresponding to $\beta=0.75$; No. 2, a two-cavity tube of the same design and coupling $K=17.75$ percent as the eight-cavity tube; No. 3, a two-cavity tube of the same cavity length as 1 and 2, but of coupling $K=9.05$ percent and terminated at a partition instead of midway between partitions; and No. 4, a two-cavity tube of the same coupling and termination as 3, but of cavity length corresponding to $\beta=0.5$.

The experimental arrangement was such that the magnitude of the accelerated beam currents could not be measured.

The experimentally determined energies were found to be in fair agreement with the theoretically predicted values where it was possible to compare the two at equal axial gradients and injection voltages. The comparison is shown in the Table I.

In the case of tubes 1 and 2, the maximum gradient was limited to the values listed because of limited r-f output power from the HK7 magnetron.

In the case of the 8-cavity tube 1, whose design was based on a 1-Mev/ft. gradient, there was evidence of a critical phase relation between beam and wave at the maximum possible gradient 0.52 Mev/ft. and a complete lack of phase focusing at 0.44 Mev/ft. Below this value there was a sharp decrease in the output voltage to a value not much in excess of the injection voltage. The theoretical study indicated an expected value of the minimum gradient for phase focusing that would be only slightly lower than 0.763 Mev/ft. The total output voltage as a function of excitation power for this tube is shown for different injection voltages in Fig. 6.

The minimum practical gradient for phase

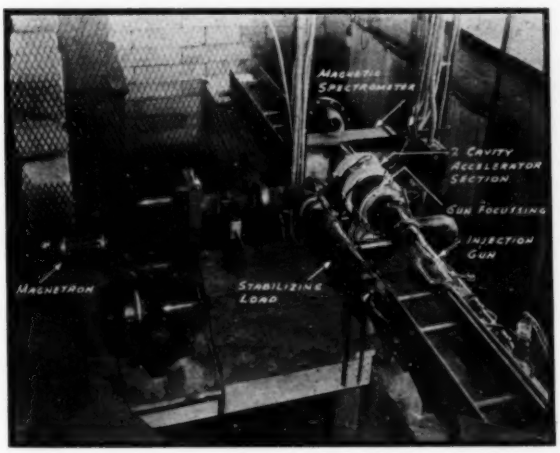

FIG. 3. Experimental set-up with a 2-cavity accelerator in the test position.

FIG. 4. Two-cavity accelerator, showing terminating cylinder and wave guide connection. $K=17.75$ percent.

[5] M. D. Fiske, Rev. Sci. Inst. **17**, 478 (1946).

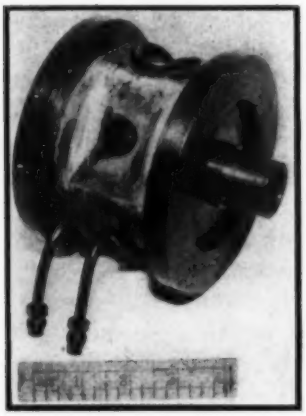

FIG. 5. Two-cavity accelerator, showing coupling hole between wave guide and cavity. Terminating is at a partition. $K=9.05$ percent.

focusing and bunching as predicted by the theoretical study was 1 Mev/ft. (see Fig. 1). The power required to excite the 1 ft. long, 8-cavity tube to 0.52 Mev/ft. corresponded to 0.360 megawatt/ft. Since excitation power appears as a copper loss in the walls of the cavity it should be proportional to

$$[(\text{Mev})^2/\text{Length}]\ 1/Q.$$

The excitation power for the 8-cavity tube extrapolated to the value required for 1 Mev/ft. would be $(1/0.52)^2\times 0.36=1.34$ megawatts/ft., a prohibitively large value. These results were confirmed by the tests of the 2-cavity tube No. 2 of the same coupling and design. The ratio of the voltage output of the 8-cavity tube to that of the 2-cavity tube at the same injection voltage and power level was 2.18, which is in agreement with the value 2.0 as predicted by the power relation.

The tests of the 2-cavity tube No. 3 of lower coupling $K=9.05$ percent indicated a larger voltage output at a given excitation power. The total voltage output *vs.* total excitation power at different injection voltages is shown in Fig. 7. In Fig. 8 is shown the voltage per gap, or average field, after deducting the injection voltage, as a function of the excitation power per gap. For comparison, the field results for the higher coupling $K=17.75$ percent, tube No. 2, are shown in Curve A. It is to be pointed out that the excitation values given for curve A are corrected for Q to compare with the 9000 value of tube No. 3. The Q of tube 2 was 6000. It will be noted that the curve for the tube 3 is drawn through the group of points for injection voltages between 41 and 93 kv where the field values are closely grouped. Below this range, 30 to 12 kv, the entering phase relations were probably such that the beam did not pick up enough energy in falling through the first gap and so emerged at a lower value. This was somewhat borne out by the behavior of the beam intensity, as at these lower values the injection beam current had to be increased by a factor of approximately 5 to 10 times to produce a visible accelerated beam on the fluorescent screen. It can be seen that the excitation power required for a given field, in the case of tube No. 3 with lower coupling, is approximately one-half of that required for tube No. 2 which had double the coupling, indicating that excitation power is directly proportional to the coupling over this coupling range. The excitation power required for a 1-Mev/ft. (120 kv/gap) gradient for this tube is 0.624 megawatt/ft., and would represent the power required for the first gun section of a limiting length of accelerator of 10 to 20 ft.

The experimental results for the shorter cavity ($\beta=0.5$) tube No. 4 of same design and coupling as tube No. 3 indicate that at a given excitation power 0.300 megawatt and 60-kv injection, the maximum output was only 0.190 Mev as compared to 0.390 Mev for the longer cavity higher Q tube No. 3. The Q of this tube was 6280 as compared to 9000 value for tube 3 and is lower in proportion to the decrease in volume due to the shorter length cavity. Since the coupling was the same in the two cases, the ratio of the two output voltages, at constant power level, would be expected to be the same as the square root of the Q times length ratio as predicted by the power relation. The agreement is only fair and is 2.05 for the voltage ratio as compared to 1.47 for the QL ratio. The discrepancy is not apparent, but might be associated with slightly different electron dynamics in the two cases. The results are sufficiently close, however, to allow an extrapolation of the data on a QL basis, and so lead to a determination of the approximate power requirements for the intermediate $\beta=0.96$ gun section and final $\beta=1.0$ stages of the accelerator.

The approximate excitation for these stages at 1-Mev/ft. gradient and extrapolated from the

0.624-megawatt/ft. value for tube No. 3 are 0.306 and 0.270 megawatt per ft. for the intermediate $\beta=0.96$ and final $\beta=1.0$ stages, respectively. The corresponding expected Q's would be 11,700 and 12,000, respectively.

For a 10-ft. accelerator, which length would approach the limiting value for the $\pi/2$ mode design and of coupling $K=9.05$ percent, the average excitation power required to maintain a 1-Mev/ft. gradient would be 0.319 megawatt/ft. In terms of the number of HK7 magnetrons required, this would amount to approximately one for each foot of accelerator.

While it has been demonstrated by the M.I.T. Accelerator Group[6] that stable parallel operation of magnetrons up to three magnetrons is possible, the usefulness of this type of accelerator as a generator of high energy particles and x-rays is greatly complicated by the large number of magnetrons and associated equipment involved. The successful outcome of the development of higher power magnetrons now in progress would greatly alter this picture.

The energy spread in the case of the two cavity tubes tested was large and of the order of $\frac{1}{3}$ to $\frac{1}{2}$ of the total output at high values of injection current. The apparent energy spread decreased as the injection beam current was decreased until at low values the spot was no larger than the injection beam spot, indicating more current coming through at the optimum phase. Although the energy spread for the 8-cavity tube was extremely low (accelerated spot same size as injection beam spot), it was felt that this was due in part to a limited range in entering angle brought about by the reduced gradient, rather than a direct indication of improved energy spread resulting from an increased number of cavities. The spread, however, should decrease with increasing number of cavities because of the greater time allowed for bunching. The theoretical study indicated that at 1-Mev/ft. gradient an energy spread of the order of 10 percent to 20 percent would be expected after the electron had traversed the first 3 ft. of tube. It is true that electrons starting at different points along the length would come through at varying energies, however, only those starting near the first few cavities would have a chance to synchronize with the wave.

TABLE I. Comparison of experimental with theoretical accelerated voltages at given axial gradients.

Accelerator section	Experimental			Theoretical		
	Inj. kv	Gradient attained Mev/ft.	Max. Mev output	Inj. kv	Gradient Mev/ft.	Expected Mev
(1) 8-cavity, $\beta=0.75$ length $K=17.75$ percent	57	0.52	0.57	50	0.763	0.625
(2) 2-cavity, $\beta=0.75$ length $K=17.75$ percent	65	0.72	0.234	50	0.763	0.190
(3) 2-cavity,* $\beta=0.75$ length $K=9.05$ percent	58	0.763	0.250	50	0.763	0.190
	58	1.00	0.315	50	1.00	0.250
	58	1.33	0.390	50	1.33	0.345

*=terminations at a partition

A mild form of r-f breakdown inside of the cavity occurred at a field of approximately 0.06 Mev/gap. This was observed as a general background illumination on the fluorescent screen. Both the background intensity and the x-ray output increased with excitation power. Also a slight increase in pressure was observed during the initial operating stages but disappeared after a short period of operation. The effect was usually encouraged by an axial magnetic field, which was probably due to a restriction of electron motion to the region of highest electric field. There was no indication that this breakdown was detrimental, as its occurrence produced no change in the r-f envelope shape.

In the case of tube 3, a well defined spot of energy approximately corresponding to that for the given excitation accompanied the breakdown, and so provided a means of determining the

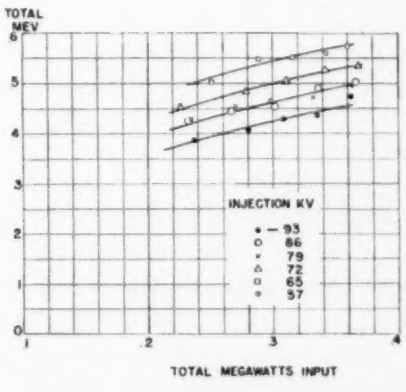

FIG. 6. 8-cavity, cavity terminated, $\beta=0.75$ tube total Mev *vs.* total megawatts input at different injection voltages. $\lambda_0=10.692$ cm (vac) (20°C); $Q=8000$; $K=17.75$ percent.

[6] Winston Bostick, Edgar Everhart, and Melvin Labitt, Tech. Report No. 14 of Research Laboratory of Electronics, Massachusetts Institute of Technology.

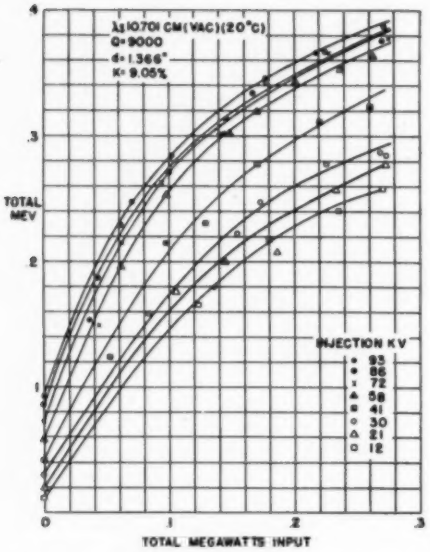

FIG. 7. Two-cavity, partition terminated, $\beta=0.75$ tube total Mev *vs.* total megawatts input at different injection voltages.

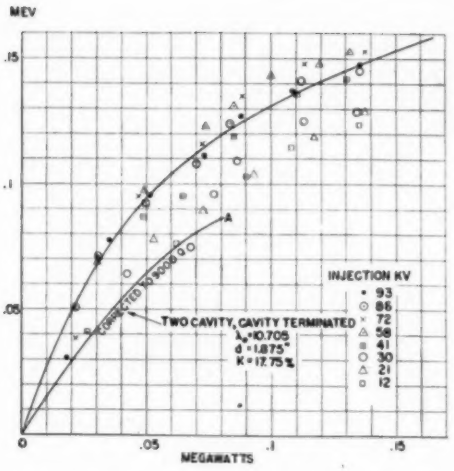

FIG. 8. Two-cavity, partition terminated, $\beta=0.75$ tube Mev *vs.* megawatt input for one cavity. $\lambda_0=10.701$ cm (vac) (20°C); $Q=9000$; $d=1.366''$; $K=9.05$ percent.

voltage at which complete breakdown occurred at different pressures. At a given cavity field, as the pressure was allowed to increase slowly, no change in spot deflection or r-f envelope shape was observed until very near the critical pressure for complete breakdown, which probably indicated that there was no predominant glow discharge period preceding the critical breakdown pressure. At the critical pressure the accelerated spot disappeared, the x-ray output decreased to zero, and the build-up and decay periods of the r-f envelope both collapsed. The critical pressures for two values of r-f field 0.09 Mev/gap and 0.14 Mev/gap (1.15 Mev/ft.) were 4.2 and 2.0 microns, respectively.

The resonance wave-length of the accelerator was observed to change with temperature and by an amount corresponding to +0.000225 cm per degree centigrade in the case of the 8-cavity tube No. 1. For a Q of 10,000 and $\lambda_0=10.7$ cm, a 4.8°C change should reduce the output to one-half. Actually the output remained essentially constant over approximately this range as the magnetron appeared to follow the resonance change. Temperature changes, in the case of short tubes such as would be used for x-ray application, should not be a serious consideration. In the case of long tubes, however, where it is important to maintain a constant cavity length so as to maintain proper phase relation between beam and exciting wave, temperature changes along the length of the accelerator would become a serious consideration.

CONCLUSIONS

The main conclusion is that although electrons can be accelerated to energies corresponding to a gradient of 1 Mev/ft. by this means, the power required to maintain this gradient is sufficiently high as to require an alarmingly large number of present day r-f power supplies such as the HK7 type magnetron. This viewpoint will change as large supplies of r-f power become more readily available.

Although the limiting length, set by mode interference, appears to be between 10 and 20 ft. at 10 cm, it is felt that this could be extended in proportion to the square root of the wave-length used. However, in doing so, the power required would be increased in proportion to the $(\lambda)^{\frac{1}{2}}$.

ACKNOWLEDGMENT

The authors wish to acknowledge the help and many suggestions offered by Dr. L. Tonks. We are also indebted to Mr. J. S. Balwit and Mr. R. Johnston for their assistance with the experimental work.

A Method for Measuring the Complex Dielectric Constant of Gases at Microwave Frequencies by Using a Resonant Cavity*

C. K. JEN
Cruft Laboratory, Harvard University, Cambridge, Massachusetts
(Received January 8, 1948)

A sensitive method has been developed for the measurement of the complex dielectric constant of low pressure gases at X-band microwave frequencies. The gas, whose complex dielectric properties are to be determined, is contained in a resonant cavity which is a part of the microwave circuit. With the introduction of the gas, the real part of the dielectric constant changes the resonant frequency of the cavity, while the imaginary part changes the amplitude and breadth of the cavity response curve. By a rapid variation of the frequency across the cavity resonance, the real and imaginary parts can be conveniently and accurately determined from measurements on an oscilloscope. Tests on such a system have been performed with satisfactory results. Sample data are presented for methylchloride and deuterated ammonia. This method can be used for the measurement of the resonant dispersion and absorption of microwaves by gas molecules. Also, the same method can be used for the measurement of loaded and unloaded Q-values of a cavity.

INTRODUCTION

THE experimental study of the complex dielectric properties of materials as a function of frequency has had a long history. Therefore, it is only natural that such measurements have now been extended to the microwave frequencies as a result of the rapid development of these very high frequency techniques in recent years. Both wave guides and resonant cavities containing the dielectric media have been commonly used for this purpose.[1–4] Until quite recently most of the attention has been directed to solid dielectrics and comparatively little to gases, but the tremendous progress made in microwave spectroscopy with gases is exciting considerable interest in measurements in gaseous media. Notable examples are found in the measurements of the absorption coefficient of O_2 by Beringer,[5] of NH_3 by Bleaney and Penrose,[6] and of NH_3 and many other gases by Hershberger.[7]

The object of the present work is to develop a more sensitive and accurate method of measuring at microwave frequencies the complex dielectric constant of gases at fairly low pressures. Such a method should be usable both for the nonresonant and the resonant dielectric properties. The X-band (8500–9750 Mc) is chosen partly because of the availability of apparatus and partly because of the anticipation that in the near future the X-band will also be a fruitful field for microwave spectroscopy. The method is, however, equally applicable to other frequency ranges. A resonant cavity has been chosen for this study because it is equivalent to a very long wave guide at its resonant frequency.

THEORY OF MEASUREMENT

A resonant cavity behaves in principle like a low frequency resonant circuit. Its properties are usually characterized by a loss factor (in this paper it will be called δ, which is the reciprocal of the customary Q-factor) and a resonant frequency. When a resonant cavity is coupled to a

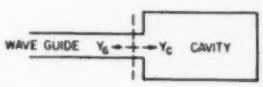

FIG. 1. Coupled cavity.

* The research reported in this document was made possible through support extended Cruft Laboratory, Harvard University, jointly by the Navy Department (Office of Naval Research) and the Signal Corps, U. S. Army, under ONR Contract N5ori-76, Task Order I. The contents of this paper have been reported earlier in Progress Report No. 2, for Contract N5ori-76, Cruft Laboratory, January 1, 1947.

[1] W. R. Maclean, J. App. Phys. **17**, 558 (1946).
[2] T. W. Dakin and C. N. Works, J. App. Phys. **18**, 789 (1947).
[3] C. N. Works, J. App. Phys. **18**, 605 (1947).
[4] S. Roberts and A. V. Hippel, J. App. Phys. **17**, 610 (1946).
[5] R. E. Beringer, M.I.T. Radiation Lab. Report No. 684.
[6] B. Bleaney and R. P. Penrose, Proc. Roy. Soc. **189**, 358 (1947).
[7] W. D. Hershberger, J. App. Phys. **17**, 495 (1946).

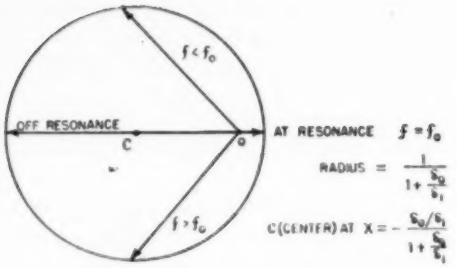

FIG. 2. Reflection factor circle diagram.

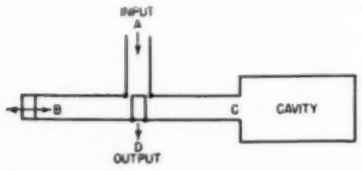

FIG. 3. Cavity coupled to magic tee.

wave guide, as shown in Fig. 1, the situation is again analogous to an ordinary coupled circuit at low frequencies. We can then derive by this analogy the admittance of the cavity (a "reflection" type in this case) as seen from the wave guide, with the following result:

$$Y_C = Y_G\left[\frac{\delta_0}{\delta_1} + j\frac{1}{\delta_1}\frac{f^2-f_0^2}{ff_0}\right], \tag{1}$$

where

Y_C = admittance of the cavity as seen from the wave guide,

Y_G = characteristic admittance of the wave guide,

$\delta_0 = \dfrac{\text{energy loss in cavity wall plus loss in medium per radian}}{\text{energy stored}}$,

$\delta_1 = \dfrac{\text{energy escaping from the input window per radian}}{\text{energy stored}}$,

f_0 = resonant frequency of the gas-filled cavity,

f = frequency of the incident wave.

In the neighborhood of the cavity resonance, i.e., $f \doteq f_0$, we have

$$Y_C \doteq Y_G\left[\frac{\delta_0}{\delta_1} + j\frac{2}{\delta_1}\frac{f-f_0}{f_0}\right]. \tag{2}$$

Defining Γ as the reflection factor which denotes

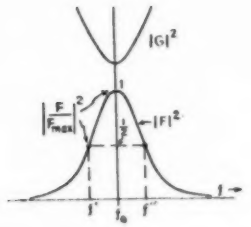

FIG. 4. Cavity resonance curves.

the ratio of the complex amplitude of the reflected wave from the cavity to that of the incident wave, we have

$$\Gamma = \frac{Y_G - Y_C}{Y_G + Y_C} \doteq \frac{1-\left(\dfrac{\delta_0}{\delta_1} + j\dfrac{2}{\delta_1}\dfrac{f-f_0}{f_0}\right)}{1+\left(\dfrac{\delta_0}{\delta_1} + j\dfrac{2}{\delta_1}\dfrac{f-f_0}{f_0}\right)}. \tag{3}$$

The vectorial plot of Γ is a circle as shown in Fig. 2. In order to translate the amplitude of the reflection factor into the usual form of a resonant response, we now adopt a so-called magic-tee arrangement as shown in Fig. 3. Here, the incident wave enters the magic tee at A, and then divides equally into branches B and C. At the end of branch B, there is a shorting plunger which always has a reflection factor $\Gamma \doteq -1$ in the immediate vicinity of the short. Depending upon the position of the plunger, this reflected wave can assume any phase difference relative to the wave reflected from the cavity when the two reflected waves combine at D. Furthermore, by the property of a magic tee, the vector difference of the two reflected waves passes through branch D, while the vector sum returns through branch A. Referring to the incident wave present in either branch B or branch C as unit amplitude, let

F = vector difference of the two reflected waves when branches B and C are equal in microwave phase,

G = vector difference of the two reflected waves when branches B and C differ by π in microwave phase;

then we have

$$\begin{aligned} F &= -1-\Gamma, \\ G &= +1-\Gamma. \end{aligned} \tag{4}$$

It follows that

$$|F|^2=\frac{1}{[1+(\delta_0/\delta_1)]^2+[(2/\delta_1)(f-f_0/f_0)]^2},$$

$$|G|^2=\frac{[(\delta_0/\delta_1)]^2+[(2/\delta_1)(f-f_0/f_0)]^2}{[1+(\delta_0/\delta_1)]^2+[(2/\delta_1)(f-f_0/f_0)]^2}.$$

At $f=f_0$, $|F|^2$ is a maximum while $|G|^2$ is a minimum. Thus, we have

$$|F|_{\max}/|G|_{\min}=\delta_1/\delta_0. \tag{5}$$

Referring to Fig. 4, at $|F/F_{\max}|^2=\frac{1}{2}$, the "half-power" frequency difference is related to the δ-values as follows:

$$(f''-f')/f_0=\delta_0+\delta_1. \tag{6}$$

Now, the left-hand terms of Eqs. (5) and (6) are two directly measurable quantities. For brevity, let

$$x=(f''-f'/f_0),$$
$$y=|F|_{\max}/|G|_{\min};$$

then we can determine δ_0 directly from the following expression:

$$\delta_0=(x/1+y). \tag{7}$$

Thus far we have not considered the differential effect of the gas. Suppose, to start with, the cavity is empty. Then in Eq. (2), we have

$$f_0=f_e,$$
$$\delta_0=\delta_e, \tag{8}$$

where the subscript e refers to quantities in an empty cavity. When the cavity is filled with gas, we must consider the changes resulting from the presence of the complex dielectric constant. Let the dielectric constant be expressed as follows:

$$\epsilon=\epsilon'-j\epsilon'', \tag{9}$$

where, for most gases, $\epsilon''\ll\epsilon'\doteq 1$. The admittance of a gas-filled cavity may then be written as

$$Y_C=Y_G\left[\frac{\delta_e}{\delta_1}+j\frac{2}{\delta_1}\frac{f-\dfrac{f_e}{(\epsilon)^{\frac{1}{2}}}}{\dfrac{f_e}{(\epsilon)^{\frac{1}{2}}}}\right]$$

$$\doteq Y_G\left[\frac{\delta_e+\epsilon''}{\delta_1}+j\frac{2}{\delta_1}\frac{f-\dfrac{f_e}{(\epsilon')^{\frac{1}{2}}}}{\dfrac{f_e}{(\epsilon')^{\frac{1}{2}}}}\right]. \tag{10}$$

Comparing Eq. (10) with Eq. (2), we see that with a gas-filled cavity,

$$f_0=f_e/(\epsilon')^{\frac{1}{2}},$$
$$\delta_0=\delta_e+\epsilon''. \tag{11}$$

We now conclude from Eq. (8) and Eq. (11), that for ϵ' very close to unity

$$\epsilon'=1-\frac{2}{(f_0)_{\text{empty}}}[(f_0)_{\text{gas}}-(f_0)_{\text{empty}}], \tag{12}$$

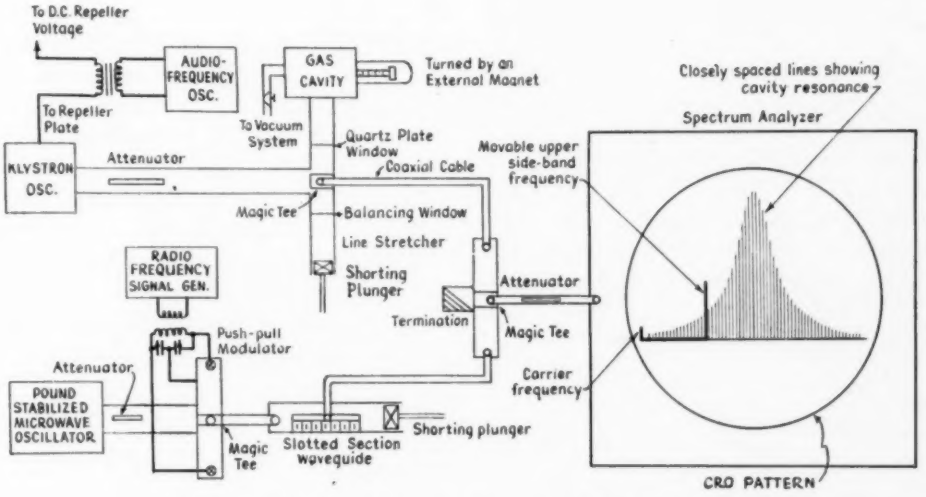

FIG. 5. Complete schematic diagram and CRO pattern.

and

$$\epsilon'' = (\delta_0)_{\text{gas}} - (\delta_0)_{\text{empty}}. \tag{13}$$

From Eqs. (12) and (13) we see that the real part of the dielectric constant can be calculated readily from the shift of the cavity resonance frequency and the imaginary part from the change in the loss factor as defined in Eq. (7). It should be remarked that the procedure of determining ϵ'' in Eq. (13) with the aid of Eq. (7) is essentially different from the apparently simpler procedure of using the following expression from Eq. (6):

$$\epsilon'' = (\delta_0 + \delta_1)_{\text{gas}} - (\delta_0 + \delta_1)_{\text{empty}}.$$

The latter statement would be true if δ_1 remains sensibly constant. Since the coupling factor δ_1 may vary with the introduction of gas, the loss factor δ_0 must be isolated from the total effect, thus necessitating the general treatment developed in Eqs. (4) to (7).

EXPERIMENTAL ARRANGEMENT

The experimental arrangement for carrying out the proposed measurements should consist essentially of one part which yields an amplitude-frequency display of the cavity resonance, and another part which serves to measure frequency differences on the same display. These objectives can be accomplished in a variety of ways, depending upon the degree of sensitivity required and the availability of instruments. It was found convenient for the present experiment to adopt a scheme as shown in Fig. 5.

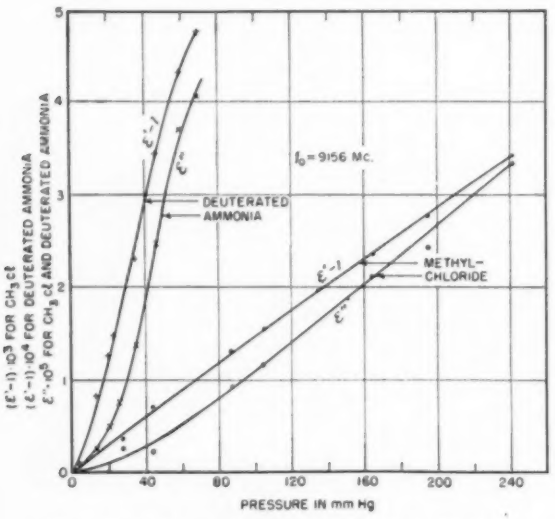

FIG. 6. $\epsilon'-1$ and ϵ'' values for methyl-chloride and deuterated ammonia.

The cavity tested here is of a type ordinarily used as an X-band wave meter, having an inner diameter of 4.952 cm. The cavity is tunable in the range 8500–9900 Mc. It has an unloaded Q-value of about 25,000. For evacuation and gas-filling purposes, the whole cavity is enclosed in a cylindrical brass housing, which is sealed on to the wave guide leading into the cavity. A sealed glass tube projecting from the same enclosure allows the cavity to be tuned by a magnetic micrometer head by means of an external magnet. The cavity is sealed from the wave guide by a window consisting of a quartz disk of about one-mm thickness with a silver-chromium evaporated film bordering the rectangular opening, which is soldered with Wood's metal to a special choke flange. To cancel the effect of the wave reflected by the quartz window, a similar window is placed symmetrically with respect to the magic-tee so that the reflected wave will not appear at the output. The microwave source is provided by a 2K25 reflex klystron, whose frequency can conveniently be swept in any desired manner.

For the measurement of frequency differences, use is made of another 2K25 klystron, frequency-stabilized by Pound's method.[8] The output is applied to a push-pull modulator, which mixes the microwave with a radiofrequency wave of a few Mc, thus producing two sideband frequencies with the carrier almost completely suppressed. One of the sideband frequencies can be conveniently used for measuring frequency differences since its position can be continuously changed relative to the stabilized carrier.

Measurement of the voltage ratios, either for determining the "half-power" points or the ratio $|F|_{\max}/|G|_{\min}$, is accomplished by comparison with a known voltage ratio in a slotted section of wave guide, in which the field distribution may be assumed to be sinusoidal.

Both the signal and frequency-measuring waves are then detected, amplified, and finally displayed on an oscilloscope. An X-band spectrum-analyzer,[9] designed by M.I.T. Radiation

[8] R. V. Pound, Proc. I.R.E. **35**, 1405 (1947).

[9] For an alternative scheme, see L. B. Young and L. G. Mann, Internal Report 55.5, M.I.T. Radiation Lab. (1945).

Laboratory, has been used for this purpose. Since the frequency of the local klystron of the spectrum analyzer is already swept at 60 cycles per second, it is necessary to sweep the signal frequency at a rate which is very much lower or higher than this. We have actually used a frequency of about 50 kc, which frequency modulates the klystron, as shown in Fig. 5. This operation results in an oscilloscopic pattern of closely spaced lines whose envelope represents the amplitude of the input wave. The frequency-measuring side frequency is superimposed on this pattern and is movable with respect to it by adjustment of the r-f oscillator. The whole pattern is also shown in Fig. 5.

In the measurement of the complex dielectric constant, two similar operations are performed, one with gas in the cavity and the other with the cavity evacuated. In each case, the center of the resonance curve is matched with one of the sideband frequencies and then the frequency difference of the "half-power" points is measured. The ratio $|F|_{max}/|G|_{min}$ is measured by adjusting the shorting plunger in the gas cavity assembly to show alternately a $|F|^2$-curve and a $|G|^2$-curve. Then, $|F|_{max}^2$ and $|G|_{min}^2$ are equalized by an attenuator at the input to the spectrum analyzer. The attenuator is calibrated from the standing-wave pattern in the slotted wave guide section of the stabilized assembly. The final results are then calculated from Eqs. (7), (12), and (13).

SAMPLE RESULTS OF MEASUREMENT

The experimental result for the sensitivity of the arrangement described above may be expressed in terms of the minimum detectable change for $\epsilon'-1$ and ϵ''. This value is estimated to be roughly 10^{-5} for $\epsilon'-1$ and 2×10^{-6} for ϵ''.

As a sample of a number of measurements, results for the complex dielectric constant of methyl-chloride (CH_3Cl) and of a mixture of deuterated ammonia (NH_3: 12.5 percent, NDH_2: 37.5 percent, ND_2H: 37.5 percent, ND_3: 12.5 percent, by volume) are presented in Fig. 6.

DISCUSSION

The above experimental results show that the proposed method can be successfully employed for the measurement of the complex dielectric constant of gases. From the magnitude of the absorption factor (ϵ'') and its dependence upon pressure, it can be concluded that the resonant absorption frequencies of deuterated ammonia are much nearer to the working frequency than those of methyl-chloride. It is well known that NH_3 exhibits "inversion" absorption for a band of frequencies around 24,000 Mc, and ND_3 is expected to absorb somewhere around 6000 Mc according to Manning's calculations.[10] It is reasonable to assume that the intermediate species have absorption frequencies between these limits. What we get here is the over-all effect of a number of selective absorptions by the mixture. For methyl-chloride the measured result may be due to resonant absorption[7] at frequencies somewhat higher than the normal K-band and partly due to non-resonant absorption (the zero-frequency contribution).

It can be seen that the present method is equally applicable to the measurement of resonant absorption and dispersion and, further, it should be able to predict the general location of the absorbing center from the dependence of the complex dielectric constant upon pressure and frequency.

From the way in which this experiment is performed, the loaded and unloaded Q-values are necessarily known quantities. Thus the method is also useful for the determination of such values, if desired.

ACKNOWLEDGMENT

The author is greatly indebted to Messrs. S. P. Cooke and J. R. Hooper, Jr. for their valuable advice and technical assistance. He is also grateful to Professor E. B. Wilson, Jr. for making deuterated ammonia available.

[10] M. F. Manning, J. Chem. Phys. **3**, 136 (1935).

Carbon Film Formation and Commutator Brush-Wear As Revealed by the Electron Microscope

ERNEST F. FULLAM AND ROBERT H. SAVAGE
The General Electric Research Laboratory, Schenectady, New York
(Received February 16, 1948)

The faces of carbon or graphite brushes, polished by rubbing against a rotating copper disk and subsequently examined with the electron microscope by means of surface replicas, are found to consist of many tilted "fingers," which are the projecting portions of the large and irregular graphite plates composing the brush. These graphite projections show a directional overlap, which is determined by the direction of motion of the disk, and when viewed stereoscopically they are found to be inclined at various angles up to nearly 90° with reference to the plane of the rotating base. They account for a previously observed "directional memory" of graphited surfaces and they show that such surfaces in general cannot be regarded as consisting simply of graphite plates oriented with the hexagonal planes flat and parallel to the plane of motion.

The brush track on the rotating copper base is found to contain small islands of carbon deposited from the brush. These islands consist of large numbers of graphite wear-fragments, which are individually of very small size in comparison with the projections of the brush face. These fragments are clearly derived from the projections by a tearing apart of their edges and are packed tightly and with random arrangement into the tool marks of the copper, smoothing over the irregularities of the latter. It is not determined whether this "carbon film" of the brush track is continuous.

The wear-dust of unlubricated graphite is found to consist of particles which are very small in average size compared with those from which brushes are manufactured. The size of these wear-fragments extends below the resolving power of the electron microscope, and this is consistent with recent data on similar particles of a size determined independently by adsorption measurements.

INTRODUCTION

THE carbon film which forms on collector-ring or commutator surfaces has been isolated and identified chemically,[1] and its importance is now well known. However, its structure—the arrangement of the crystals within the film—has not been revealed. The film has been presumed to consist of graphite platelets oriented with their slip-planes flat on the surfaces and parallel to the direction of motion. This view has been drawn from analogy with the established structure of "graphoid films" on bearing surfaces.[2]

Lately it has been suggested[3] that this view might not be correct but that the platelets may overlap in the direction of stroke to form a "shingled" layer. The initial evidence for this new viewpoint was based upon observations of steel ball bearings lubricated with graphite (containing small amounts of Apiezon grease) and operated in a sliding contact apparatus[3] in vacuum. It was found that the bearings operated quietly, with low friction, when revolving in the usual direction of rotation (clockwise) but that after reversal of rotation the bearings temporarily were noisy and showed high friction (at least 3×normal as estimated from deceleration measurements). In the course of a few minutes of operation in the new direction the bearing operation returned to normal. It was possible to repeat the high friction effect merely by reversing the rotational direction. The apparatus showed a directional memory and was even sensitive to a single slight displacement (e.g., a fraction of one revolution) in the direction producing frictional disturbance.

It was possible to understand this curious effect by assuming the overlapping already referred to. Subsequent experiments with carbon brushes operating upon slip-rings have shown supporting evidence of this directional effect. For example, the films formed under graphite brushes containing small amounts of inorganic salts, and operating with low friction under high altitude conditions in which less than the adequate concentration of water vapor was present,[4] were suddenly torn up simply by a reversal of rotation, the brushes then wearing out within a few minutes (unless given additional water vapor.)

[1] C. Van Brunt, unpublished reports (1937); also C. Van Brunt and R. H. Savage, Gen. Elec. Rev. **47**, 16 (1944).
[2] R. O. Jenkins, Phil. Mag. **17**, 457 (1934).
[3] R. H. Savage, J. App. Phys. **19**, 1 (1948).
[4] R. H. Savage, Gen. Elec. Rev. **48**, 13 (1945).

The practical and fundamental importance of the film structure thus became evident, and work has been done to learn more about the associated phenomena using the electron microscope. During this work it was found essential to investigate also the structure of the faces of brushes which were used to form the films, and the carbon dust formed by wear of brushes in vacuum equipment. The initial report on this work follows.

PREPARATION OF CARBON SAMPLES

Representative collector-films and polished brush faces were made by operating graphite brushes in a friction apparatus[3] on a copper disk rotating at 1750 r.p.m. This disk had been turned in a lathe to as smooth a face as could be conveniently machined in the laboratory. Abrasives and polishing powders were excluded, and precautions were taken to prevent contamination of the face after cleaning. The brushes were small rods of square cross section, machined from electrographitized carbon blocks made from a coke base and having the following physical characteristics: resistivity 1800 microhmcentimeter, scleroscope hardness 50, density 1.75. They

FIG. 1. Carbon motor-brush replica.

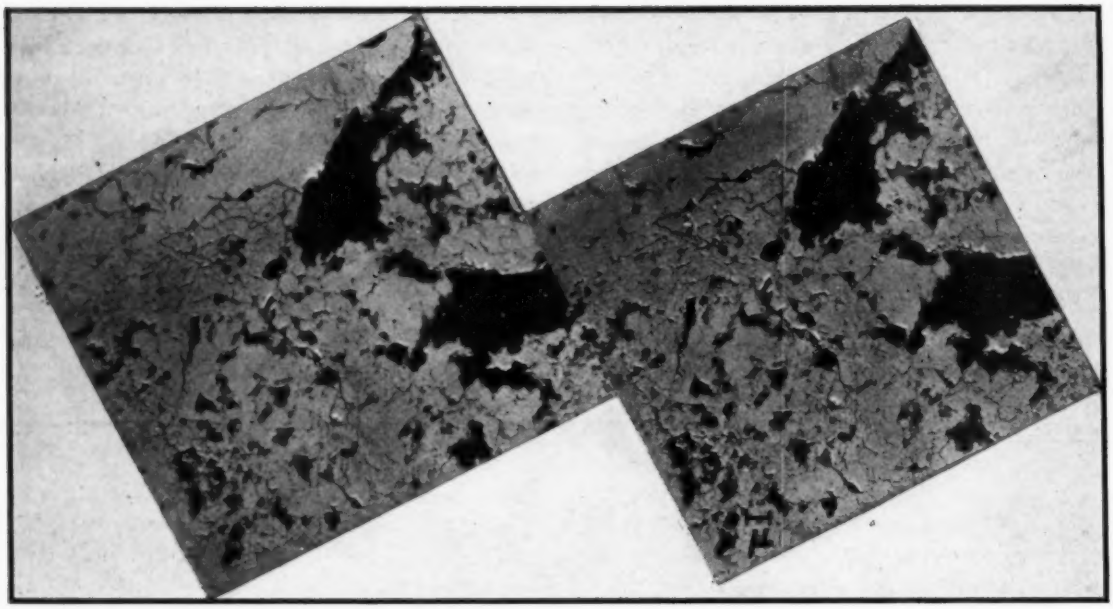

FIG. 2. Stereo of carbon motor-brush replica.

bore normally against the disk with apparent bearing areas of 0.06 cm^2 under spring loads of 0.092 kg. They did not carry current. The atmosphere was water vapor at the pressure of 7 mm (mercury), and the wear rate was observed to be nearly zero during the entire run, which was limited to one hour in order to limit the film thickness to partial transparency. Following this run the brush surfaces showed characteristic specular polish, and the unmagnified track was light gray against pale copper in general appearance. The brushes and disk were removed from the apparatus with considerable care so as to avoid any reversing motion upon the contact surfaces, which would tend to disturb the surface arrangement of the crystals and particles. Immediately following, these samples were transferred to covered petri dishes for examination.

ELECTRON MICROGRAPHS

To employ the high resolution and great depth of field of the electron microscope for this examination of the surfaces that had been in contact with one another, it was necessary to use surface

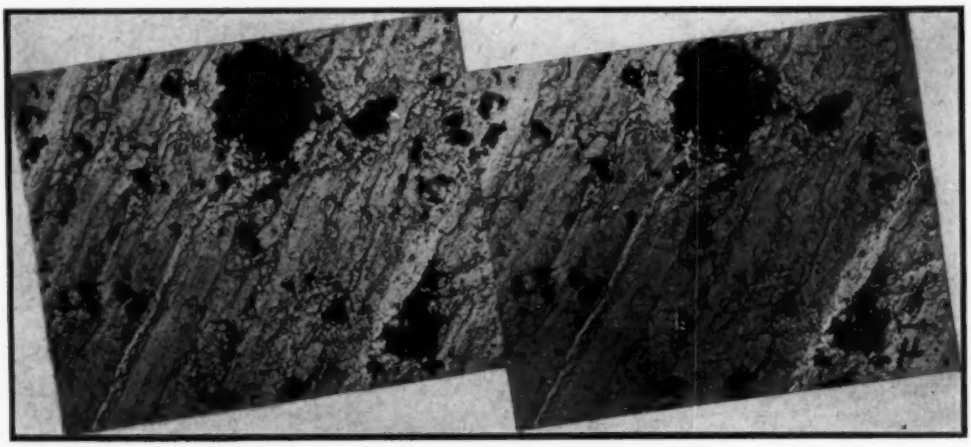

FIG. 3. Stereo of carbon film on copper surface.

replicas. These replicas were prepared in the following manner: a 10 percent solution of purified nitrocellulose in amyl acetate was placed on the surfaces to be examined and the solvent allowed to evaporate slowly. When the nitrocellulose film was hard, it was stripped mechanically from the surfaces, removing with it that material not firmly attached to the surface and reproducing in replica all other structures. Onto this surface a thin film of silica was evaporated in a vacuum by heating 1 mg of silica in a tungsten coil filament at a distance of 6.5 cm from the resin replica. The desired area of the replica was then selected under a light microscope and an electron microscope specimen screen fastened over it with the thin silica film in contact with the screen wires. The original replica was then dissolved away and the silica replica washed by the condensation of amyl acetate vapors directly on them. This operation leaves a thin silica replica over the openings of the specimen screen, retaining without displacement or alteration whatever material has been removed from the original surface by the nitrocellulose. Care must be exercised in the interpretation of an electron micrograph of such a combination of graphite and replica-of-graphite structures.

Figure 1 is a replica of a representative small area of one brush face. The magnification may be calculated from the superimposed micron scale. In this micrograph we see that plate-like particles comprising a portion of the surface protrude above the plane of the surface and overlap in the direction of motion of the copper, indicated by the arrow, thus forming many overlapping tongues or projections. These vary in diameter, in respect to surface, from less than 0.02 micron to particles larger than one micron, some of which are torn off by the original replica. Their number and distribution may vary over wide limits, as indicated by other pictures. The average area of the projections may be estimated at about 0.5 square micron although the great majority are much smaller with areas of the order 0.01 square micron. The edges of the projections are ragged and suggest that the process of normal friction is accompanied by continual tearing away of fragments from the edges.

In view of the extreme raggedness of the projections on the brush face, the term "shingles"

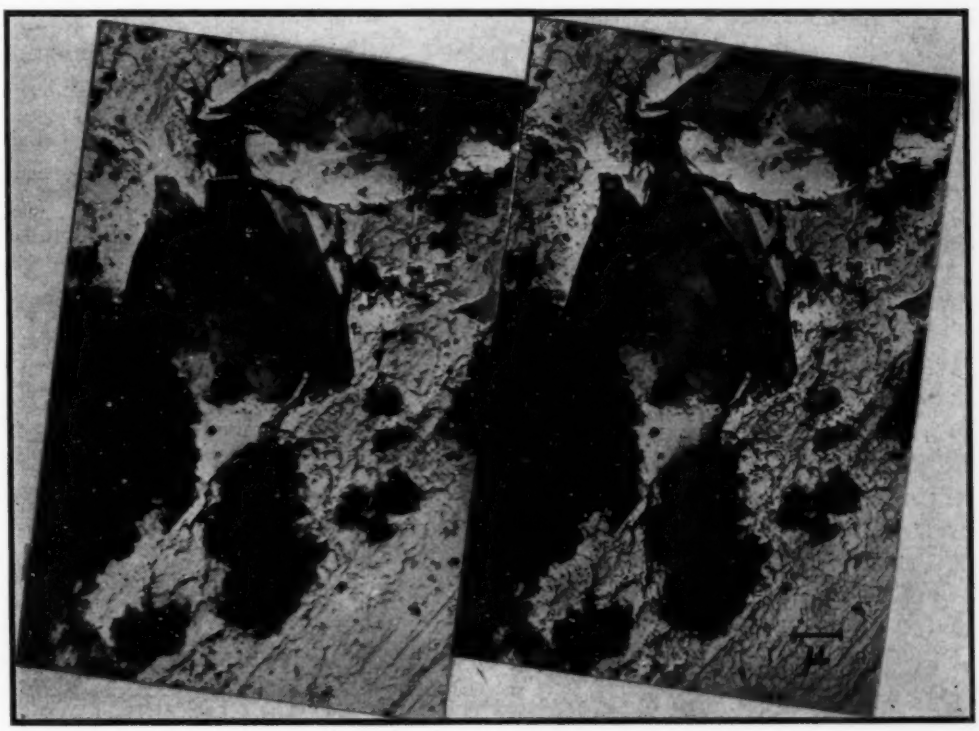

FIG. 4. Stereo of carbon film on copper surface.

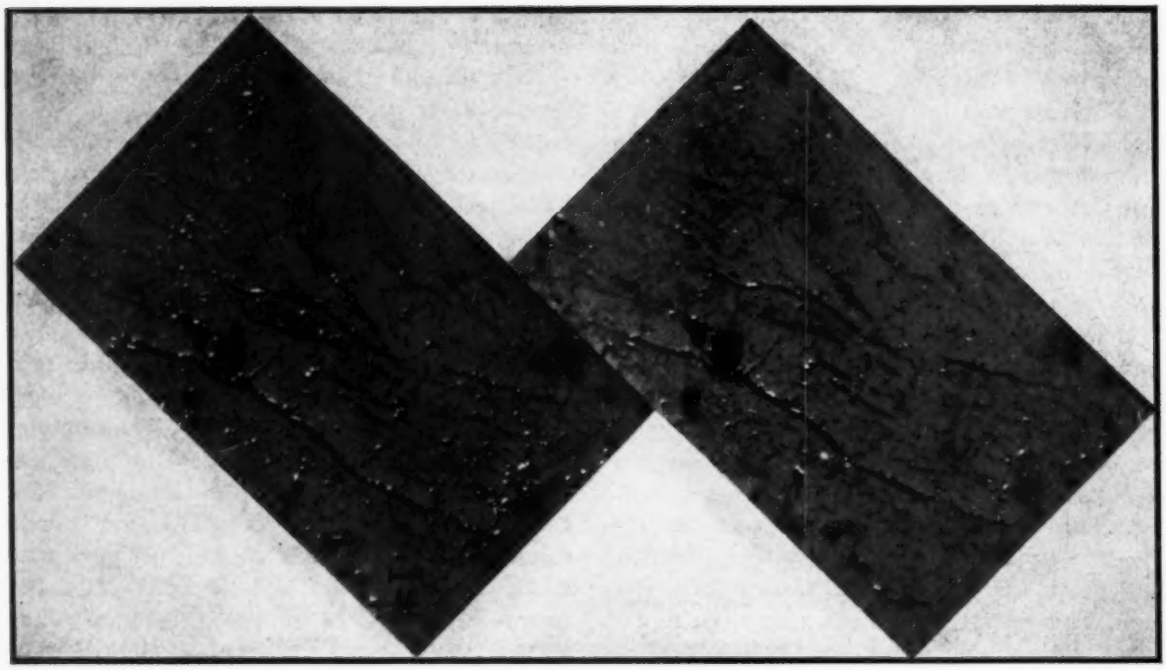

FIG. 5. Stereo of carbon motor-brush replica.

is now misleading, but it was originally used before any real conception of surface structure had been obtained, simply to suggest a directional overlapping.

Figure 2 is a stereoscopic electron micrograph of another brush-face replica. It is similar to Fig. 1, but stereoscopically one may see that the overlapping tongues are inclined to all angles up to nearly 90 degrees from the base plane, with most at less than 45 degrees. From this the suggestion is made that the areas of contact consist of individual surfaces formed by these tongues which are isolated tilted planes scattered over the entire face.

Electron diffraction patterns, contrary to these observations, have generally been interpreted as indicating that the crystals lie flat and parallel to the surface. However, such patterns do not reveal the detailed structure at the surface.

Figure 3 is a stereoscopic electron micrograph of a replica of the carbon film on the copper surface from which some loose carbon particles as aggregates have been transferred to the thin replica. The replica itself shows the tool marks in the copper and also reproduces the structures formed by the carbon particles that are tightly packed into these marks over scattered areas. Many irregularities of the copper surface evidently collect the carbon particles and are quickly encased by firmly packed particles. These protrusions then become relatively smooth, after which they remove little more material from the brushes. Some of the protrusions are no doubt broken, and rebuilt by the desposition of other particles. In the study of this type of brush no indications have been found that the copper contributes to this smoothing process by a localized flow, as might occur under the influence of increased temperature or pressure.

The direction of motion of the copper may be determined by the shape of some of the protrusions and by the preferred location of the loose carbon particles *on the trailing side of these*, as may be observed in the stereoscopic pictures. The direction of motion of the copper is indicated by the arrow in Fig. 3.

The pioneering work of Van Brunt[1] on carbon films clearly indicated a porous* but nevertheless *continuous* structure under the optical microscope at 100 diameters' magnification. Relatively large

* Pores were not actually observed, but the reagents quickly penetrated the film and attacked the underlying base.

sheets were isolated intact, and were found to be transparent over small thin areas, but were streaked and mottled in general appearance because of the opacity of thicker areas which were themselves discontinuous although contained within the whole film. The electron micrograph at high magnification (Fig. 3) was at first interpreted as indicating a discontinuous film structure, the only apparent film consisting of replicas of the isolated carbon-particle patches and clusters of carbon particles themselves. (The fine lines clearly represent the roughness elevations and depressions, or secondary tool marks in the copper.) However, such an interpretation of this micrograph is difficult to reconcile with the optical observations already referred to. Furthermore, it does not account for the observed fact that the nitrocellulose is much more easily stripped from the brush track than from the untouched copper. Accordingly, two alternative possibilities should be recorded. (a) The carbon film over the copper surface may be incompletely developed in the present instance. Its rate of formation may have decreased enormously after the first few traverses of the brush during which time enough islands were formed to support the brush face continuously. The film which had been found to be continuous under the optical microscope[1] had been prepared by a much longer run of 72 hours compared with the present film of 1 hour. Or (b) an extremely thin carbon film may actually cover these tool marks, conforming to them in such a way as to indicate no superimposed structure such as is shown by the large and semi-opaque graphite crystals occasionally noted.

Figure 4 is another stereoscopic electron micrograph of a replica of a brush track on the copper surface and shows in this instance a few graphite crystals which are very large and undistorted compared to the mass of particles on the surface. Here again the great majority of the particles have the same size and structure as the wear dust (see later) and were apparently produced by a breaking away from the edges of the tongues on the brush face, since their size is comparable with the irregularities of the tongues.

None of the micrographs of the brush track has shown evidence of even partial orientation of the graphite crystals relative to the base plane. The indicated crystalline arrangement is completely random wherever visible.

From the foregoing electron micrographs we are led to conclude that the brush face normally

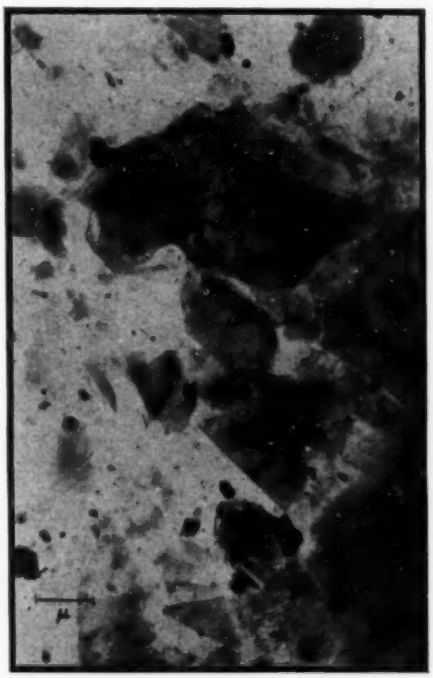

FIG. 6. Graphite stock powder No. 1107.

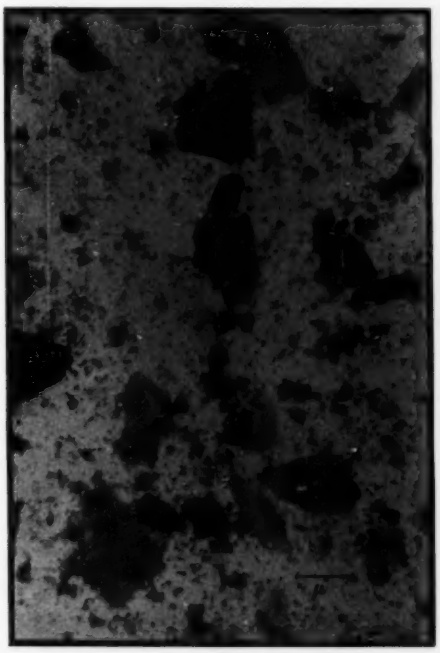

FIG. 7. Wear dust from No. 1107 brush.

contains a myriad of individually isolated graphite projections (tongues) stroked in the direction of motion so as to lie at varying obtuse angles to the base plane. These projections evidently provide the surfaces of true contact. They are undoubtedly flexible and elastic, and should support the load as a unified system which is probably unique in its resiliency and adaptability when in contact with irregular metal surfaces rotating at high speed.

The process of wear is expected to be a normal accompaniment of the friction between the brush-face projections and the collector surface and may occur intermittently as a gradual erosion of these projections until, as a limit, flat areas have developed. We should then expect renewed deposition of graphite over these flat and presumably inelastic areas or a tearing of them, under the excessive pressures of nonconforming surfaces, to uncover fresh projections. Film formation and wear are thus fundamental counterprocesses accompanying normal friction. Evidently, upon reversal of rotation a major rearrangement of the projections is required, which accounts for the directional memory of graphited surfaces as observed.

SUPPLEMENTARY OBSERVATIONS

An additional study has been made to check and to extend the foregoing observations. In this a second copper disk and new brushes were used. These were operated first in vacuum with high wear rates (track 1) in order to fit the rather irregular brush faces to the disk surface, then on a fresh area in a water vapor atmosphere at 6-mm (mercury) pressure for 6 minutes (track 2) to form a relatively thin film, and, finally, in the water vapor for 4 hours (track 3) to form a "well developed" film. The electron micrographs of the surface replicas made from these new samples confirmed the initial observations in all of their fundamental aspects. Small tilted projections on the brush face were again noted, and these were characterized by the directional overlap. Incidentally it was noted that the 6-minute film was similar to the 4-hour film, indicating that the time factor within these limits had not been an important variable. One difference was noted, however, between the first micrographs and the later ones: in the latter the projections were seemingly *more rounded* (Fig. 5). The suggestion is made tentatively that this difference may have resulted from slight structural or particulate differences between the different carbons which were used, or even between different successive cross sections of the same carbon, or, on the other hand, from different evaporation rates of silica from the filament during the formation of the replicas. Much more work is needed in order to clarify points such as this, and it is suggested that one approach which should also yield much other useful information will be through the use of carbons which differ greatly in their apparent physical properties, such as electrographitized black-carbon in comparison with crystalline natural graphite.

WEAR DUST

In order to understand more clearly the nature of the wearing process in relation to film formation and to film structure, attempts were made to determine the extent to which the individual particles in the brush are subdivided as a result of the wear. For this purpose it was essential to have reference micrographs of the particles initially making up the brushes and comparison micrographs of the dust produced by the wear of these same brushes. It was not possible to obtain satisfactory reference micrographs for the brushes which were used in the film study reported in the preceeding discussion because those brushes contained a large proportion of graphite derived from the coked binder; this had been crystallized from organic material during the final firing process so that the determination of its structure and form was greatly complicated. Therefore in place of the electrographitized brush a study was made of a natural-graphite type. This type had been made by firing a pressed crystalline natural-graphite powder (No. 1107) with about 2 percent coked binder, to about 1350°C.

Figure 6 is an electron micrograph of the No. 1107 graphite stock powder before the brush was pressed from this material. The sample was mounted by dispersing the particles in a nitrocellulose solution and drawing down the suspension on glass with a spatula.[5] The particles are seen to be predominantly very large in area,

[5] M. C. Schuster and E. F. Fullam, Ind. Eng. Chem. Anal. Ed. **18**, 653 (1946).

and so thin in many instances as to be penetrated by the electron beam. The characteristic hexagonal plate-like crystal structure may be easily identified.

Figure 7 is the comparison micrograph and shows the dust produced by wear of the No. 1107 brushes in the vacuum equipment. This dust shows a few large particles that have been chipped from the brush, and a large number of fine particles occurring in a size range which evidently extends below the resolving power of the electron microscope. It is thus evident that the process of wear and removal of debris results in a subdivision of the original graphite particles to very small fragments.

Electron micrographs of the wear dust made from the electrographitized brushes used in the film study were very similar to Fig. 7, showing a few chips of large size and a great number of small fragments. Many of the latter were of a size and thickness corresponding to edge irregularities and thickness of the projections of Fig. 1. From these observations it may be concluded that the process of wear involves the continual tearing away of the tongues of the brush face into many smaller fragments. Many of these fragments may be broken further into still smaller particles before being thrown from the copper disk. (Such an abrasive and crushing action as might be expected may partly separate at the edges the sheets of graphite comprising the particles so as to expose a large surface area.) Specific surface measurements[6] of the dust by nitrogen adsorption at $-195°C$ indicate a surface area of about 400 sq. m/gram.

ACKNOWLEDGMENTS

The authors are indebted to Miss Ruth Hager who prepared the replicas and the electron micrographs, and made many helpful suggestions in the course of the work.

One of the authors (R.H.S.) wishes especially to thank Raymond M. Fuoss of Yale University for having suggested to him initially the fundamental importance of applying the electron microscope to research on graphite sliding and brush wear, this suggestion having started the present work.

[6] R. H. Savage and Callaway Brown, J. Am. Chem. Soc. (in press).

The Radiation Patterns of Dielectric Rods—Experiment and Theory*

R. B. Watson and C. W. Horton

Defense Research Laboratory, The University of Texas, Austin, Texas

(Received January 19, 1948)

A theory is developed describing the electromagnetic radiation from dielectric rods used as terminations to rectangular wave guides. The radiation patterns are computed from the fields due to equivalent magnetic and electric currents on the surfaces of the rods. These equivalent currents are determined by use of Schelkunoff's equivalence principle applied to approximate fields within the dielectric. Specific calculations are carried out for rods whose average dimensions are $0.9'' \times 0.25''$ and whose lengths vary from three to ten wave-lengths. Experimental patterns are obtained for eight polystyrene rods, some of which are variable in length. Agreement with theory is found for rods from three to six wave-lengths long; differences between experiment and theory are discussed.

INTRODUCTION

A THEORY has been developed describing the electromagnetic radiation from dielectric rods used as terminations to rectangular metallic wave guides. In particular, the theory leads to expressions for the radiation patterns for certain dielectric rods, which are in agreement with experimental observations for rods not longer than six wave-lengths.

The theory is an application to dielectric rods of the equivalence principle stated by

* The work described in this paper was done at the Defense Research Laboratory under the sponsorship of the Bureau of Ordnance, Navy Department, Contract NOrd-9195.

Schelkunoff.[1] This principle leads to the establishment of equivalent magnetic and electric currents over the surface of a particular rod; from these currents the radiation pattern may be computed. The equivalent currents are calculated from the tangential components of the electric and magnetic vectors at the surface of the rod. In order to carry out this calculation exactly, the electromagnetic field in the dielectric must be known. Although the problem of finding this field has not been solved, reasonable approximations may be made for the field. The radiation patterns thus computed agree with experiment. Specifically, patterns are calculated for a dielectric rod whose average dimensions are $0.9'' \times 0.25''$ and whose length varies from three to ten wave-lengths. This dielectric rod is inserted in a wave guide which is excited in the $TE_{0,1}$ mode.

Experimental patterns are obtained for eight different polystyrene rods of rectangular cross section. These patterns agree well with the corresponding ones based on theory; detailed analysis is made of the differences in terms of the theoretical approximations and experimental variations.

THEORY

The equivalence principle states (in part) that the electromagnetic field inside a surface Σ due to sources outside the surface can be produced by sheet electric currents $\mathbf{J}$ and sheet magnetic currents $\mathbf{M}$ over Σ given by

$$\mathbf{J} = -\mathbf{n} \times \mathbf{H}^0, \tag{1}$$

$$\mathbf{M} = \mathbf{n} \times \mathbf{E}^0, \tag{2}$$

where $\mathbf{n}$ is the unit normal vector directed outward from Σ, $\times$ denotes the vector product, and $\mathbf{E}^0$ and $\mathbf{H}^0$ are the values of the electric and magnetic vectors $\mathbf{E}$ and $\mathbf{H}$ on the surface Σ. In terms of these equivalent currents, the magnetic vector potential $\mathbf{A}$ and the electric vector potential $\mathbf{F}$ at a point P within the surface are given by:

$$\mathbf{A} = \frac{1}{4\pi} \int_\Sigma \mathbf{J} \frac{\exp(jkr')}{r'} d\Sigma, \tag{3}$$

$$\mathbf{F} = \frac{1}{4\pi} \int_\Sigma \mathbf{M} \frac{\exp(jkr')}{r'} d\Sigma, \tag{4}$$

where r' = distance from $d\Sigma$ to the point P, $k = 2\pi/\lambda$, λ = wave-length in free space, and $j = (-1)^{\frac{1}{2}}$. In terms of these potentials, the electric and magnetic fields at the point P are:

$$\mathbf{E} = j\omega\mu\mathbf{A} - (1/j\omega\epsilon) \text{ grad div}\mathbf{A} - \text{curl}\mathbf{F}, \tag{5}$$

$$\mathbf{H} = j\omega\epsilon\mathbf{F} - (1/j\omega\mu) \text{ grad div}\mathbf{F} + \text{curl}\mathbf{A}, \tag{6}$$

where ω = angular frequency, ϵ = dielectric constant, μ = permeability. These six equations allow calculation of the radiation pattern provided that $\mathbf{E}^0$ and $\mathbf{H}^0$ are known.

In the application of these general statements to the problem of the radiation from a dielectric rod it is necessary to examine the detailed nature of the fields $\mathbf{E}^0$, $\mathbf{H}^0$. The dielectric rod serves as a termination for a rectangular metallic wave guide, as shown in Fig. 1. The dimensions of the rod are the same as the wave guide dimensions at the junction point and are assumed to vary only slowly with distance from the end of the wave guide. The surface corresponding to Σ consists of the outside surfaces of the wave guide and dielectric rod and is closed by an infinitely large sphere about the origin. The sources are within the wave guide. It is assumed that for short distances (a few wave-lengths) outside of the wave guide, the field within the dielectric is not far different from the field in the guide. This is reasonable, for the dielectric is inserted within the guide a considerable distance. A tapered termination is included to prevent excessive reflections and generation of harmonic waves at the junction between air and dielectric. Also, the shape of the dielectric is sensibly the same as that of the guide. Hence the field in the portion of the dielectric within the guide is

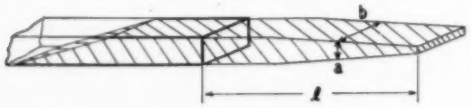

FIG. 1. Dielectric rod as termination for rectangular wave guide.

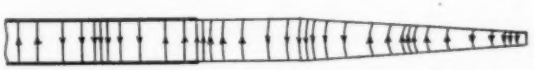

FIG. 2. Variation in electric field along length of dielectric rod.

[1] Bell Sys. Tech. J. **15**, 93 (1936).

accurately the same as the field in the empty guide; the considerable difference in dielectric constant between the dielectric and air should prevent excessive changes in the field in the dielectric outside of the guide, at least for short distances.

The tangential components of the electric and magnetic vectors at the surface Σ are the only quantities giving rise to the sheet currents, as is indicated by Eqs. (1) and (2). The tangential components over the surface of the wave guide will be assumed zero. This is a very good approximation for the electric vector, since the wave guide is a good conductor. The fields are further assumed to vanish at large distances, so that the only part of the surface Σ on which the tangential components of the field are significant is that portion in contact with the surface of the dielectric.

APPLICATION TO $TE_{0,1}$ MODE OF EXCITATION

The transverse electric wave in the wave guide designated $TE_{0,1}$ is of especial interest. The electric vector has the form

$$\mathbf{E}_{0,1} = \mathbf{i}\left(\cos\frac{\pi y}{b}\right)\exp(-j(\omega t - k'z)), \qquad (7)$$

where $k' = 2\pi/\lambda_g$, λ_g = wave-length inside the guide, $\mathbf{i}$ = unit vector in the x direction, and b = width of wave guide, and also of dielectric rod. The magnetic vector has the form

$$\mathbf{H}_{0,1} = \left\{\mathbf{j}\frac{k'}{\omega\mu}\cos\frac{\pi y}{b} + \frac{\mathbf{k}}{j\omega\mu}\sin\frac{\pi y}{b}\right\} \times\exp(-j(\omega t - k'z)), \qquad (8)$$

where $\mathbf{j}$ and $\mathbf{k}$ are unit vectors in the y and z directions, respectively.

The field at the surface of the dielectric will produce (in general) five categories of equivalent currents. The first three of these will be considered in detail.

(a) Magnetic currents on top and bottom (wide surfaces).

(b) Electric currents on the sides (narrow surfaces).

(c) Electric currents on the top and bottom.

(d) Magnetic currents on the sides. These currents arise from the tangential component of the electric vector at these surfaces. The electric vector vanishes at the sides in the wave guide, and therefore cannot be of appreciable magnitude in the dielectric. These currents are then assumed negligible.

(e) Electric and magnetic currents on the end. Because of the small radiation area of the end face compared to the other surface areas of the dielectric rod, the effect of any equivalent currents on the end is neglected.

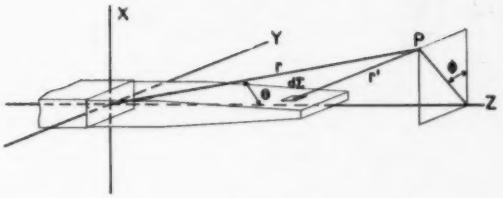

FIG. 3. Coordinate systems used in pattern computations.

(a) Magnetic Currents on Top and Bottom

The electric field inside the wave guide has zero tangential components on these surfaces; if the field in the dielectric were exactly the same as in the wave guide, the magnetic currents would vanish. There is undoubtedly a flow of energy through these surfaces, and hence it is concluded that the electric vector departs from the normal and has a tangential component parallel to the z axis. A suggested variation of the field is indicated by Fig. 2. The tangential components at top and bottom are in opposite directions, but so are the corresponding vectors $\mathbf{n}$; hence the magnetic currents $\mathbf{M}$ are in the same direction. The resultant magnetic currents are assumed to vary across the width of the guide as does the x component of the electric field, since it is the distortion of this component that leads to the currents. Hence

$$\mathbf{M} = \mathbf{j}M_0\cos(\pi y/b)\exp(-j\omega t)\sin k'z. \qquad (9)$$

Here $k' = 2\pi/\lambda_w$, where λ_w is the wave-length in the dielectric. These currents are distributed over the length and width of the dielectric rod. The general form for the variation in the z direction, $\exp(jk'z)$, is particularized here to $\sin k'z$ in order that the currents shall vanish at the opening of the wave guide as required by the absence of a tangential component within the guide. Since only the magnetic currents on the surfaces of the dielectric are to be considered, the electric currents are taken as zero, and, correspondingly, $\mathbf{A}$ from Eq. (3) is zero. The

value of $\mathbf{F}$ is given by Eq. (4) as:

$$\mathbf{F}=\frac{\mathbf{j}}{4\pi}\int_{\Sigma} M_0\left(\cos\frac{\pi y}{b}\right)(\sin k'z) \times\exp(-j\omega t)\frac{\exp(jkr')}{r'}d\Sigma. \quad (10)$$

In evaluating this integral it is convenient to designate the field point P by polar coordinates (r,θ,ϕ), while the location of the surface element $d\Sigma$ on the dielectric rod is specified by the Cartesian coordinates (x,y,z). The relationship between these coordinate systems is illustrated in Fig. 3. It is easily seen that when r is very much larger than the length of the rod, by neglecting higher order terms

$$r'=r-x\sin\theta\cos\phi-y\sin\theta\sin\phi-z\cos\theta. \quad (11)$$

The variation of r' over the length of the dielectric rod is insignificant in determining the value of the integral in Eq. (10), except for the exponential term $\exp(jkr')$. Thus r' is put equal to r in the denominator, and this term may be removed from the integral together with the term $\exp(jkr)$ resulting from substitution of Eq. (11) for r' in the exponential. Hence Eq. (10) becomes

$$\left.\begin{aligned}\mathbf{F}&=\mathbf{j}P_1(\theta,\phi)\frac{\exp(jkr-j\omega t)}{4\pi r},\\ P_1(\theta,\phi)&=\int_{\Sigma} M_0\left(\cos\frac{\pi y}{b}\right)(\sin k'z)\\ &\quad\times\exp(-jk(z\cos\theta+y\sin\theta\sin\phi\\ &\quad+x\sin\theta\cos\phi))d\Sigma.\end{aligned}\right\} \quad (12)$$

This integral is a function of the variables (θ,ϕ), and of the parameters, M_0, k, k', and the dimensions of the dielectric rod; the integration is to be carried out over the surfaces of the dielectric.

Next, the vector operations of Eqs. (5) and (6) must be carried out to find $\mathbf{E}$ and $\mathbf{H}$ at the field point P. Since $\mathbf{A}$ is zero, Eqs. (5) and (6) reduce to the following:

$$\mathbf{E}=-\text{curl}\mathbf{F}, \quad (13)$$

$$\mathbf{H}=j\omega\epsilon\mathbf{F}-\frac{1}{j\omega\mu}\text{ grad div }\mathbf{F}. \quad (14)$$

These operations are to be taken with respect to the coordinates (r,θ,ϕ), and hence $P_1(\theta,\phi)$ must be explicitly considered. However, if r is taken large, the terms involving derivatives of $P_1(\theta,\phi)$ become negligible. Hence P_1 will be taken as a scalar constant in the evaluation of Eqs. (13) and (14). Neglecting terms in $(1/r^2)$,

$$\text{curl}\mathbf{F}=\frac{1}{4\pi}\left\{\mathbf{i}\left(\frac{jk}{r}\cos\theta\right)-\mathbf{k}\left(\frac{jk}{r}\sin\theta\cos\phi\right)\right\}\times\exp(jkr-j\omega t)P_1(\theta,\phi). \quad (15)$$

Now $\mathbf{E}=-\text{curl}\mathbf{F}$, which is the negative of Eq. (15); when $\mathbf{k}$ and $\mathbf{i}$ are converted to polar coordinates, then (the term $\exp(jkr-j\omega t)/4\pi r$ which represents a spherical diverging wave is omitted throughout the remainder of this section)

$$\left.\begin{aligned}E_r&=0,\\ E_\theta&=(jk\cos\phi)P_1(\theta,\phi),\\ E_\phi&=(-jk\sin\phi\cos\theta)P_1(\theta,\phi).\end{aligned}\right\} \quad (16)$$

A complete solution requires the detailed evaluation of $P_1(\theta,\phi)$. As is shown in Fig. 1, the rod is supposed to be of rectangular cross section, of length l, average width a and depth b. Accordingly, the limits on the integral over Σ run from 0 to l in the z direction, and from $-(b/2)$ to $+(b/2)$ in the y direction; but x has only two values, $+(a/2)$ and $-(a/2)$. The integrand arises from the evaluation of $(\exp(jkr')/r')$. Since x takes on only the values $\pm(a/2)$, x may be replaced immediately by these values, so that two terms arise in the integrand. Also, $d\Sigma$ may be replaced by $dS=dydz$. Thus:

$$P_1(\theta,\phi)=\int_s M_0\left[\exp\left(-jk\frac{a}{2}\sin\theta\cos\phi\right)+\exp\left(jk\frac{a}{2}\sin\theta\cos\phi\right)\right]\cos\frac{\pi y}{b}\cdot(\sin k'z)\times\exp(-jk(z\cos\theta+y\sin\theta\sin\phi))dydz. \quad (17)$$

Consolidating terms gives:

$$P_1(\theta,\phi)=M_0\cos\left[\frac{ka}{2}\sin\theta\cos\phi\right]\cdot\int_s\left(\cos\frac{\pi y}{b}\right)(\sin k'z)\times\exp(-jk(z\cos\theta+y\sin\theta\sin\phi))dydz. \quad (18)$$

Separating the y and z portions of the integral then gives:

$$\left.\begin{aligned} P_1(\theta,\phi) &= M_0 \cos\left[\frac{ka}{2}\sin\theta\cos\phi\right]\cdot I_1\cdot I_2, \\ I_1 &= \int_{-(b/2)}^{+(b/2)} \left(\cos\frac{\pi y}{b}\right) \\ &\qquad \times\exp(-jky\sin\theta\sin\phi)dy, \\ I_2 &= \int_0^l (\sin k'z)\exp(-jkz\cos\theta)dz. \end{aligned}\right\} \quad (19)$$

An evaluation of I_1 and I_2 leads to:

$$\left.\begin{aligned} I_1 &= \frac{2b}{\pi}\frac{\left(\frac{\pi}{2}\right)^2\cos\left(\frac{kb}{2}\sin\theta\sin\phi\right)}{\left(\frac{\pi}{2}\right)^2-\left(\frac{kb}{2}\sin\theta\sin\phi\right)^2}, \\ I_2 &= \frac{1}{2k}(A-jB), \\ A &= \frac{1}{n-\cos\theta}[1-\cos\{(n-\cos\theta)kl\}] \\ &\quad +\frac{1}{n+\cos\theta}[1-\cos\{(n+\cos\theta)kl\}], \\ B &= \frac{\sin\{(n-\cos\theta)kl\}}{n-\cos\theta}-\frac{\sin\{(n+\cos\theta)kl\}}{n+\cos\theta}, \\ n &= k'/k. \end{aligned}\right\} \quad (20)$$

From Eq. (16) it is seen that for large distances from the dielectric rod the electric vector forms a plane wave. The magnetic vector may be found directly without recourse to Eq. (14), as:

$$\left.\begin{aligned} H_r &= 0, \\ H_\theta &= -\frac{k}{\omega\mu}E_\phi = j\frac{k^2}{\omega\mu}\sin\phi\cos\theta P_1(\theta,\phi), \\ H_\phi &= \frac{k}{\omega\mu}E_\theta = j\frac{k^2}{\omega\mu}\cos\phi P_1(\theta,\phi). \end{aligned}\right\} \quad (21)$$

The terms in Eq. (16), as amplified by Eqs. (19) and (20), have the following explanation:

(a) The term $\cos(\frac{1}{2}ka\cos\phi\sin\theta)$ in Eq. (19) arises because of the fact that the magnetic currents are present on two plane parallel surfaces separated by a distance a.

(b) The $\sin\phi$ and $\cos\phi$ terms in Eq. (16) arise because the electric field is polarized.

(c) The term $\cos\theta$ in E_ϕ arises because the magnetic currents in a surface element dS behave like dipole oscillators parallel to the y axis. (Later it appears that the factor $\cos\theta$ occurs in E_θ when the source is electric currents on the side.)

(d) The integral I_1 in Eq. (19) represents the part of the pattern contributed by the finite width b of the dielectric rod. The term $\cos(\pi y/b)$ in the integrand of I_1 represents the shading of the magnetic currents in accordance with the $TE_{0,1}$ excitation.

(e) The integral I_2 in Eq. (19) represents the effect of the length of the dielectric rod. Both k and k' enter into the expression; the significant quantity appears to be k'/k, which depends on the thickness of the dielectric rod.

Experimental patterns are usually confined to certain planes: specifically, measurements of the E-vector in the planes $\phi=0$ and $\phi=\pi/2$. The equations for E simplify: for the E-plane, $\phi=0$,

$$\left.\begin{aligned} I_{10} &= \frac{2b}{\pi}, \\ I_2 &\text{ remains the same,} \\ P_1(\theta,0) &= M_0\cos\left[\frac{ka}{2}\sin\theta\right]\cdot\frac{2b}{\pi}\cdot I_2, \\ E_\theta &= jk\cdot P_1(\theta,0), \\ E_\phi &= 0. \end{aligned}\right\} \quad (22)$$

Likewise for the H-plane, $\phi=\pi/2$,

$$\left.\begin{aligned} I_{1(\pi/2)} &= \frac{2b}{\pi}\frac{\left(\frac{\pi}{2}\right)^2\cos\left(\frac{kb}{2}\sin\theta\right)}{\left(\frac{\pi}{2}\right)^2-\left(\frac{kb}{2}\sin\theta\right)^2}, \\ I_2 &\text{ remains the same,} \\ P_1(\theta,\pi/2) &= M_0\cdot I_{1(\pi/2)}\cdot I_2, \\ E_\theta &= 0, \\ E_\phi &= -jk\cos\theta\cdot P_1(\theta,\pi/2). \end{aligned}\right\} \quad (23)$$

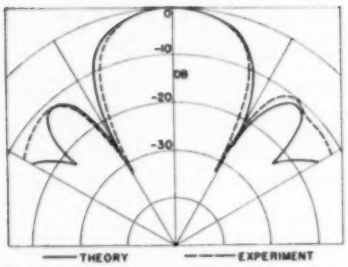

FIG. 4. Patterns in E-plane for dielectric rod with $l=4.22\lambda$, $n=1.10$.

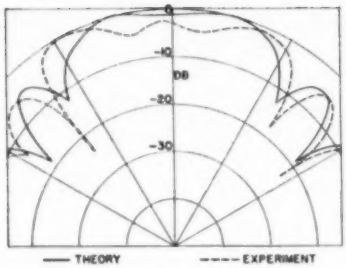

FIG. 5. Patterns in E-plane for dielectric rod with $l=4.22\lambda$, $n=1.30$.

(b) Electric Currents on the Sides

A similar theoretical analysis may be carried out for the electric currents on the sides of the dielectric rod. These currents are given by Eq. (1); for the $TE_{0,1}$ mode, the field at the surface should have a tangential component corresponding to the component of the field in the z direction inside the wave guide:

$$H_z = B \sin(\pi y/b) \exp(jk'z - j\omega t), \tag{24}$$

where B is an arbitrary constant. Evaluating the term in y for the sides of the rod, the surface electric currents are:

$$\mathbf{J} = \mathbf{i} J_0 \sin k'z \exp(-j\omega t). \tag{25}$$

In this equation, the term $\exp(jk'z)$ has been replaced by the term $\sin k'z$, indicating that the currents in the neighborhood of the opening of the wave guide are insignificant in contributing to the radiation pattern. This choice of the variation with z is based primarily on experimental evidence. Making use of Eq. (11) and putting in the appropriate values of r' as before leads to the value of the vector potential $\mathbf{A}$:

$$\left.\begin{aligned} \mathbf{A} &= \mathbf{i}\frac{\exp(jkr - j\omega t)}{4\pi r} P_2(\theta,\phi), \\ P_2(\theta,\phi) &= \int_\Sigma J_0 \sin k'z \exp(-jk(z\cos\theta \\ &\quad + y\sin\theta\sin\phi + x\sin\theta\cos\phi))d\Sigma. \end{aligned}\right\} \tag{26}$$

Considering only the contributions from these currents, and therefore putting $\mathbf{F}=0$, Eq. (6) simplifies to: $\mathbf{H}=\text{curl}\mathbf{A}$. Ignoring the action of the vector operations on $P_2(\theta,\phi)$ in Eq. (26) and neglecting terms of the order of $1/r^2$, the components of $\mathbf{H}$ are found to be (omitting the factor $\exp(jkr - j\omega t)/4\pi r$ throughout the rest of this section):

$$\left.\begin{aligned} H_r &= 0, \\ H_\theta &= jk(\sin\phi)P_2(\theta,\phi), \\ H_\phi &= jk(\cos\theta\cos\phi)P_2(\theta,\phi). \end{aligned}\right\} \tag{27}$$

These equations are recognized as those for a plane wave when r is large, and therefore instead of using Eq. (5) for $\mathbf{E}$, more directly:

$$\left.\begin{aligned} E_r &= 0, \\ E_\theta &= (\omega\mu/k)H_\phi = (j\omega\mu)(\cos\theta\cos\phi)P_2(\theta,\phi), \\ E_\phi &= -(\omega\mu/k)H_\theta = -(j\omega\mu)(\sin\phi)P_2(\theta,\phi). \end{aligned}\right\} \tag{28}$$

As before, the integrand in $P_2(\theta,\phi)$ arises in part from the evaluation of $(\exp(jkr')/r')$. Since here y takes on only the values $\pm\frac{1}{2}b$, two terms arise in the integrand: these two terms become constants so far as the integration is concerned, and the surface element reduces to $dxdz$. Thus,

$$\left.\begin{aligned} P_2(\theta,\phi) &= -J_0 \cdot 2\cos[(kb/2)\sin\theta\sin\phi] \\ &\quad \cdot I_3 \cdot I_4, \\ I_3 &= \int_{-(a/2)}^{+(a/2)} \exp(-jkx\sin\theta\cos\phi)dx, \\ I_4 &= \int_0^l \sin k'z \exp(-jkz\cos\theta)dz. \end{aligned}\right\} \tag{29}$$

It is seen that I_4 is the same as I_2 in Eq. (19); this integral is evaluated in Eq. (20). I_3 has the value:

$$I_3 = \frac{2}{k}\frac{\sin[(ka/2)\sin\theta\cos\phi]}{\sin\theta\sin\phi}. \tag{30}$$

Evaluating the equations for the E- and H-planes

gives: E-plane: $\phi=0$

$$\left.\begin{aligned} I_{30}&=-\frac{2}{k}\frac{\sin[(ka/2)\sin\theta]}{\sin\theta},\\ I_4&=I_2 \text{ remains unchanged,}\\ P_2(\theta,0)&=-2J_0\frac{2}{k}\frac{\sin[(ka/2)\sin\theta]}{\sin\theta}\cdot I_2,\\ E_\theta&=j\omega\mu(\cos\theta)\cdot P_2(\theta,0),\\ E_\phi&=0. \end{aligned}\right\} \quad (31)$$

H-plane: $\phi=\pi/2$:

$$\left.\begin{aligned} I_{3(\pi/2)}&=a,\\ I_2&\text{ remains unchanged,}\\ P_2\left(\theta,\frac{\pi}{2}\right)&=-2J_0 a\cos\left[\frac{kb}{2}\sin\theta\right]\cdot I_2,\\ E_\theta&=0,\\ E_\phi&=-j\omega\mu P_2[\theta,(\pi/2)]. \end{aligned}\right\} \quad (32)$$

The expressions for the patterns for the E- and H-planes for magnetic currents on top and bottom and electric currents on the sides as summarized in Eqs. (22), (23), (31), and (32) are seen to have certain similarities and differences. For electric currents the pattern in the E-plane indicates a null at $\theta=\pi/2$ due to the factor $\cos\theta$. This null is absent in the pattern for the magnetic currents. Equation (22), however, indicates a null in this latter pattern if $(\frac{1}{2}ka\sin\theta)=\pi/2$. This means $\sin\theta=\pi/ka$; but for $ka=1.96$, the experimental value, $\pi/ka>1$ and the null is not possible. Again, for electric currents the pattern in the H-plane indicates a null if $(\frac{1}{2}kb\sin\theta)=\pi/2$, or $\sin\theta=\pi/kb$; the experimental value of $kb=4.5$ gives $\pi/kb=0.7$, whence $\theta=45°$. The pattern for magnetic currents does not lead to such a null, but contains a factor of $\cos\theta$ leading to a null at $\theta=\pi/2$. Other nulls for both cases may arise for smaller angles nearer $\theta=0$, because of the term I_2 which is common to both pattern expressions. Such nulls are found in computed values for I_2, and are also observed experimentally.

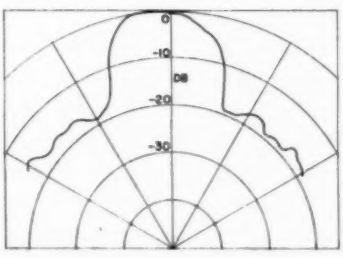

FIG. 6. Experimental pattern in E-plane for dielectric rod with $l=10.2\lambda$, $n=1.10$.

(c) Electric Currents on Top and Bottom

These currents arise from the tangential component of the magnetic vector on the top and bottom surfaces. The magnetic vector has the components:

$$H_y=B_2\cos\frac{\pi y}{b}\exp(jk'z-j\omega t),$$

$$H_z=B_1\sin\frac{\pi y}{b}\exp(jk'z-j\omega t).$$

These expressions have the same values on the two faces, since they do not vary with x; the evaluation of the electric currents then gives currents which are everywhere parallel, but of opposite direction on the bottom compared to the top. Hence these currents can produce no contribution in the field at large distances in the z direction ($\theta=0$). Some contribution should be expected at moderate angles, but no contribution at right angles to the rod ($\theta=\frac{1}{2}\pi$). The resultant pattern should be somewhat on the order of the pattern due to a quadrupole. No detailed evaluation is given here of this pattern, since it does not appear to give contributions near $\theta=0$, the direction of primary interest.

PATTERN COMPUTATIONS

The fields given by Eqs. (22) and (23) have been calculated for specific values of the parameters. These expressions were modified in the

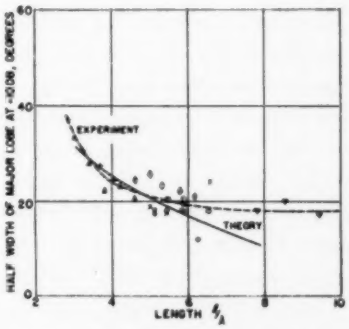

FIG. 7. Half-width of major lobe as a function of length of dielectric rod.

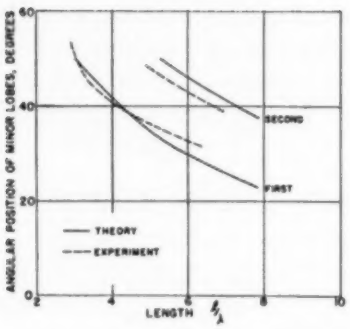

FIG. 8. Angular position of minor lobes as a function of length of dielectric rod.

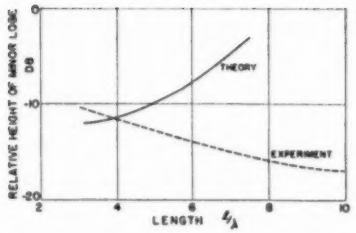

FIG. 9. Relative height of first minor lobe as a function of length of dielectric rod.

calculation to find the magnitude of the complex expressions involved, and to produce normalized values for the fields. The maximum value of the magnitude was used as a normalizing factor, whether this maximum occurred at $\theta=0$ or elsewhere. Unfortunately, the expressions for A and B cannot be evaluated in terms of a general parameter, but must be computed for each choice of n and kl. To allow comparison with experiment, several values for n were chosen, namely, 1.00, 1.05, 1.10, 1.20, 1.30, and 1.50, for $kl=26.4$. Typical computed patterns are shown in Fig. 4 for $n=1.10$, $kl=26.4$, and in Fig. 5 for $n=1.30$, $kl=26.4$. After comparison with experiment, the value of 1.10 was chosen for further computations, using a range of values of kl from 19.0 to 64.1. A summary of data for these several patterns computed for the E-plane is shown in Figs. 7, 8, and 9, together with comparable experimental data. The parameter n varies with the thickness of the dielectric rod. In very thin rods $k'\sim k$, and n is very nearly unity. In thick rods $k'>k$, and n becomes nearly equal to the refractive index for the dielectric. In experimental practice it is found desirable to taper the rod (see Fig. 1) so that the thickness a decreases along the length. This procedure reduces reflection effects and improves the radiation pattern. For such a situation, k' would actually be a function of z in the equations. This variation is allowed for by choosing a mean value of k' in correspondence with experimental evidence.

In the same way, the fields given by Eqs. (31) and (32) were calculated, but for only one or two values of the parameters. Because of the common term I_2, essential agreement was observed between these patterns and those for Eqs. (22) and (23), the only differences arising in the heights of the minor lobes. These differences were not considered significant, and hence no further values were computed, it being concluded that the patterns calculated from the effects of the magnetic currents were sufficient to describe the fields.

EXPERIMENT

Experimental Arrangement

Experimental patterns for a number of polystyrene rods as terminations for a wave guide were obtained by rotation of the rods in a plane polarized electromagnetic field. This field was produced by a dipole antenna mounted in a 24-inch parabolic reflector and connected to a magnetron operating at X-band frequency. This source was placed on the roof of one building and directed at another building 400 feet away, on the roof of which was mounted the receiving equipment. Such an arrangement produced a plane polarized field at the receiving position and reduced reflections from the ground and other surroundings to a minimum. A rotating stand coupled to a motor drive was used for rotation of the rods in the field. The signal received by a rod actuated a suitable receiver whose output was recorded on the chart of an Esterline-Angus recording milliammeter. A marking relay on this recorder allowed interpretation of the record in terms of the rotation of the rod on its stand.

The rods were all of rectangular cross section, designed to fit the wave guide snugly near one end, and ending within the wave guide in a tapered section designed to prevent reflections at the interface between dielectric and air. The outer section was tapered uniformly to give an average thickness of slightly more than half the thickness of the wave guide. This section had

different lengths for the several rods. A typical shape is illustrated in Fig. 1.

Pattern Measurements

Patterns in E- and H-planes were taken for eight different polystyrene rods of various lengths and thicknesses. To obtain a pattern in the E-plane, the rod and associated wave guide were rotated about an axis perpendicular to the axis of the rod and the electric field direction. To obtain a pattern in the H-plane, the rod and associated wave guide were rotated about an axis again perpendicular to the axis of the rod but parallel to the electric field direction. In each case the orientation of the field from the source was such as to produce the $TE_{0,1}$ mode in the receiving wave guide.

Seven of these rods had constant width equal to the inside dimension of the wave guide, but were tapered in the E-plane so that the average thickness was the same for each. As is shown in Fig. 1, the taper does not begin exactly at the junction with the wave guide; the taper itself may differ somewhat from rod to rod. Hence the several average thicknesses are not precisely the same. The eighth rod had a length comparable to one of the first seven, but a considerably different thickness. Typical patterns are shown in Figs. 4, 5, and 6. The pattern in Fig. 4 is for the E-plane for a rod whose length is $l=4.22\lambda$ and whose average thickness is 0.195λ. On this same figure is also shown the theoretical pattern. It is observed that agreement is very good out to about 45°. The general shapes of the curves are the same, the widths of the major lobes at the -10-db points are the same, and the positions of minima agree well. The heights of the first minor lobes are very nearly the same, but the second minor lobe is only suggested by a slight dip on one side of the experimental curve. The theoretical curve shows a minimum about 45°, but at this same angle it was shown in the section on theory that other effects there neglected might be of some importance. In addition, reflections from surrounding objects are more likely to affect the low level fields represented by minor lobes than the strong signal of the major lobe. Hence the deviation of the experimental curve is not unexpected. The pattern in Fig. 5 is for the E-plane for a rod of length $l=4.22\lambda$ and thickness of 0.390λ. The agreement between the experimental and theoretical patterns is here not as good; the experimental curve has some variations near 0° not evident from theory, and the positions of the nulls do not coincide. A small variation in the choice of n in the calculation would improve the agreement of the nulls. The pattern in Fig. 6 is for the E-plane for a rod of length 10.2λ, and average thickness 0.195λ. It is seen that the major lobe has coalesced with one or more minor lobes, while other minor lobes are considerably smaller. The theory developed above indicates for such lengths very prominent first minor lobes, but no major lobe at all. This discrepancy is attributed to the failure of the continuing assumption that the fields in the dielectric rod are similar to the fields within the wave guide throughout the length of the rod.

The seven rods of comparable thickness each had a portion of uniform rectangular cross section about the junction between the rod and wave guide; by inserting more or less of the rod into the wave guide a certain variation of length was available for each rod without appreciable change in the average thickness. About 30 different patterns could thus be obtained for the seven rods, with some overlapping of values for length. Figure 7 shows the resulting values of half-width of the major lobe, illustrating the scattering of the experimental points. A smooth curve shows the general tendency of these points; this curve is not far different from the curve obtained from theoretical patterns, for lengths as great as about 6λ. For rods of longer length, coalescing of the major and first minor lobes begins, whereas the theory indicates a continuing narrowing of the major lobe. A set of data is shown in Fig. 8 for the angular position of the minor lobes as a function of length of rod. The experimental points have been omitted here for purposes of clarity; the scattering is much the same as that shown in Fig. 7. Agreement with theory is again quite good up to $l=6\lambda$, but is less satisfactory thereafter; the minor lobes tend to disappear or to coalesce with the major lobe. Agreement between theory and experiment for angles greater than 45° or so is not good, that is, for further minor lobes. For these large angles the theoretical assumptions are not expected to hold accurately, and reflections from surrounding objects may

well upset experimental conditions. Similar data for the nulls of the patterns show equally good agreement between theory and experiment as for the positions of minor lobes.

The relative height of the first minor lobe obtained from experiment as a function of length is compared to the theoretical curve in Fig. 9. Here there is little or no agreement except for order of magnitude; the theory indicates increasing minor lobe height, while experiment leads to decreasing height. The heights of minor lobes are likely greatly affected by the approximations of the theory and by the experimental conditions, whereas the positions of lobes and nulls are less affected by these factors. Thus the good agreement of positions of minor lobes and nulls is not accompanied by good agreement in minor lobe height.

A comparable set of data was compiled for the *H*-plane patterns. The same agreements and deviations were noted as discussed above for the *E*-plane, without producing any fundamental differences between the results for the two planes.

SUMMARY

A theory is developed for computing radiation patterns for a dielectric rod used as a termination for a rectangular wave guide. Subject to some restrictions, the theory is applied to the $TE_{0,1}$ mode of excitation in the wave guide, and specific expressions are worked out for the radiation patterns. The expressions contain as parameters the length, width, and thickness of the dielectric rod, and its apparent index of refraction. Suitable choice of the index of refraction produces computed patterns agreeing in considerable detail with patterns for polystyrene rods whose lengths vary from 3λ to 6λ, and whose average thicknesses and widths are the same. Also, a comparable computed pattern is obtained for a considerably thicker rod in the same length range.

It is concluded that, given the physical parameters, the analysis may be used to compute radiation patterns for the $TE_{0,1}$ excitation of rectangular dielectric rods.

The Attenuation of Spherical Shock Waves in Air*

RICHARD G. STONER AND WALKER BLEAKNEY

Palmer Physical Laboratory, Princeton University, Princeton, New Jersey

(Received February 13, 1948)

The peak pressure of spherical shock waves from small explosive charges has been determined as a function of distance by measuring the velocity of propagation and applying the velocity-pressure relation derived from the Rankine-Hugoniot equations. The charges were composed of TNT or pentolite (TNT/PETN 50/50 by weight), weighed from 1.45 to 8 lb., and were spherical or cylindrical in shape, except for one series of small rectangular blocks. Measurements on the non-spherical charges were made in the plane through the center of the charge, perpendicular to the axis.

The pressure-distance relations for the four principle charge types are given by the following fitted equations, in which Π represents excess peak pressure in atmospheres, and the distance, scaled according to charge weight, is given by the non-dimensional variable $Z=R/(\rho\tau)^{\frac{1}{3}}$ where R is the distance from a charge of volume τ and specific gravity ρ:

½-lb. rectangular blocks, TNT,
$$\Pi_Q=13.50/Z-769.9/Z^2+36280/Z^3;$$
8-lb. cylinders, Pentolite,
$$\Pi_A=10.49/Z-135.5/Z^2+21070/Z^3;$$
4-lb. cylinders, TNT,
$$\Pi_B=11.34/Z-185.9/Z^2+19210/Z^3;$$
3.75-lb. spheres, Pentolite,
$$\Pi_C=8.63/Z+295.1/Z^2+7823/Z^3.$$

These equations are valid for values of Z between approximately 18 and 110. The indicated probable error of the fitted curves is of the order of one percent for intermediate distances, increasing to from two to seven percent at the extremes of the distance range covered.

The curve for spherical charges is in agreement with the Kirkwood theory, and the results for cylinders having various length/diameter ratios indicate large dependence of pressure on charge shape for values of Z up to 50 at least.

I. INTRODUCTION

IT has long been recognized that pressure waves of finite amplitude in mediums like air propagate at greater than sound velocities, the velocity increasing with amplitude. For this reason, a continuous wave of finite amplitude changes its form with time, a pressure front becoming steeper until limited by the viscosity

* This work was supported in part by the Office of Naval Research, Contract No. N6ori-105 Task II.

and heat conductivity of the medium. When this relatively stable form is reached, the pressure rise occurs within an extremely narrow region, and for most purposes may be considered a perfect discontinuity. Such a disturbance is called a shock wave. The conditions governing the propagation of such discontinuities were formulated by Rankine and Hugoniot, who gave expressions for the conservation of mass, momentum, and energy across the shock front.[1]

The spherical wave produced by the detonation in free air of an explosive charge is a wave of this type, having the characteristic form shown in Fig. 1 for a pressure jump of the order of 0.5 atmosphere.[2] The initial rapid rise to a peak pressure P is followed by a more gradual decay, a shallow suction phase, and a return to atmospheric pressure P_0, either gradual, or including a small secondary shock. The peak pressure decays as the wave propagates outward for two reasons: (1) because the energy must be distributed over a constantly increasing area, and (2) because there is a finite dissipation of energy in the transition through the shock front. Exact solution of the hydrodynamical equations, subject to initial conditions describing the release of energy in the explosive process and to the Rankine-Hugoniot conditions at the shock front, is not possible because of the non-linear nature of the equations of motion, and direct numerical integration is, in general, prohibitively laborious. In a recently published paper,[3] Kirkwood and Brinkley, by imposing a similarity restraint on the energy-time curve of the shock and using the second law of thermodynamics to determine, at an arbitrary distance, the distribution of the initial energy, have reduced the problem to two ordinary differential equations which are amenable to numerical integration. Their computations then provide a theoretical peak pressure *vs.* distance relation.

Experimental determination of the peak pressure of shock waves has also proved to be difficult. The most common method and that which was for a long time considered the most promising, has been the use of piezoelectric crystals, which produce a charge proportional to the applied pressure. The fundamental objection to such gauges, which has only recently become clear, results from the disturbance of the flow caused by the presence of the gauge itself. This effect makes the apparent pressure as read by the gauge less than the true pressure (i.e., the pressure that would exist in the absence of the gauge). The true pressure, moreover, is not a linear function of the gauge reading. Calibration of the gauges therefore becomes a difficult matter. These difficulties can be reduced considerably by suitable streamlining of the gauge and mount, but a complete solution requires a method of dynamic calibration exactly duplicating the conditions under which the gauge is used, which has not so far been achieved.

A technique for pressure measurements which is not subject to these objections has been suggested in the application of the relation between the peak pressure and the velocity of propagation of a shock. If gauges are used simply to time the passage of the shock over a known distance, the need for calibration is eliminated, and the local effect due to the presence of the gauges is unimportant so long as the over-all speed of propagation of the wave is not reduced. While the experiment requires careful planning to obtain satisfactory precision, the elimination of systematic errors should assure more reliable results than have been obtained previously.

The derivation of the pressure-velocity relation has been given in numerous places.[4] Using the

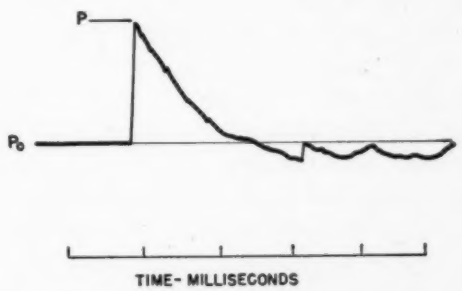

FIG. 1. Typical shock wave from a small charge. (8 feet from 0.5 lb. of TNT. $P-P_0 \sim 0.5$ atmosphere.)

[1] W. J. M. Rankine, Phil. Trans. **A160**, 277 (1870). H. Hugoniot, J. de l'ecole polyt. **57**, 3 (1887); **58**, 1 (1888).

[2] The form of very weak shock waves is somewhat different, and has been investigated by J. W. M. DuMond, E. R. Cohen, W. K. H. Panofsky, and E. Deeds, J. Acous. Soc. Am. **18**, 97 (1946).

[3] S. R. Brinkley, Jr. and J. G. Kirkwood, Phys. Rev. **71**, 606 (1947).

[4] G. I. Taylor and J. W. Maccoll, "Dynamics of Compressible Fluids," from *Aerodynamic Theory*, ed. by W. F. Durand (Julius Springer Verlag, Berlin, 1935) Vol. III, Div. H; H. W. Liepmann and E. E. Puckett, *Aerodynamics*

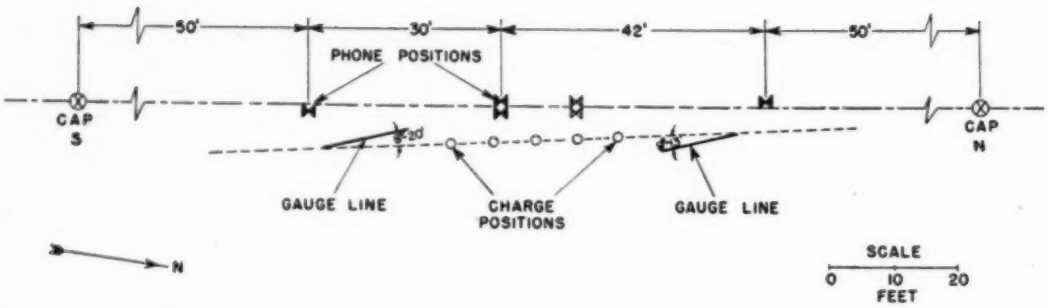

FIG. 2. Plan of experimental set-up. Ten gauges were mounted uniformly, 18 inches apart, along each gauge line.

Rankine-Hugoniot relations and calculating the internal energy of the gas from the ideal gas law, we obtain

$$(P-P_0)/P_0=[2\gamma/(\gamma+1)][(V^2/a^2)-1], \quad (1)$$

where P is the absolute pressure immediately behind the shock front, P_0 is the atmospheric pressure ahead of the shock, V is the velocity of the shock relative to the medium ahead, a is the velocity of sound in this medium, and γ is the ratio of specific heats C_P/C_V. At high pressures the ideal gas approximation with constant γ in the energy equation is not correct. Comparison of Eq. (1), using $\gamma=1.40$ for air, with more exact calculations[5] indicates, however, that for an excess pressure $P-P_0$ of 100 lb./in.^{2} the error in $P-P_0$ is less than 0.7 percent and that this error diminishes rapidly for lower pressures.

Examination of Eq. (1) shows that the ratio of the percent error in excess pressure $P-P_0$ to the percent uncertainty in the velocity ratio V/a is never less than two, and is very large for pressures only slightly greater than P_0. In the pressure region of interest in this investigation ($\sim$0.1 to 10 atmos. excess) the error ratio is about ten in order of magnitude. Thus in order to determine the excess pressure within 1 percent, velocity measurements must be good to about 0.1 percent. This was taken as the design criterion, and the experiment was planned so that this precision could be expected in all the measured quantities involved in determining the velocity ratio.

II. EXPERIMENTAL PROCEDURE

To measure shock wave velocity, quartz piezoelectric gauges were chosen as being best suited to the requirements of the problem. These consist of an x-cut quartz disk, 0.9 inch in diameter and 0.1 inch thick, mounted in a sealed brass housing with a thin dural face plate which communicates the external pressure to the x face of the crystal. Used "face-on" (the blast incident normally on the sensitive face) these gauges provide an extremely fast response to pressure changes, and the flat face furnishes a definite point from which to measure the baseline distance. Ten such gauges were mounted rigidly at intervals of 18 inches and connected in parallel on a single channel of a multichannel cathode-ray oscilloscope unit. This was part of a mobile unit developed especially for blast recording, and provided amplifiers with good high frequency response and exceptionally well focused traces so that the time of arrival of a shock wave at a gauge could be determined within about a micro-second.

Two lines of ten gauges each were set up on opposite sides of the charge, with a distance of 40 feet between the first gauge of each line, as shown in Fig. 2. With a spacing of 18 inches between gauges, a total distance range of about 7 feet to 47 feet could be covered by moving the charge position back and forth between the two gauge lines, 18 pressure points being obtained from the two gauge lines on each shot. Charge positions were located at the point midway between the gauge lines, and symmetrically on each side of this point. In this way the two independent sets of gauges could be checked against each other directly (charge in center position) and in effect interchanged in covering distances close to and far from the charge by taking shots at corresponding positions on opposite sides of the center. Excellent agreement was observed between the results of the two groups of gauges.

of a Compressible Fluid (John Wiley and Sons, Inc., New York, 1947).

[5] J. G. Kirkwood, S. R. Brinkley, Jr. and J. M. Richardson, unpublished work.

To reduce the risk of the nearer gauges blanketing those behind, each gauge line was rotated at an angle of about 9° from the line joining the farthest gauge of each line. A test showed that with the gauges staggered to this extent there was no observable attenuation of the shock wave due to its passage along the gauge line. Careful measurements of the angle and distance of each gauge line with respect to each charge position were made, as well as of the intergauge distances along each gauge line, so that the differences in the radial distances of successive gauges from the charge could be calculated. These represent the true baselines over which the spherical shocks were timed. When the charge position was changed each gauge was rotated about a vertical line through the center of its sensitive face so as to remain normal to the radial line from the charge.

Short pulses of about five microsecond duration were superimposed at a rate of 10,000 per second on each recording channel to facilitate timing the intervals between the arrival of the shock at successive gauges. These pulses were produced by a crystal controlled oscillator checked against the standard carrier frequency of station WWV.

The charges used were either spherical or cylindrical in shape, weighing between ½ and 8 pounds. The cylinders were hung with their axes vertical, so that all the gauges were in the equatorial plane of the charge. In measuring "free air" peak pressure, the charge and gauges must be sufficiently far above the ground to eliminate interference with the incident wave arising from reflection phenomena at the ground. In the present experiments the gauges and charges were located in a horizontal plane 10 feet above the ground, a height sufficient to guarantee that the effect of the ground could not be felt until the shock wave had passed the farthest gauge.

The velocity of sound in the medium must also be known in applying the pressure-velocity relation. Because of the difficulty of controlling or measuring random local variations in the temperature, humidity, local velocity, etc., of the outdoor atmosphere, which affect the velocity of both sound and shock waves, the velocity of sound was measured directly and as nearly as possible at the same time and place as were the shock waves themselves. Ordinary telephone receivers were set up as indicated in Fig. 2 to provide two independent baselines of 30 and 42 feet over which the velocity of the wave produced by the detonation of a blasting cap could be measured. The caps were located at a sufficient distance for the velocity of the pressure wave to have decayed to sound velocity within the limits of observation. Two caps were detonated in close succession at positions *N* and *S* (Fig. 2) to provide determinations of sound

TABLE I. Charges used in experimental program.[a]

Designation	Composition	Average[b] weight (pounds)	Shape	Height[c] (inches)	Diameter[c] or width (inches)	Height / diameter ratio	Number of shots	Number of pressure observations
Q	Pressed TNT	0.5	Rectangular block	3.50	1.75	—	17	117
A	Cast Pentolite[d]	8.00[f]	Cylinder	8.75	4.50	1.94	5	88
B	Cast TNT[e]	4.10[g]	Cylinder	7	3.62	1.93	8	144
C	Cast Pentolite[d]	3.75	Sphere	—	5	—	8	142
D	Cast TNT[e]	2.89[h]	Cylinder	5	3.62	1.38	5	90
E	Cast TNT[e]	2.89[h]	Cylinder	12	2.31	5.20	5	90
F	Cast TNT[e]	1.45[i]	Cylinder	2.5	3.62	0.69	1	18
G	Cast TNT[e]	1.45[i]	Cylinder	6	2.31	2.60	3	52
H	Cast TNT[e]	1.45[i]	Cylinder	8	2.00	4.0	3	45
K	Cast TNT[e]	1.45[i]	Cylinder	12	1.62	7.4	1	18

[a] The spherical pentolite charges were prepared by the Woods Hole group of Division 2, NDRC. All cylindrical charges were supplied by the Picatinny Arsenal.
[b] The weights of individual charges varied by as much as ±5 percent in some cases from the average values listed. Accurately measured weights were used in scaling to reduce results to a common basis.
[c] Dimensions given are nominal values. Variations of the order of ±5 percent occur in some cases.
[d] 50 percent TNT and 50 percent PETN, by weight. Specific gravity ~1.60.
[e] Specific gravity of cast TNT ~1.55.
[f] Includes 0.031-lb. tetryl pellet booster.
[g] Includes 0.096-lb. tetryl pellet booster.
[h] Includes 0.067-lb. tetryl pellet booster.
[i] Includes 0.030-lb. tetryl pellet booster.

velocity in opposite directions, from which the velocity of sound relative to still air and the component of wind velocity in the direction parallel to the gauge lines could be determined. The effect of cross wind velocity (although it was not measured) is entirely negligible since it is a second-order effect, and, by good fortune, the prevailing wind direction during the period of shooting was very nearly parallel to the gauge lines, so that the cross-wind component was in any case only a fraction of the parallel wind component which was measured. The two caps and the main charge were set off automatically at intervals of about 0.1 second to eliminate as far as possible the danger of fluctuations in the atmosphere between the time of the sound measurements and the shock measurements.

The proper wind velocity correction was added to the shock velocity measured over each interval of the gauge line, and the corrected shock

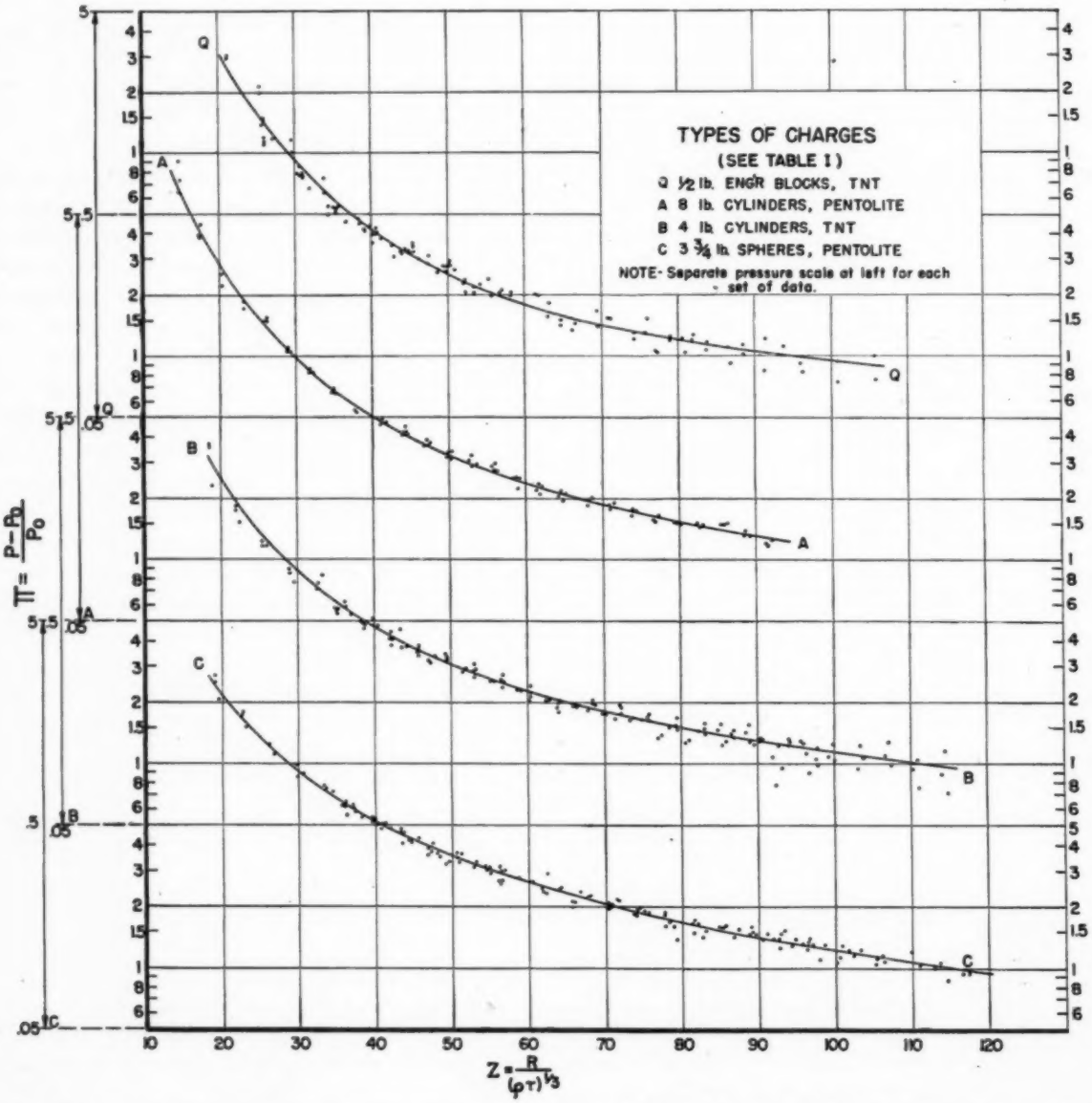

FIG. 3. Experimental pressure *vs.* distance results for four types of charges. Excess shock wave pressure in non-dimensional units, $\Pi = (P-P_0)/P_0$, is plotted against the non-dimensional distance $Z = R/(\rho_T)^{\frac{1}{3}}$. For specific gravity $\rho = 1.60$, $Z = 1.06R/D$, where D is the diameter of a sphere having the same volume as the charge. Thus Z represents approximately the distance in charge diameters, for the explosives used. (For TNT, $\rho = 1.55$; for pentolite, $\rho = 1.60$.)

TABLE II. Fitted curves giving best values of experimental pressure measurements on four series of charges.

Type of charge	Distance range covered by experimental data $[Z=R/(\rho\tau)^{\frac{1}{3}}]$	Fitted curve for pressure $\Pi=(P-P_0)/P_0$	Standard deviation[a] of Π (expressed in percent) σ_1	σ_{min}	σ_2
TNT Eng'r Blocks (Q)	$21 < Z < 107$	$\Pi_Q = 13.50/Z - 769.9/Z^2 + 36280/Z^3$	±3.9%	±2.1%	±4.9%
Pentolite Cylinders (A)	$14.7 < Z < 91$	$\Pi_A = 10.49/Z - 135.5/Z^2 + 21070/Z^3$	7	0.9	1.4
TNT Cylinders (B)	$18.6 < Z < 111$	$\Pi_B = 11.34/Z - 185.9/Z^2 + 19210/Z^3$	6.5	0.8	2.2
Pentolite Spheres (C)	$18.6 < Z < 119$	$\Pi_C = 8.63/Z + 295.1/Z^2 + 7823/Z^3$	2.1	0.6	1.4

[a] σ_1 is the standard deviation at the smallest Z indicated in column 2 and σ_2 at the largest Z. σ_{min} represents the minimum value of standard deviation reached usually at about the midpoint of the Z range. The curve for σ is generally flat in the neighborhood of σ_{min}, and the standard deviation is roughly $<1.5\sigma_{min}$ in the region $40 < Z < 90$.

velocity V was inserted in Eq. (1), along with the measured sound velocity a, and the corresponding pressure calculated. Since the shock velocity changes appreciably with distance, the pressure calculated from the measured average velocity over the interval corresponds to the instantaneous pressure at a point within the interval determined by the relation

$$V(R_V) = (1/R_m q) \int_{R_{m-}}^{R_{m+}} V(R)dR, \qquad (2)$$

where R_V is the distance from the charge at which the instantaneous pressure equals the pressure computed from the average velocity, R_m is the distance from the charge to the midpoint of the interval over which the velocity is measured, q is the ratio of the length of the interval to R_m, $R_{m+} = R_m(1+q/2)$, $R_{m-} = R_m(1-q/2)$, and V is the function expressing shock velocity in terms of distance from the charge.

An approximate expression for R_V may be obtained by assuming that the pressure over a short interval may be represented by an expression of the form $P - P_0 = AR^{-n}$, where A and n are constants, and expanding the resulting expression for $V(R)$ obtained by substituting this in Eq. (1). The expression valid for low pressures was first given by Carr, Schwarzschild, and Weiss, working at Aberdeen, and has the form

$$R_V = R_m\{1 - (1+n/2)q^2/24\}. \qquad (3)$$

A slightly different expression is obtained when an expansion valid at high pressures is used. A more detailed derivation of Eq. (3) shows that it actually holds for moderately high pressures, and that in the most unfavorable case in the experiments reported here the error in R_V is only 0.18 percent.

III. RESULTS

The physical characteristics of the types of charges investigated are given in Table I. In order to compare results from charges of different weights, the data have been reduced to a common basis by scaling the distances according to the principle of similitude. For similar charges of equal density, equal pressures are expected at distances proportional to the linear dimensions of the charges, and hence to the cube root of the charge weight. This scaling law has been shown experimentally to be valid over a large range of charge weights. The scaled distances are given in terms of the non-dimensional variable $Z = R/(\rho\tau)^{\frac{1}{3}}$, where R is the actual distance from the charge, having a volume τ and specific gravity ρ relative to water.[6] The pressure is expressed non-dimensionally in units $(P-P_0)/P_0$, denoted hereafter by Π.

The charges designated A, B, and C in Table I formed the major part of the experimental program, and the complete sets of pressure-distance points for these three series and for the pre-

[6] It has been customary in the past to represent the scaled distance by the dimensional variable $z = R/w^{\frac{1}{3}}$ where R is the distance in feet, and w is the charge weight in pounds. The quantity z thus has dimensions ft./(lb.)$^{\frac{1}{3}}$. The relation between z and the non-dimensional variable $Z = R/(\rho\tau)^{\frac{1}{3}}$, which we have introduced, is obtained by replacing w by $62.43\rho\tau$. It follows that $Z = (62.43)^{\frac{1}{3}}z = 3.967z$. Thus a distance in Z units when divided by 4 represents roughly the distance in feet from a one pound charge.

The convenient relationship between the Z units and charge diameters may be seen by substituting $V = \pi D^3/6$ where D is charge diameter. We then have $Z = (\pi\rho/6)^{-\frac{1}{3}} \times (R/D)$. Thus Z represents exactly the number of charge diameters (R/D) when $(\pi\rho/6)^{-\frac{1}{3}} = 1$; i.e., for $\rho = 6/\pi = 1.910$. Because of the cube root involved, Z also represents approximately the distance in charge diameters for a considerable range of values of ρ. For $\rho = 1.50$, for example, $(\pi\rho/6)^{-\frac{1}{3}} = 1.084$, and Z differs from the number of charge diameters by 8.4 percent.

The "density of loading," as the term is customarily used, is the same as the specific gravity ρ used here. Hence R will be in feet if τ is in cu. ft., in cm if τ is in cc, etc.

liminary series (Q) using U. S. Corps of Engineers Demolition Blocks of pressed TNT are shown as small dots in Fig. 3, A, B, C, and Q, respectively.

The curves shown represent least square fits of an expression of the form $\Pi = AZ^{-1} + BZ^{-2} + CZ^{-3}$, introduced by Reynolds,[7] which has been found to give a satisfactory representation of the data over the range of Z involved. Asymptotic solutions of the propagation equations show a decay in pressure proportional at large distances to Z^{-1} except for a slowly varying logarithmic factor, and experimental measurements in general point to Z^{-3} as a possible limiting value for the dependency at small distances. The Z^{-2} term provides a third parameter necessary for fitting the data successfully. Since the pressure in the explosive is known to be finite, an expression of this form cannot hold for very small Z. For this reason the fitted curves should be extrapolated only with great caution beyond the range of the experimental data. The equations of the fitted curves for the first four groups of charges in Table I are given in Table II. The limiting values of Z indicate the range covered by the experimental data. The quantity σ is an estimate of the reliability of the fitted curve, expressed as a standard deviation; that is, if the experiment were repeated, in $\frac{2}{3}$ of the cases the value of Π given by the fitted curve would lie within $\pm\sigma$ of the "true" curve which would be obtained from a very large number of observations in the same kind of experiment. The values of σ given in Table II are expressed as a percentage of the value of Π as given by the fitted curve, which represents the best value of the pressure as indicated by the experimental data. The standard deviation of an individual point is ~ 5 times the σ for the curve. The statistical treatment by which these σ's were calculated took into account the non-independence (in the statistical sense) of data from adjacent gauge line intervals.[8]

The relationship of the various experimental determinations to each other and to the theory are shown in Fig. 4. To emphasize the comparison of the various curves, the pressure curve for pentolite spheres (Π_c in Table II) has been chosen arbitrarily as standard, and the difference of each of the other curves from it, expressed as a percentage of excess pressure, is plotted as ordinate. The ordinate is thus the quantity $100(\Pi - \Pi_c)/\Pi_c$ (equivalent to $100(P - P_c)/(P_c - P_0)$). The abscissa is the non-dimensional scaled distance Z. Thus the curve for pentolite spheres is represented by the horizontal axis.

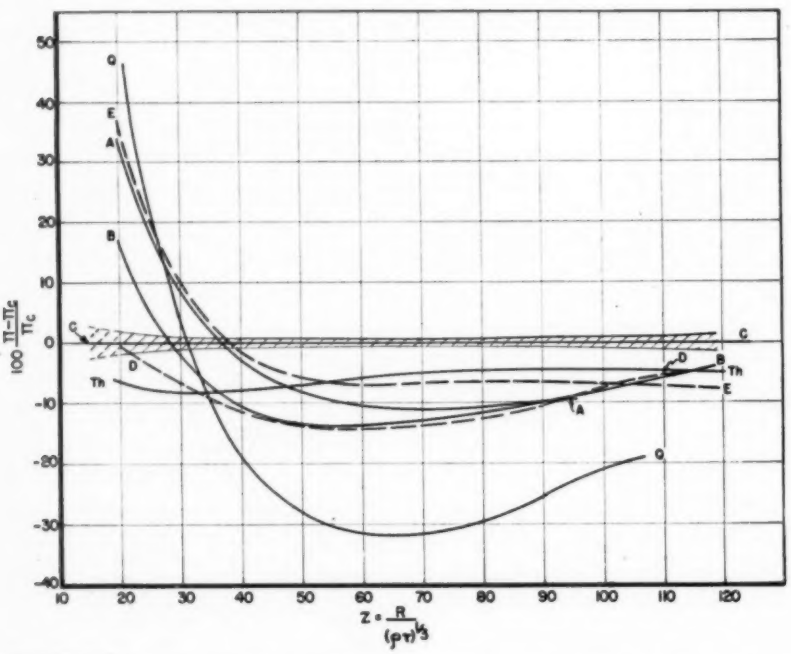

FIG. 4. Comparison of results. Each curve represents the percent deviation of excess pressure, $100(\Pi - \Pi_C)/\Pi_C$, from the value for pentolite spheres Π_C, plotted as a function of the non-dimensional distance Z. The experimental curves are designated by letters as in Table I. Curve *Th* represents Kirkwood and Brinkley's theoretical prediction for TNT spheres.

[7] G. T. Reynolds, "Small charge air blast experiments," OSRD Report No. 1518 (1943).
[8] We are indebted to Dr. H. Sheffe for developing a form of statistical treatment appropriate to this problem.

(The choice of this curve as standard is only for convenience in making the greatest number of meaningful comparisons and, of course, implies no fundamental distinction in the reliability of this curve relative to the others.) The shaded region indicates the standard deviation band $\pm\sigma$ (expressed in percent). Bands of similar width apply to the other experimental curves. The various curves are identified according to the designations used in Table I.

Curve *Th* represents the theoretical curve for spherical charges of TNT computed by Kirkwood and Brinkley on the basis of their recently reported theory.[3] A curve for pentolite, which could be compared directly with the experimental results, is not available, but experimental work at Woods Hole indicates that 5 percent probably represents the superiority in pressure level of pentolite over TNT, averaged over the whole distance range involved. Thus the approximate constancy of the difference between curve *Th* and curve *C*, with an average value of from five to seven percent, represents good agreement between the theory and the experimental data.

The effect of charge shape may be seen directly from curves *C* and *A* which represent pentolite spheres and cylinders, respectively. Curve *B* is for TNT cylinders having the same length/diameter ratio as the pentolite cylinders. Its approximate similarity to curve *A* is a further confirmation that the observed difference between cylinders and spheres is real, but the two curves raise some question whether (at least in the case of cylindrical charges) the ratio of the pressures from TNT and pentolite is a constant, independent of distance. The shape of curves *A* and *B* may be explained qualitatively by the observation that the shock wave from the sides of a cylindrical charge should at first be more nearly cylindrical than spherical, and thus show a slower decay and relatively higher pressure at small distances from the charge. At some point, the rarefaction propagating in from the ends would begin to take effect, and the wave could then be expected to decay more rapidly than the corresponding spherical wave. It is somewhat surprising that this effect is apparently so pronounced at distances greater than 20 charge diameters, but in view of the indicated precision of the experimental determinations, the observed effect must be considered real. The explanation suggested is of course only qualitative.

The remaining types of charges in Table I, consisting of smaller cylinders of TNT having a larger range of length/diameter ratios, were not used in sufficient numbers to make it advisable to treat the data statistically, but curves could be fitted by eye with reasonable assurance. Because of the smaller size of the charges and the smaller number of observations, the results are less reliable, but are almost certainly good to better than 10 percent, except at the extremes of the distance range. Curves *D* and *E* are for 2.9-lb. TNT cylinders with length/diameter ratios of 1.38 and 5.20, respectively. The former is somewhat less than the ratio for the charges of curve *B*, the latter considerably larger. The relative values of the three curves at small distances are consistent with the argument suggested above, and the three curves approach agreement at large distances, which is to be expected. The data from 1.45-lb. cylindrical TNT charges with four different length/diameter ratios varying from 0.69 to 7.4 also showed similar behavior, but the number of shots was so small (only 2 shots, providing 18 pressure points each, with no overlap in distance, in the case of the smallest and the largest L/D ratios) that an accurate comparison is of little significance, and the curves have not been included in Fig. 4.

An extreme example of the effect of charge shape is seen in curve *Q*, representing measurements made with standard Corps of Engineers Demolition Blocks of pressed TNT, whose measurements are given in Table I. These blocks have a square cross section, with slightly rounded corners, and measurements were made in the equatorial plane in a direction normal to a flat face. Thus the effect of both corners and ends may be expected, and a large divergence from the pressure-distance law for spherical charges is observed, considerably larger than in the case of even the most elongated cylinders investigated.

There have been published, as far as the authors are aware, no experimental results with which the data in this paper can be compared. They are aware, however, of the existence of other results to which reference cannot be made at this time because they have not been published.

IV. CONCLUSION

The velocity method of measuring shock wave pressures which has been developed appears to offer a means of determining absolute peak pressure which is (1) free from the systematic error inherent in direct gauge measurements due to the physical presence of the gauge in the flow, and (2) capable of precision of better than 1 percent in the excess pressure when a sufficiently large number of measurements is made. A fundamental limitation appears to be the nonuniformity of the atmosphere under even the best field conditions. On the basis of such measurements, Kirkwood's theory has been checked experimentally, and a difference in the decay of pressure with distance arising from the shape of the charge has been observed which persists at relatively large distances from the charge.

The authors wish to take this opportunity to express their appreciation to Professor A. H. Taub for many helpful consultations during the early development of the program, and to Messrs. L. Christiansen, H. Krieg, R. W. Symons, and R. W. Weston, who constituted the field crew.

Chromatic Aberration and Resolving Power in Electron Microscopy

E. G. Ramberg and J. Hillier
Radio Corporation of America Laboratories, Princeton, New Jersey
(Received February 17, 1948)

Contrast difficulties in the observation of fine detail in thin specimens may be overcome by employing dark-field observation. This introduces the added complication, however, that the imaging electrons are now inhomogeneous, having experienced a most probable energy loss of the order of 20 volts. The present calculations of the effect of chromatic aberration and diffraction show that with an objective aperture smaller than the "optimum aperture," and centered optics, such inhomogeneities do not appreciably affect the resolution, even in the extreme case that the electrons are uniformly distributed in energy.

THE recognition of fine detail attainable in electron micrographs depends on the ultimate resolving power of the instrument, as determined by lens aberrations[1] and diffraction effects, on the one hand, and by the image contrast under the given operating conditions on the other. The condition generally regarded as favorable for attaining the highest resolutions—namely, bright-field observation of very thin objects with a physical objective aperture at least equal to the "optimum aperture"—inherently leads, unfortunately, to relatively low contrasts. Apart from contrast limitations, the resolution is here limited by spherical aberration and diffraction, leading, according to Glaser's wave-mechanical theory,[2] to the expression

$$d_{\min}=0.56\lambda(Cf/\lambda)^{\frac{1}{4}} \tag{1}$$

for an "optimum aperture"

$$\alpha_{\text{opt}}=1.13(Cf/\lambda)^{-\frac{1}{4}}. \tag{2}$$

Here $d_{\min}$ is the least resolvable separation of two object points, C the dimensionless spherical aberration constant of the objective, f its focal length, and λ the de Broglie wave-length of the imaging electrons. Equation (1) represents a lower limit to the resolution obtained with the

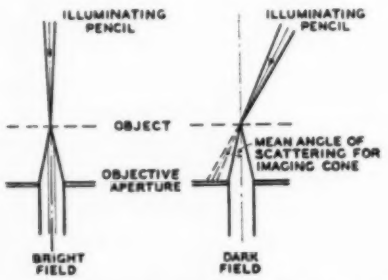

FIG. 1. Arrangement of illumination for bright-field and dark-field observation.

[1] The effects of field asymmetries as well as voltage fluctuations (effective because of the chromatic aberrations of the lenses) are included herein.

[2] W. Glaser, "Image formation and resolving power of the electron microscope from the standpoint of wave mechanics," Zeits. f. Physik 121, 647 (1943).

electron microscope by any means. As already indicated, unfavorable contrast conditions prevent a close approach to this limit for the majority of specimens.

An obvious remedy for this contrast difficulty consists in the employment of dark-field observation; here the background brightness is greatly reduced since only radiation scattered by the specimen is utilized for the formation of the image. If the illuminating beam is made to impinge on the specimen at an angle and the objective aperture is centered as for bright-field work (Fig. 1), the geometric aberrations and diffraction effects may, in principle, be made approximately the same as for bright field. However, most of the scattered electrons, unlike those which pass through the specimen without deflection, experience an appreciable loss in kinetic energy. These energy losses lead to enhanced chromatic aberration effects in the image which, in the past, have been considered responsible for the reduction in resolving power always observed when an electron microscope is used as a dark-field instrument. Since this increase in chromatic aberration appears to be an essential concomitant in the passage from bright field to dark field it becomes of interest to investigate the velocity distribution in the scattered electrons used for dark field imaging and to examine to what extent chromatic aberration reduces resolving power.

Figure 2 shows the energy spectra of 50-kv electrons which have been scattered by a 100-A.U. collodion foil through the small angles indicated. These curves, obtained with the microanalyzer arranged as shown in Fig. 3, have been corrected for the sensitometric properties of the photographic plate, but not for the finite slit width of the instrument. Hence they represent simply the electron distribution obtained on the analyzer plate. The geometry of the apparatus was such that the electrons passing through any portion of the entrance slit had been scattered by the object over an angular range 0.0008 radian in width. With the slit adjusted so as to coincide with the electron probe (Fig. 4) the angular deflection of the electrons could be computed from the displacement of a particular point of the spectrum from the overexposed image of the probe; it is obtained simply by

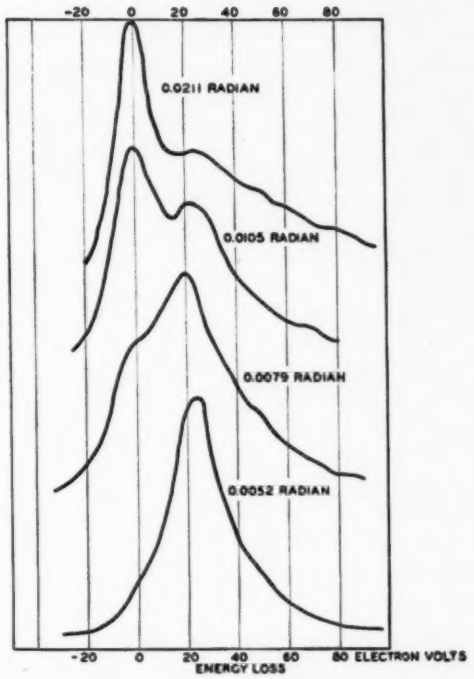

FIG. 2. Electron distributions in velocity spectrograms formed by electrons scattered by a thin collodion film through the indicated small angles.

dividing this displacement by the length of the electron path from the object to the plate. Quite similar results were obtained, of course, from spectra obtained by displacing the slit; here the angular deflection is given by the ratio of the slit displacement to the object-slit separation.

The curves in Fig. 2 show a predominance of the inelastic scattering at very small angles, of elastic scattering (zero energy loss), at greater angles. This is in accord with theoretical expectation.[3] The most probable energy loss of the inelastically scattered electrons is seen to be of the order of 20 electron volts, which presumably represents an averaged energy of excitation from the uppermost occupied to the nearest unoccupied energy bands of the nitrocellulose lattice.

In order to compute the effect of chromatic aberration resulting from such velocity distributions the simplifying assumption was made that the physical aperture of the objective corresponded to an angular aperture appreciably smaller than the optimum aperture given by

[3] See, e.g., L. Marton and L. I. Schiff, "Determination of object thickness in electron microscope," J. App. Phys. 12, 759 (1941).

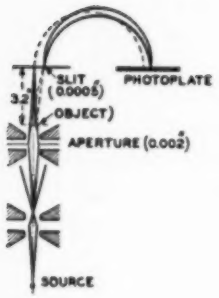

FIG. 3. Arrangement of microanalyzer for the determination of velocity distribution of electrons scattered through a definite angle.

Eq. (2). Under these circumstances the effect of spherical aberration is negligible, so that only chromatic aberration and diffraction need be considered in determining the fundamental resolving power of the microscope. Since preliminary calculations for the velocity distributions in question indicated that the effect of chromatic aberration, also, was very small, it seemed of interest to treat the most extreme case of chromatic aberration—namely, that obtained with uniform energy distribution of the electrons.

If f_0 is the focal length of the objective for V_0-volt electrons, the displacement of the point of convergence of the wave in image space corresponding to a change $e\Delta V$ of the kinetic energy of the electrons is

$$\Delta z = M^2 K(\Delta V/V_0) f_0. \tag{3}$$

Here M is the magnification and K a factor of the order of unity. Hence, if $u(z,r)$ is the amplitude of the wave at an axial separation z and a radial separation r from the point of convergence, the intensity (or concentration of electrons) at a point a distance r from the axis is, for uniform energy distribution of the electrons, given approximately by

$$I = \int_{-\infty}^{\infty} |u(z,r)|^2 dz. \tag{4}$$

This relation implies the validity of Eq. (3) throughout the range of kinetic energies, and neglects the effect of the variation of the de Broglie wave-length λ with kinetic energy as well as the variation in the solid angle intercepted by the objective aperture at the point of convergence. It applies, thus, most accurately for small values of r, where electrons with small values of ΔV contribute most to the value of the integral.

The value of $u(z,r)$ for a converging spherical wave limited by a distant diaphragm (the objective aperture) to a cone of half-angle α is given, according to Debye,[4] by

$$\begin{aligned} u(z,r) &= \frac{ik}{2\pi} \int_0^{\alpha} \int_0^{2\pi} \exp(ik(z\cos\vartheta_0 \\ &\quad + r\sin\vartheta_0 \cos\varphi_0))\sin\vartheta_0 d\vartheta_0 d\varphi_0 \\ &= ik \int_0^{\alpha} \exp(ikz\cos\vartheta_0) \\ &\quad \times J_0(kr\sin\vartheta_0)\sin\vartheta_0 d\vartheta_0. \end{aligned} \tag{5}$$

Here $k = 2\pi/\lambda$ and α, the half-angle of the wave cone, will be regarded as constants, corresponding to the values for the wave with its convergence point at $z=0$. $J_0(x)$ is the Bessel function of order zero. The intensity expression in Eq. (4) may then be evaluated with the aid of a series of transformations and a change in the order of integration as follows:

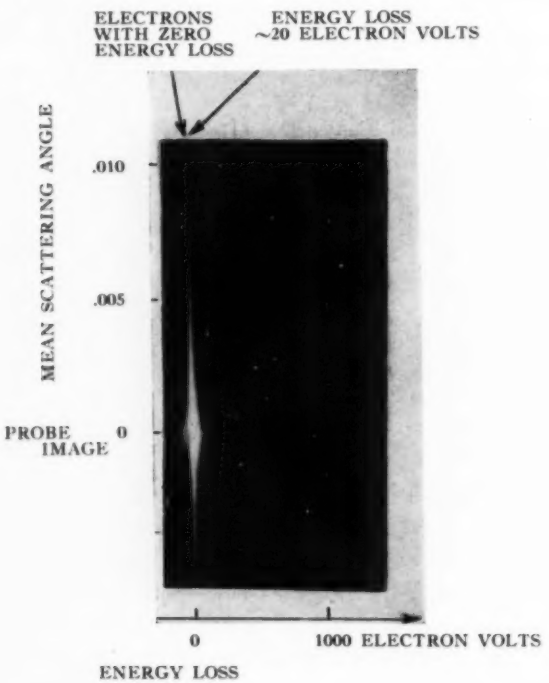

FIG. 4. Velocity spectrogram of 50-kv electrons which have passed through a thin collodion film.

[4] P. Debye, "Light near a focal point or line," Ann. d. Physik **30**, 755 (1909). The calculation given applies for an unpolarized wave.

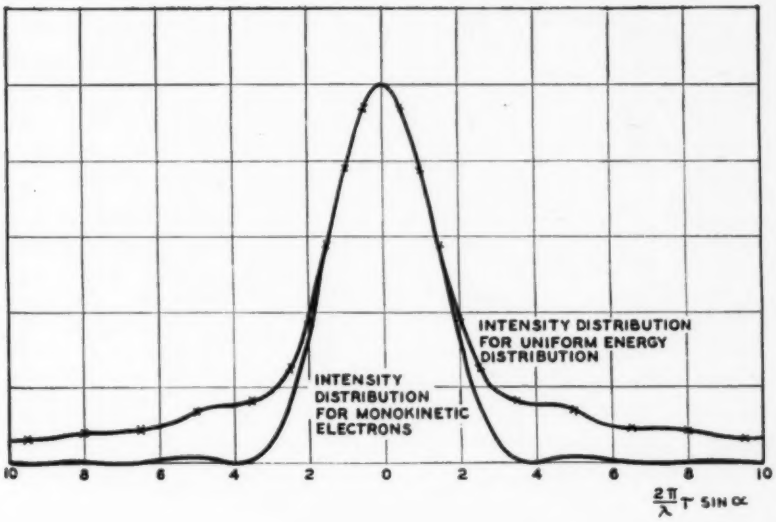
INTENSITY DISTRIBUTION FOR UNIFORM ENERGY DISTRIBUTION
INTENSITY DISTRIBUTION FOR MONOKINETIC ELECTRONS
10 8 6 4 2 0 2 4 6 8 10
$\frac{2\pi}{\lambda} r \sin\alpha$

FIG. 5. Intensity distribution in image of a point source.

$$I(r)=k^2\int_{-\infty}^{\infty}dz\left\{\left|\int_0^{\alpha}\cos(2kz\sin^2(\vartheta_0/2))\times J_0(kr\sin\vartheta_0)\sin\vartheta_0 d\vartheta_0\right|^2+\left|\int_0^{\alpha}\sin(2kz\sin^2(\vartheta_0/2))\times J_0(kr\sin\vartheta_0)\sin\vartheta_0 d\vartheta_0\right|^2\right\}$$

$$=k^2\int_{-\infty}^{\infty}dz\int_0^{\alpha}\sin\vartheta_0 d\vartheta_0\int_0^{\alpha}\sin\vartheta_0' d\vartheta_0'\times\{\cos 2kz[\sin^2(\vartheta_0/2)-\sin^2(\vartheta_0'/2)]\times J_0(kr\sin\vartheta_0)J_0(kr\sin\vartheta_0')\}$$

$$=k^2\int_0^{\alpha}\sin\vartheta_0 d\vartheta_0\int_0^{\alpha}\sin\vartheta_0' d\vartheta_0'\times\left\{\left[\frac{\sin 2kz(\sin^2(\vartheta_0/2)-\sin^2(\vartheta_0'/2))}{2k(\sin^2(\vartheta_0/2)-\sin^2(\vartheta_0'/2))}\right]_{-\infty}^{\infty}\times J_0(kr\sin\vartheta_0)J_0(kr\sin\vartheta_0')\right\}$$

$$=2k\int_0^{\sin^2(\alpha/2)}dy\int_0^{\sin^2(\alpha/2)}dy'\times\left\{\left[\frac{\sin 2kz(y-y')}{y-y'}\right]_{-\infty}^{\infty}\times J_0(2kr(y-y^2)^{\frac{1}{2}})J_0(2kr(y'-y'^2)^{\frac{1}{2}})\right\}.$$

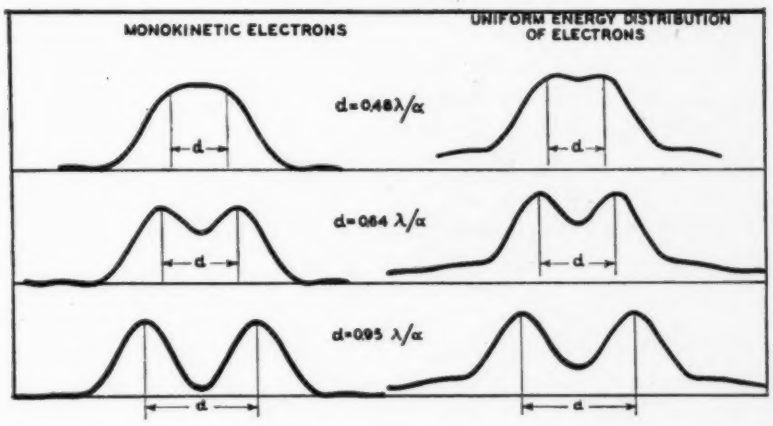

FIG. 6. Intensity distribution along line joining the image centers of two point sources.

$$I(r)=4\pi k\int_0^{\sin^2(\alpha/2)} J_0^2(2kr(y-y^2)^{\frac{1}{2}})dy$$

$$=2\pi k\int_0^1 J_0^2(krx\sin\alpha)\frac{x\sin^2\alpha}{(1-x^2\sin^2\alpha)^{\frac{1}{2}}}dx$$

$$=\frac{2\pi}{kr^2}\int_0^{kr\sin\alpha}\frac{J_0^2(u)\cdot u\cdot du}{(1-(u^2/k^2r^2))^{\frac{1}{2}}}.$$

The last expression is readily integrated if the quantity $u^2/(kr)^2$ is neglected as compared with unity. This is quite generally permissible, since, even if the pattern is referred to the object plane, $u^2/(kr)^2$ has a maximum value less than 0.0001. We then find:

$$I(r)=\pi k\sin^2\alpha\{J_0^2(kr\sin\alpha)+J_1^2(kr\sin\alpha)\}, \quad (6)$$

where $J_1(x)$ is the Bessel function of the first order. For very large r this approaches the distribution to be expected for chromatic aberration alone:[5]

$$I(r)\rightarrow\frac{2\sin\alpha}{r}$$

since

$$J_0(x)\rightarrow(\pi x/2)^{-\frac{1}{2}}\cos(x-\pi/4);$$

$$J_1(x)\rightarrow(\pi x/2)^{-\frac{1}{2}}\sin(x-\pi/4).$$

Close to the Gaussian image point, on the other hand, the distribution is closely approximated by the distribution for a monokinetic imaging pencil in the plane of sharp focus:

$$I_0(r)=(\sin^2\alpha/r^2)J_1^2(kr\sin\alpha), \quad (7)$$

since for small values of the argument x the functions $J_0^2(x)+J_1^2(x)$ and $4J_1^2(x)/x^2$ are both given by $1-(x^2/4)+$ terms of the fourth and higher orders in x.

Figure 5 compares the intensity distribution calculated for uniform energy distribution (Eq. (6)) with that obtained for monokinetic electrons (Eq. (7)). Inspection indicates that the resolving power obtainable with the two distributions is practically the same. This is further confirmed by the distributions obtained for two scattering centers separated by small distances, plotted in Fig. 6. If the least resolved distance is defined as that for which a minimum appears between the two maxima corresponding to the individual scattering centers, a slightly smaller separation may actually be resolved with the uniform energy distribution than with the monokinetic radiation. In any case, the energy distribution of the electrons reduces the contrast. This contrast reduction is, however, not so great as to impair materially the discrimination of particles in dark-field images. It would be more serious in bright-field observations.

The conclusions regarding the effect of chromatic aberration on resolving power which have here been reached apply throughout the portion of the image field in which axial chromatic aberration exceeds chromatic change in magnification and rotation. In a magnetic electron microscope with centered lenses this is commonly true for the entire observed field.[6]

These calculations indicate that objectives with physical apertures somewhat smaller than the optimum for the lens should be capable of approximately equal resolving powers in both bright and dark fields. The reduced resolution demonstrated in the published dark-field images may reasonably be attributed to the fact that sufficiently small apertures were not generally used. In this laboratory some dark-field images have been obtained with apertures of 4×10^{-3} rad. and 10^{-4} rad. in which the resolution obtained was nearly equal to that in the bright-field images. However, in neither type of image did the resolution approach the theoretical value. This last discrepancy has been ascribed to the effects of the charging of contamination layers on what were originally clean apertures.

It now appears that lack of resolution in dark-field images has been due to technical rather than fundamental limitations. This means that properly directed development should make it possible to exploit the high contrast possibilities of dark-field images.

[5] In this case

$$I=4\pi\sin^2\frac{\alpha}{2}\cdot 2\int_{r/\tan\alpha}^{\infty}\frac{dz}{\pi z^2\tan^2\alpha}=\frac{8\sin^2\frac{\alpha}{2}}{\tan^2\alpha}\cdot\frac{\tan\alpha}{r}\leqq\frac{2\alpha}{r}.$$

[6] See, e.g., Zworykin, Morton, Ramberg, Hillier, and Vance, *Electron Optics and the Electron Microscope* (John Wiley and Sons, Inc., New York, 1945), p. 646.

The Young's Modulus and Strain Coefficient of Resistivity of Some Bismuth Rich Alloys*

G. C. KUCZYNSKI
Sylvania Electric Products, Inc., Bayside, New York

AND

J. T. NORTON
Department of Metallurgy, Massachusetts Institute of Technology, Cambridge, Massachusetts

(Received February 24, 1948)

The Young's modulus and strain coefficient of electrical resistivity were determined for some Bi-Pb, Bi-Sn, Bi-Se, and Bi-Ni alloys. It was found that the modulus of elasticity decreases rapidly in the regions of solid solution contrary to the predictions of Guillet. The strain coefficient of resistivity was found to increase rapidly within the limits of solid solubility while the stress coefficient of electrical resistivity remained constant.

THE alloys of bismuth with lead and tin exhibit unusually rapid increases of specific electrical resistivities with small concentration of these elements.[1,2]

On the other hand, the work of Nishayama[3] and Guillet[4] seems to indicate that in the range of terminal solid solutions, in general, no unusual variations of Young's modulus should be expected. Therefore, it seemed of interest to investigate the Young's modulus and the influence of strain upon electrical resistivity of these particular alloys.

METHOD AND MATERIALS USED

The static method of Young's modulus determination was used because it facilitated the measurement of elastic and electrical properties at the same time. The apparatus designed for this purpose in the Metallurgical Department of Massachusetts Institute of Technology is described in another place.[5] The increments of stress were plotted against the corresponding increments of strains. The slope of the linear part of the curve thus obtained was accepted as the value of Young's modulus of a given metal or alloy. The temperature was maintained at 28°C and controlled within the range ±0.1°C. The total systematic error in Young's modulus determination was estimated not to exceed 5 percent.

At the same time, using the same apparatus the electrical resistance at increasing strain was measured and its change ΔR divided by original resistance. R_0 was plotted against increment of strain $\Delta\epsilon$. The slope of the obtained curve at $\Delta\epsilon=0$ (extrapolated) is defined as strain coefficient of electrical resistance $\Delta R/R_0\Delta\epsilon$. The relationship between this coefficient and the corresponding coefficient $\Delta\rho/\rho\Delta\epsilon$ of electrical resistivity ρ in the elastic region can be expressed by the following equation:

$$\Delta\rho/\rho\Delta\epsilon=(\Delta R/R\Delta\epsilon)-(1+2\mu), \qquad (1)$$

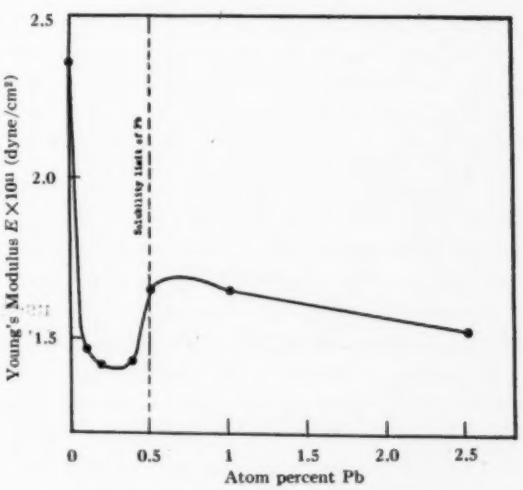

FIG. 1. Young's modulus as a function of composition for Bi-Pb alloys.

* This paper is based upon the ScD thesis of G. C. Kuczynski, Massachusetts Institute of Technology, 1946.

[1] N. Thompson, Proc. Roy. Soc. **A155**, 111 (1936).

[2] A. Thomas and G. Evans, Phil. Mag. **16**, 329 (1903).

[3] Z. Nishayama, Sci. Rep. Tohoku Imp. Univ. **18**, 359–400 (1930).

[4] L. Guillet, Bull. Tech du Bur. Veritas.

[5] J. T. Norton and G. C. Kuczynski, Instruments, **21** 328 (1948).

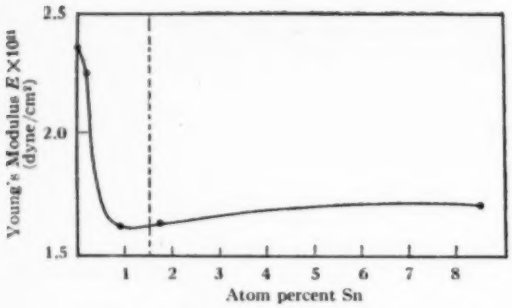

FIG. 2. Young's modulus as a function of composition for Bi-Sn alloys.

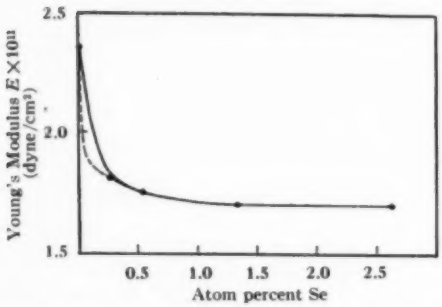

FIG. 3. Young's modulus as a function of composition for Bi-Se alloys.

where μ is the Poisson's ratio which, in the case of bismuth and its diluted alloys, is equal to 0.33.[6] The changes in length were measured with a cathetometer, down to 0.0005 cm. The permanent elongation never exceeded 0.01 percent. The total systematic error in the determination of this factor was estimated not to exceed 8 percent.

Some Bi-Pb, Bi-Sn, Bi-Se, and Bi-Ni were investigated. Bismuth metal was supplied by the American Smelting and Refining Co. and contained no more than 0.0023 percent Pb, 0.0013 percent Cu, and 0.0005 percent Fe. Lead used was chemically pure containing more than 99.9 percent of lead. Tin was of the Bureau of Standard purity. Selenium containing more than 99.9 percent of selenium used for preparation of bismuth-selenium alloys was supplied by the American Smelting and Refining Company. Nickel used for making bismuth nickel alloy was Mond Nickel containing more than 99.9 percent of Ni.

The alloys were prepared by melting in vacuum then extruded to 0.004-inch diameter wires. These wires were examined microscopically and

[6] *Smithsonian Physical Tables* (1934), Eighth edition, p. 137.

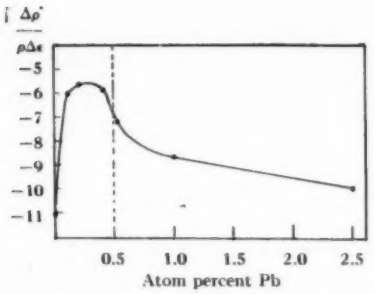

FIG. 4. Strain coefficient of resistivity for Bi-Pb alloys.

only those with smooth surfaces were selected for investigation. From these only pieces which exhibited uniform cross section to 3 percent were tested. All wires were vacuum annealed at 100°C for 15 minutes. The modulus of elasticity and strain coefficient of resistivity for each metal or alloy was determined at least from five specimens. The current passed through the wire never exceeded few milliamperes. The electrical resistivities of the investigated wires indicated that the axis of the wire was parallel to the trigonal axis of the bismuth unit cell. All factors measured refer to this direction only.

EXPERIMENTAL RESULTS

The following Bi-Pb alloys were investigated: 0.1, 0.2, 0.4, 0.5, 1.0, and 2.5 atomic percent of

TABLE I.

Concentration in atom percent	Young's Modulus $\times10^{11}$ (dyne/cm²)	$\Delta\rho/\rho\Delta\epsilon$	$\Delta\rho/\rho\Delta\sigma\times10^{-11}$ (cm²/dyne)
	Bi-Pb alloys		
0.00	2.36	−11.11	−4.10
0.10	1.46	− 6.00	−4.10
0.20	1.43	− 6.30	−4.30
0.40	1.41	− 6.10	−4.25
0.50	1.66	− 7.00	−4.30
1.00	1.64	− 8.66	−5.30
2.50	1.53	− 9.98	−6.50
	Bi-Sn alloys		
0.17	2.25	− 9.60	−4.2
0.87	1.60	− 0.32	
1.77	1.62	− 5.82	
8.45	1.70	− 2.32	
	Bi-Se alloys		
0.27	1.81	− 9.16	−5.05
0.54	1.76	− 8.68	−5.00
1.33	1.70	− 8.06	−5.05
2.63	1.70	− 7.68	−4.80
	Bi-Ni alloy		
13.00	2.25	− 4.68	−2.08

lead. The results are represented in Fig. 1 and in the Table I. The smallest addition (about 0.1 atomic percent) of lead lowers Young's modulus by about 40 percent. After the minimum point at about 0.3 atom percent of lead is reached, Young's modulus increases rapidly. After 0.5 atom percent of lead the alloys exhibit only slight changes in Young's modulus. The rapid decrease of modulus of elasticity followed by its rapid increase takes place in the region of solid solubility of lead in bismuth. The solubility limit of lead in bismuth was estimated by Guertler and other investigators[7,8] at 0.5 atom percent of lead.

The bismuth-tin alloys behave initially similar to bismuth-lead alloys (Fig. 2, Table I). They exhibit a shallow minimum at about 1.3 atom percent of tin. According to M. Hansen[8] the solubility limit of tin in bismuth is about 1.5 atom percent.

Bismuth-selenium alloys (Fig. 3, Table I) show the same rapid decreases of Young's modulus at low concentrations of selenium, but the modulus of elasticity of the alloys containing more than 0.27 atom percent of selenium falls down slowly and finally assumes a constant value. The initial decrease due to the addition of one atom percent of selenium is about 30 percent. The solubility of selenium in bismuth is not known but most probably is very low, of the order of a tenth of atom percent.

Only one alloy of bismuth-nickel containing 13 atom percent of nickel was investigated. Its Young's modulus was found to be 2.25×10^{11} dynes/cm^2 almost equal to that of pure bismuth (2.3×10^{11} dynes/cm^2).

The above observations seem to contradict Guillet's contention[4] that in the range of terminal solid solutions, Young's modulus does not change appreciably.

The strain coefficients of electrical resistivity are given in the third column of Table I and Figs. 4–6. The comparison of these curves with those of Young's modulus for the corresponding alloys reveal striking relationship. Abrupt changes of both properties occur within the same regions of concentrations. In all cases Young's modulus decreases rapidly as strain coefficient of electrical resistivity increases (algebraically). In the case of Bi-Pb alloys Young's modulus reaches its minimum at 3 atom percent of lead and at the same concentration $\Delta\rho/\rho\Delta\epsilon$ has its maximum. In the case of Bi-Sn alloys the increase of strain coefficient of resistivity is so rapid that at about 0.8 atom percent of tin it reaches value zero and then becomes positive and as high as 6.0 at 1.75 atom percent. After solubility limit of tin in bismuth (about 1.5 atom percent) is exceeded, $\Delta\rho/\rho\Delta\epsilon$ falls slowly to the value of 2 for 8.45 atom percent of tin.

In the case of Bi-Se alloys the change of strain coefficient does not seem to be so abrupt as in

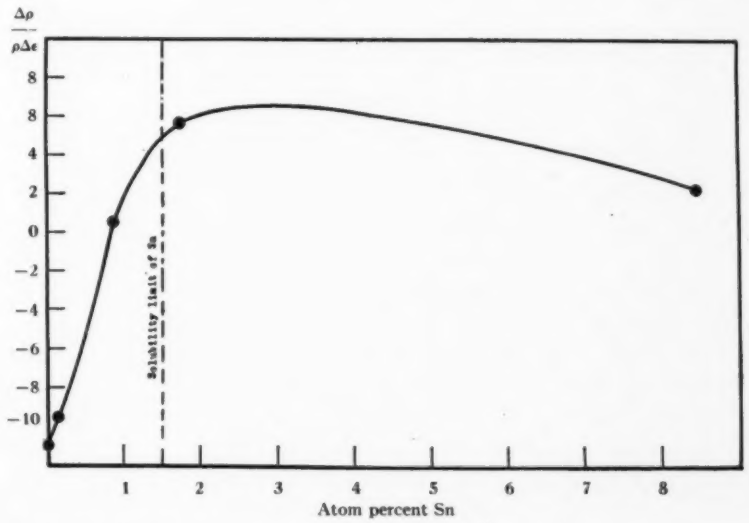

FIG. 5. Strain coefficient of resistivity for Bi-Sn alloys.

[7] W. Guertler, Zeits. f. anorg. allg. Chemie **51**, 911 (1906).
[8] M. Hansen, *Aufbau der Zweistofflegierungen* (Verlag Julius Springer, Berlin, 1936).

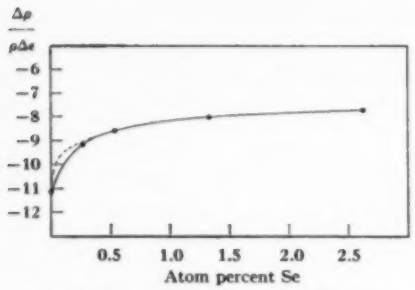

FIG. 6. Strain coefficient of resistivity for Bi-Se alloys.

the previous cases. This is most probably due to the fact that the solubility of selenium in bismuth is well below 0.1 atom percent of selenium, so the line joining the value of $\Delta\rho/\rho\Delta\epsilon$ for pure bismuth and that for 0.27 atom percent of selenium should be much steeper (like the dotted lines on Figs. 3 and 6). The same refers to Young's modulus curve described above.

The strain coefficient of resistivity for Bi-Ni alloy with 13.0 atom percent nickel was also determined and found to be -4.68.

The above results show that there seems to be a definite relationship between $\Delta\rho/\rho\Delta\epsilon$ and Young's modulus within solubility region. The shape of the curves suggests that the ratio $(\Delta\rho/\rho\Delta\epsilon)/E$ where E is Young's modulus should remain constant. In view of $E\Delta\epsilon=\Delta\sigma$ where $\Delta\sigma$ is the increase of stress, we can express our relationship in the following equation:

$$\Delta\rho/\rho\Delta\sigma=\text{constant}.$$

In other words the relative change of the electrical resistivity of a terminal solid solution of Bi-Pb and Bi-Sn alloys is proportional only to the stress and independent of either its elastic deformation produced or the initial resistivity or the composition. Therefore, it is the same as in the pure bismuth, namely, 4.10.

Indeed, the fourth column of Table I shows that this factor remains reasonably constant for Bi-Pb alloys for concentrations lower than solubility limit (about 0.5 atom percent of Pb). After this limit is exceeded $\Delta\rho/\rho\Delta\sigma$ decreases. Of course no such analysis is possible for Bi-Sn alloys because some have zero or even positive strain coefficients of resistivity. Bi-Se alloys exhibit low value of the stress coefficient of resistivity (around -5.0×10^{-11} (cm²/dyne) instead of -4.1×10^{-11} (cm²/dyne)), indicating once more that the solubility limit of selenium in bismuth is well below 0.27 atom percent of selenium, $\Delta\rho/\rho\Delta\sigma$ for Bi-Ni alloy is unusually high, -2.08×10^{-11} (cm²/dyne).

ACKNOWLEDGMENT

The authors wish to express their gratitude to Baldwin Southworks Company in Philadelphia for making these investigations possible.

Letter to the Editor

Electron Optical "Schlieren" Effect

L. MARTON
National Bureau of Standards, Washington, D. C.
April 19, 1948

SEVERAL months ago the problem came up of measuring the magnetization produced on ferromagnetic wires in a wire-recording system. Several possibilities were explored and finally an electron optical method was chosen as one of the possible methods for measuring the fringe field extending from the recording wire. This method was conceived in close analogy to the light optical "schlieren" method (often also called Töpler's shadow method). It consists in forming an image of a light source on a convenient stop which intercepts all direct rays (Fig. 1). If in

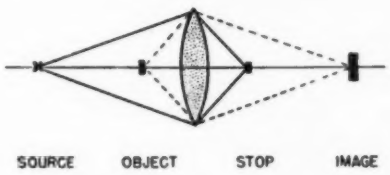

FIG. 1. Schematic representation of the optical path for the production of a "schlieren" image.

the space between the source and lens there is a variation of the index of refraction, an image of that inhomogeneity will be produced by means of the same lens in a conjugate image plane beyond the stop. Thus a dark-field image of the variation of the refractive medium is formed.

This method is readily adaptable to electron optical investigations. In fact, the isolated observations of striae occur often enough in electron microscopical work when either the objective lens aperture is not properly centered or the action of the beam on some unexpected impurities in the system produces a charge on some part of the instrument. The patterns thus produced in electron microscopes are usually very disturbing and every effort has been made to avoid them. In our work here we deliberately produce conditions under which these patterns are formed and use them for the observation of the fields making these patterns.

The most convenient application to electron optical systems is that of a beam-producing system like that of an electron microscope with a sufficient number of lenses to give the required flexibility in concentrating the transmitted beam and a convenient stop for the production of the dark-field image. The first experiments of this nature had for object a determination of the magnetization produced by a recording head on a steel or other wire used for recording purposes. For producing a "schlieren" image of a magnetized wire, the wire was placed at a distance of about 5 cm from a magnetic lens with a free bore of about 16 mm and irradiated with a 40-ekv electron beam. An approximately 6-to-1 image was formed on a fluorescent screen. Sharp focusing is facilitated by the fact that the image of the magnetized wire appears straight only when in focus, whereas out-of-focus images show the magnetized regions out of line with non-magnetic parts of the wire. Thus the out-of-focus image of a straight magnetized wire appears as a zigzag line.

After the image of the wire is properly focused, a center stop of about 1-mm diameter is used to intercept the direct rays. Figure 2 shows how, by placing the center stop partially across the visual field, a partly bright-field and partly dark-field image of such magnetized wires can be obtained. The "schlieren" image of the magnetic fields extending on both sides of the wire is readily recognizable.

Once images of fields are produced by this method the intensity distribution in the image can be used for calculating the actual field distribution at the sample. Such calculations have been carried out recently in this laboratory by Mr. S. H. Lachenbruch for the case of an ideal magnetic dipole. In the case of a magnetized wire which was our first example, it is reasonable to assume that the field around the wire behaves as if it were produced by an ideal dipole. By means of this assumption we can calculate from the intensity distribution in the image the actual field strength in the immediate vicinity of the wire.

This electron optical method can be made into a very useful tool for the observation of electrostatic or magnetic fields where such fields are not susceptible to any other type of investigation. As an example, the field distribution in electromagnetic wave guides may be cited where the field distribution in elbows is rather incompletely known. Experiments have been undertaken here by Mr. D. Reverdin to produce such "schlieren" images by using standing waves in a straight portion of a wave guide. It is also an interesting tool for the exploration of space charge fields, or any other phenomena which do not always allow an analytical treatment because of their complicated geometries.

Further applications include a study of contact potentials, mosaic structure of crystals, ferromagnetic domains, etc. A preliminary study of ferromagnetic domains

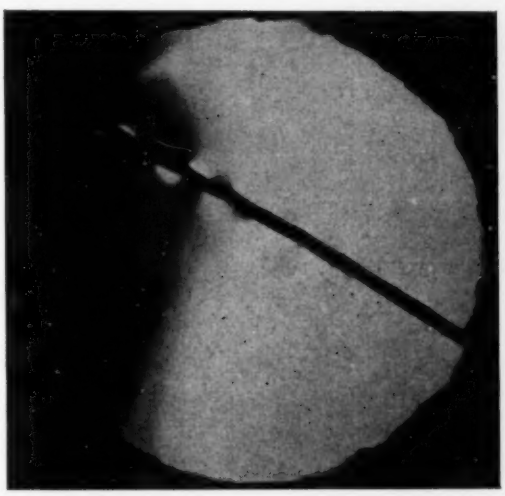

FIG. 2. "Schlieren" image of short magnetic pulses on steel wire. Left side: dark field; right side: bright field.

has been undertaken and is being published elsewhere.[1] It may be worth mentioning in this respect also an early work of Boersch, who observed dark-field images produced by a vapor jet.[2] Strictly speaking, his observation does not belong here because the primary phenomenon is scattering instead of deflection produced by a variation of the electromagnetic index of refraction.

[1] L. Marton, Phys. Rev. **73**, (1948).
[2] H. Boersch, Zeits. f. Physik. **107**, 493 (1937).

Here and There

Personnel

J. Howard Dellinger, Chief of the Central Radio Propagation Laboratory of the National Bureau of Standards, retired on April 30 after 40 years of government service. He is now acting as a radio consultant and adviser.

Isidor Fankuchen is the first incumbent of the new Chair of Applied Physics at Polytechnic Institute of Brooklyn.

Christopher E. Barthel, Jr., has been named Chairman of Physics Research at Armour Research Foundation of Illinois Institute of Technology.

Carroll Stansbury has been appointed to the Electronics Division of the National Bureau of Standards, where he will do research in the engineering electronics laboratory.

T. Keith Glennan was inaugurated as the fourth President of Case Institute of Technology, Cleveland, Ohio, on May 20 and 21. The program featured a symposium with the theme: The Increasing Responsibility of the Scientist and Engineer in Public Affairs.

Lehigh Valley Physics Club

The Physics Club of the Lehigh Valley was recently elected to the status of an Affiliated Society of the American Institute of Physics. The Club at present has a membership of about one hundred scientists and engineers.

Eisenhart Elected Fellow of British Society

Churchill Eisenhart, Chief of the Statistical Engineering Laboratory, National Bureau of Standards, has been elected a fellow of the Royal Statistical Society of Great Britain

North American Philips Sponsors Course

A group of nationally known authorities on x-ray diffraction lectured on their specialties before the third annual spring course in x-ray diffraction, spectrometry, and fluorescence analysis, held recently in the New York offices of North American Philips Company, Inc. Discussion of medical applications of x-ray diffraction was included in the course for the first time. Seventy persons, from 15 States and Canada, enrolled in the week-long course.

New Booklets

The Proceedings of the 1947 National Electronics Conference has been printed and is now available at $4 a copy from Dr. R. R. Buss, Secretary N.E.C., Care of Electrical Engineering Department, Northwestern Technological Institute, Evanston, Illinois.

Lenkurt Electric Company, Inc., 1105 County Road, San Carlos, California, has issued its Bulletin 40A, entitled *Trancors*. 24 pages.

Industrial Photographic Division of Eastman Kodak Company, Rochester 4, New York, recently issued two new booklets which are available free on request: *Magnifying Time* (12 pages) and *Kodak Linagraph Films and Papers, for Instrument Trace Recording* (4 pages).

RCA Laboratories Division, Princeton, New Jersey, published this spring an index to *RCA Technical Papers*, Volume II (b), 1947. 24 pages.